Universitat de Girona

EFFECT OF PRE-BOND MOISTURE ON THE STATIC AND FATIGUE BEHAVIOUR OF BONDED JOINTS BETWEEN CFRP LAMINATES FOR STRUCTURES REPAIRS

Sandip Rudha Budhe

Dipòsit legal: Gi. 1798-2014
http://hdl.handle.net/10803/283567

Universitat de Girona

DOCTORAL THESIS

EFFECT OF PRE-BOND MOISTURE ON THE STATIC AND FATIGUE BEHAVIOUR OF BONDED JOINTS BETWEEN CFRP LAMINATES FOR STRUCTURAL REPAIRS

Sandip Rudha Budhe

2014

Universitat de Girona

DOCTORAL THESIS

EFFECT OF PRE-BOND MOISTURE ON THE STATIC AND FATIGUE BEHAVIOUR OF BONDED JOINTS BETWEEN CFRP LAMINATES FOR STRUCTURAL REPAIRS

Sandip Rudha Budhe

2014

Supervised by

Dr. Jordi Renart Canalias Dra. Anna Rodriguez Bellido

A thesis submitted for the degree of Doctor by the

University of Girona

Universitat de Girona

To whom it might concern,

Dr. Jordi Renart Canalias, Lecturer at the University of Girona of the Department of Enginyeria Mecànica i de la Construcció Industrial and **Dra. Anna Rodriguez Bellido** at the Material and Processes Department, Airbus,

CERTIFY that the study entitled *Effect of Pre-bond Moisture on the Static and Fatigue Behaviour of Bonded Joints Between CFRP Laminated for Structural Repairs* has been completed under our supervision and meets the requirements to opt for a Doctorate.

For all intents and purposes, I hereby sign this document

Dr. Jordi Renart Canalias
Universitat de Girona, Spain

Dra. Anna. Rodriguez Bellido
Materials and Processes, Composite Technology, Airbus, Madrid, Spain

Girona, June 2014

Dedicated to my family

Acknowledgment

It would not have been possible to complete the doctoral thesis without help and support of the kind people around me from last 3 year journey of Phd.

I am really happy to have Dr. Jordi Renart as my supervisor, his support, guidance help me a lot. He is very cool and friendly in nature so i could discuss thing other than academic also. I would like to thank him for his valuable guidance and encouragement leads to complete my doctoral study at University of Girona. He plays an important role for the completion of my thesis and specially a multifatigue test and analysis. With his support, guidance and help, I could finish multifatigue test on time.

Secondly I would like to thanks to Dra. Ana Rodriguez for her guidance, valuable comment and directions help me to achieve the final goal. Discussion with her solves the many problems and it gives me new direction for thinking.

My greatest appreciation and gratitude goes to Prof. Josep Costa Balanzat, for his trust and support. I would like to thank him for his talented comment, discussion and encouragement leads to give new way of thinking. He is busy person and involve in many activities then also he make time for discussion with me. He is good person and asks many times about my staying in Girona and my personal life.

I am very grateful to Joan Andreu who helps me a lot for the academic and technical support. I never in trouble for academic process, work contract letter and other related work; it's because of Joan Andreu. I thanks to Rina who helps me a lot for my paper work, contract related work and specially translate my mail from Catalan to English language.

I would also thanks to all members of our AMADE research group; all are really helpful in nature. I never have any difficulty

in the initial days and all the work gone smoothly because of helpful, kind and lovable person in our group. I feel lucky to be part of such research group. We have the group lunch, Christmas, lunch and other event where we enjoyed and share our personal life and thought, so I never feel lonely. I also thank the wonderful staff in the Mechanical and structural department for always being so helpful and friendly.

The library facilities, Informatics facilities, computer facilities and fully equipped laboratory of the Girona University have been indispensable. I would also thanks to all co-author of article for their effort and valuable comment.

I would like thank to the INTA (Instituto Nacional de Tecnica Aeroespacial) for providing the material and also manufacture the material of our required specification during research. Special thanks to Dr. Jose Maria Pindado to discuss about the manufacturing process and help us to sort out the doubt related to material manufacturing.

I spent more time in laboratory as most of my work is experimental. I also like to have in around machine it feel good, so my bound with the lab members (Yunior, Jaume, Javi and Magdalena) was strong like as a good friend and their help and kind support and guidance really help me to carry my work in proper procedure. I would thank to Tina about the quality of test and methods and her vigilance on the test procedure and on calculation help me to avoid any mistake during testing and data analysis.

My stay in Girona would not be possible without Sabi, Shubho, Alicia and Santanu. We were like families and we thoroughly enjoyed the Friday Nights and Barracus festival. Sabi help me a lot for the official work like permission for residence card and other miscellaneous work, thank you. My friends in Sweden, India and other part of the world were sources of laughter, joy and support. Special thanks go to Nilesh, Sachin, Dilip, Yogesh who always ready to talk with me and increase my energy when I was down.

I especially thank my father, mother, brother and sister. My hard-working parents have sacrificed their lives for me and provided unconditional love and care. I would not have made it this for without them. I would like to thank my wife Tanushree for her personal support, care and love even though she was in India. I really appreciate her patience and support especially after marriage; we were 8000km away from each other but never fight, really feel lucky to have you in my life.

Finally, I want mention that doing Phd in AMADE research group, university of Girona is a memorable journey in my life. I learned so many things and experiences that I have gained through this journey would help me to complete the rest of journey in my life successfully.

Thank you all again!!

Moltes gracies!!!!

Funding

This work has been partially supported by an AIRBUS contract: TOLEDO project, and by the Spanish Ministerio de Economía y Competitividad through the grant MAT 2012-37552-C03-03.

List of figures

List of tables

List of symbols

Symbol	Description
δ	Displacement
P	Load
a	Crack length
C	Compliance
P_{max}	Maximum load
B	Specimen width
da/dN	Fatigue crack growth
dC/da	Variation of compliance with crack length
m	Material constant of paris law
F_p	Load after the pre-crack
a_p	Crack length after the pre-crack
R	Load ratio $(\delta_{min}/\delta_{max})$
ERR	Energy Release Rate
δ_{max}	Maximum displacement
δ_{min}	Minimum displacement
G_{IC}	Mode I Fracture Toughness
G_{IIC}	Mode II Fracture Toughness
G_C	Critical Fracture Toughness
G	Fracture Toughness
G_{Ith}	Mode I threshold energy
G_{Imax}	Maximum mode I energy release rate
N	Fatigue loading cycles

List of acronyms

Acronym	Description
CFRP	Carbon Fiber Reinforced Polymer
CBT	Classical Beam Theory
DCB	Double Cantilever Beam
NL	Nonlinear Point
CCM	Compliance Calibration Method
VIS	Visual Inspection Point
5 %Max	Minimum value between the 5% increment of the compliance and the maximum point
LEFM	Linear Elastic Fracture Mechanics
PROP	Propagation point
SBT	Simple Beam theory
SEM	Scanning Electron Microscopy
% w/w	Percentage of weight of water
RH	Relative Humidity

Table of Contents

Summary

In recent years, the use of composite materials in the aeronautic, automotive, marine construction, etc. has increased significantly. Hence, there is an increasing need for repair technologies on primary structural components, as replacing a damaged component by a new one is not cost effective in many cases. The composite structures experience damage in service that comes from accidental impacts, mechanical stresses, environmental factors (moisture and temperature), etc. Thus, maintenance and repair is the concern of the end users as well as of the manufacturers. Suitable material systems and controlled curing conditions are essential to fabricate reliable repairs.

In particular, moisture absorption is one of the most important factors for the performance of composite structures. This phenomenon is well known and is taken into account during the design phase. However, very few authors study the effect of pre-bond moisture on composite bonded repairs and its effect in the bond performance. Most authors found a negative influence on the fracture toughness but some noticed that there is a positive influence or no effect. There is no single theory with sufficient experimental support to provide a general relation between the pre-bond moisture and the mechanical properties of the joints. So, there is a need to study the effect of pre-bond moisture and to correlate it with the fracture toughness of the bonded joint. A better understanding of the effects of the pre-bond moisture will permit the optimization of the drying process prior to bond. This is a common practice which implies time and energy costs. Adjusting the drying time and the drying temperature to the minimum required is an objective of the aeronautical industry.

In this work, the effect of pre-bond moisture is analyzed for co-bonded adhesive joints subjected to static and fatigue loads. Specimens with three levels of pre-bond moisture (0%, 0.33% and 1.25%) and two different adhesive films (F1, F2) have been used in the analysis.

The first part of the study is carried out under mode I static loading. The results of the tests show that the fracture toughness of both adhesive films, F1 and F2, is highly sensitive to the pre-bond moisture present in the CFRP substrates. Pre-bond moisture decreases, as a general rule, the fracture toughness energy, although the influence of the test temperature and the post-bond conditioning modulate the fracture toughness values.

Pre-bond moisture also changes dramatically the failure mode. In absence of pre-bond moisture, the specimen failure is driven by the test temperature and the post-bond conditioning, with a variety of failure modes as a consequence of the relative resistance of each component (material) of the bond to those factors, temperature and moisture. In the presence of pre-bond moisture, whatever the test temperature or the post-bond conditioning, all specimens failed in the interface between the co-bonded material and the adhesive film.

The second part of the study is carried out under mode I fatigue loading. The design of a device for multiple-fatigue testing of 6 specimens, and the development of the methodology to obtain a complete fatigue characterization in one single step is presented. The test device and the methodology are used to investigate the effect of pre-bond moisture under fatigue loading. Results show that, an increase of the moisture absorbed by the substrate before performing the joint has a negative effect on the fatigue behaviour of the adhesively-bonded joints.

Resumen

En los últimos años, el uso de materiales compuestos en la industria aeronáutica, automoción, construcción marina, etc. ha experimentado un gran crecimiento. Por consiguiente, resulta cada vez más necesario el desarrollo de metodologías para su reparación, en especial en componentes estructurales primarios, principalmente porque la substitución del componente no resulta económicamente rentable en muchos casos. Es un hecho conocido que las estructuras de compuesto en servicio sufren daños provocados por impactos accidentales, tensiones mecánicas, efectos ambientales (humedad y temperatura), etc. Por consiguiente, el mantenimiento de estas estructuras y su reparación son considerados de vital importancia para los usuarios finales así como para los fabricantes. Una buena elección de los materiales así como un buen control del proceso de curado son esenciales para obtener reparaciones confiables.

En especial, la absorción de la humedad por parte de los materiales es uno de los factores que más influyen en el rendimiento de las estructuras de material compuesto. Este fenómeno es bien conocido y tenido en cuenta durante la etapa de diseño. Sin embargo, se han realizado muy pocos estudios sobre el efecto de la presencia de humedad en el sustrato antes de los procesos de uniones encoladas en reparaciones de estructuras de compuesto. La mayoría de los autores han obtenido que la presencia de humedad en el proceso de curado tiene un efecto negativo en los valores de tenacidad a la fractura de la unión, muy pocos autores han obtenido resultados positivos o un efecto nulo. No existe una sola teoría con soporte experimental suficiente para explicar una relación general entre los efectos de la presencia de la humedad en los substratos y su efecto en las propiedades mecánicas de la unión. Por consiguiente, hay una necesidad de realizar estudios sobre este efecto de la humedad y poderlo relacionar con la tenacidad a la fractura de la unión adhesiva. Una mejor caracterización de los posibles efectos de la presencia de humedad en los componentes a reparar, permitiría la optimización del proceso de secado del sustrato previo a la instalación de una reparación encolada. Estos procesos de secado son una práctica habitual y son costosos en tiempo y energía. Ajustar los tiempos y las temperaturas a lo estrictamente necesario es un objetivo de la industria.

En este trabajo se ha analizado el efecto de la absorción de la humedad en el substrato antes del proceso de curado en uniones co-encoladas sometidas a ensayos estáticos y de

fatiga. Para el análisis se han utilizado probetas con tres niveles de absorción de humedad (0%, 0.33% y 1.25%) y dos tipos de adhesivos laminados (F1 y F2).

En la primera parte del estudio el análisis se ha realizado mediante ensayos estáticos. Los resultados de estos ensayos muestran que la tenacidad a la fractura de los dos adhesivos, F1 y F2, es sensible a la humedad del sustrato, disminuyendo como regla general a medida que aumenta el porcentaje de humedad en el sustrato. La influencia de la temperatura de ensayo y del acondicionamiento en humedad de las probetas co-encoladas previo al ensayo también se hace notar, modulando los valores finales de tenacidad. La humedad presente en el sustrato cambia también dramáticamente los modos de fallo. En ausencia de humedad, el fallo de las uniones está determinado por la temperatura de ensayo y el acondicionamiento posterior a la unión, obteniendo una variedad de modos de fallo como consecuencia de la resistencia relativa a ambos factores, temperatura y humedad, de los materiales que componen la unión. La presencia de humedad en el sustrato, provoca en todos los casos, el crecimiento de la grieta en la interfaz entre el material co-encolado y el adhesivo, independientemente de la temperatura de ensayo y del acondicionamiento posterior a la unión.

En la segunda parte del estudio el análisis se ha realizado mediante ensayos de modo I a fatiga. En primer lugar se presenta el diseño de un utillaje para poder realizar múltiples ensayos al mismo tiempo, y de una metodología para la caracterización de las propiedades de un lote de probetas. El equipamiento, así como la metodología, se han utilizado para investigar el efecto de la absorción de la humedad en el substrato en uniones sometidas a cargas cíclicas. Los ensayos han dado como resultado un efecto negativo de la absorción de humedad en el comportamiento a fatiga de las uniones adhesivas.

Resum

Durant els últims anys, la utilització de materials compòsits en la indústria aeronàutica, automoció, construcció marina, etc. ha tingut un gran creixement. Es per aquesta raó, que cada vegada té més importància el desenvolupament de mètodes per a la seva reparació, i especialment la definició mètodes de reparació en components que realitzen una funció estructural, doncs la substitució del component no és econòmicament viable en molts dels casos. És un fet conegut, que les estructures de material compòsit en condicions de servei pateixen danys provocats per impactes accidentals, tensions mecàniques, efectes ambientals (humitat i temperatura), etc. Per tant, el manteniment i la reparació d'aquestes estructures són considerats processos de vital importància per a l'usuari final i també per als fabricants. Una bona tria dels materials, així com un bon control dels processos de curat, tenen un gran efecte en l'obtenció de reparacions fiables.

Especialment, l'absorció de la humitat per part dels materials és un dels factors que més influència té en el rendiment de les estructures de material compòsit. Aquest és un fenomen ben conegut i que es té en compte durant l'etapa de disseny. No obstant, s'han dut a terme molts pocs estudis sobre els efectes de la humitat en el substrat abans de realitzar el procés d'encolat en reparacions entre estructures de compòsit. La major part dels autors han obtingut valors inferiors de la tenacitat a la fractura de la unió, molt pocs treballs han obtingut resultats positius o un efecte nul. No existeix cap teoria amb un suport experimental suficient que proporcioni una relació general entre l'absorció d'humitat en el substrat i el seu efecte en les propietats mecàniques de la unió. Per tant, hi ha una necessitat per dur a terme estudis relacionats amb aquesta temàtica i poder-los quantificar mitjançant la tenacitat a la fractura de la unió adhesiva. Una millor determinació dels efectes provocats per la presència d'humitat en els components a reparar permetria l'optimització del procés d'assecat del substrat abans de la realització d'una reparació encolada. Aquests processos d'assecat són una pràctica habitual i són costosos en temps i energia. L'ajust del temps i de la temperatura al que és estrictament necessari, per tal d'obtenir una bona reparació, és un objectiu de la indústria.

En aquest treball s'ha analitzat l'efecte la l'absorció de la humitat en el substrat abans del procés de curat en unions co-encolades sotmeses a càrregues estàtiques i de fatiga.

L'anàlisi s'ha dut a terme amb provetes amb 3 nivells d'absorció d'humitat (0%, 0.33% y 1.25%) i dos tipus d'adhesius laminats (F1 i F2).

En la primera part de l'estudi s'ha dut a terme una campanya d'assaigs estàtics. Els resultats obtinguts mostren que la tenacitat a la fractura dels dos adhesius, F1 y F2, es sensible al contingut d'humitat en el substrat, disminuint, com a regla general, a mesura que augmenta el percentatge d'humitat en el substrat. La influència de la temperatura de l'assaig i del condicionament en humitat de les provetes abans de realitzar l'assaig també es fa palès, modificant els valors de la tenacitat. La humitat continguda en el substrat modifica dràsticament els modes de falla. En absència d'humitat, el mode de falla de les unions està determinat per la temperatura d'assaig i el condicionament posterior de la unió, obtenint una varietat de modes de falla com a conseqüència de la resistència relativa a la temperatura i humitat dels materials que conformen la unió. La presencia d'humitat en el substrat provoca, en tots els casos, el creixement de l'esquerda en la interfície entre el material co-encolat i l'adhesiu, amb independència de la temperatura d'assaig i el condicionament posterior que se li faci a la proveta.

En la segona part de l'estudi s'ha dut a terme una campanya d'assaigs de mode I a fatiga. En primer lloc es presenta el disseny d'un utillatge per a poder realitzar més d'un assaig a fatiga al mateix temps, i també una metodologia per a la caracterització de les propietats d'un lot de provetes. L'equipament així com la metodologia s'han utilitzat per a l'estudi de l'efecte de l'absorció d'humitat en el substrat en unions sotmeses a càrregues cícliques. Com a resultat dels assaigs s'ha obtingut un efecte negatiu de l'absorció d'humitat en el comportament a fatiga de les unions adhesives.

En la primera part de l'estudi s'ha dut a terme una campanya d'assaigs estàtics. Els resultats obtinguts mostren que la tenacitat a la fractura dels dos adhesius, F1 y F2, es sensible al contingut d'humitat en el substrat. Hi ha una variació del mode de fallada de les provetes, passant d'un estat amb múltiples fronts d'esquerda a un sol front d'esquerda quan s'augmenta el contingut d'humitat en el substrat d'un 0% a un 0.33% o un 1.25%. El mateix efecte té lloc pels dos adhesius. Per altra banda, la tenacitat a la fractura s'incrementa amb la temperatura, això succeeix amb provetes envellides per un procés d'acondicionament que posteriorment han sigut assajades a 80ºC i a 120ºC. L'increment de la ductilitat de la matriu és una possible explicació d'aquest efecte.

Chapter1

Introduction

1.1 Background

Adhesive bonding has gained lots of popularity during the last decades due to the many advantages that it offers when compared to classical mechanical fastening techniques, such as welding, riveting or bolting. In fact, adhesive bonding has found application in various areas such as aeronautics, electronics, automobile and even sports and construction also. The application of adhesive bonded joints in structural components made of fibre-reinforced composites has been increased significantly in the recent years because of lightweight. Adhesive bonding offers ease fabrication, improved fatigue performance, potential reductions in life-cycle maintenance costs, and also allows for greater flexibility in design.

In recent years, the use of composite materials in the aeronautic, automotive, marine construction, etc. has increased significantly. Hence, there is an increasing need for repair technologies on primary structural components, as replacing them by a new component is not cost effective in many cases (Armstrong et al. 2005). The application of bonded repairs in composite components is well established and spread in the aeronautical industry, especially for minor accidental damages during the operational life of the aircraft. The frequency of minor accidental damages during the operational life of the aircraft is high and their repair operations have a significant impact on the maintenance costs. Severe damages, if less frequent, have also an important influence on the maintenance costs, because they might imply to stop the normal aircraft operation and require costly and time-consuming repairs. Figure 1.1 shows the on-site structural repair of aeroplane.

Figure 1.1 On-site structural repair of an aeroplane

Common damage can arise from accidental impacts, mechanical factors, environmental factors, etc. (Cheng et al. 2011). The main environmental factors to be taken into account are moisture absorption and temperature, as they can affect the strength of the composite structure. After several years of service, a composite component will normally contain a significant amount of moisture. The amount of moisture absorption depends mainly on the exposure condition, the material type, etc. Material qualification includes extensive determination of the detrimental effect of moisture, and temperature and Environmental Know Down Factors (EKDF) are derived and applied in the design phase. But moisture is not only affecting the mechanical performance of the component: in composite bonded joints, especially in those used for repairs, the amount of moisture absorbed in the adherend, called as pre-bond moisture, might have an influence on the final performance of the joint. Thus, the usual repair procedure is to avoid the uncertainty caused by the effect of moisture by drying the structure before the bonded repair is made. The drying process is long and can take several days even for thin skins, moreover when the skins have to be conservatively assumed to be fully saturated with moisture, as it is the case for in-service repairs. The time to dry increases the repair costs dramatically, not only because of the energy wasted in the process, but also due to the lost revenue during this extended repair time. The current trends in aircraft operations are showing an increasing demand for lower operational and maintenance costs. Practically, this translates into aircrafts with longer design lives, with longer inspection intervals, shorter inspection downtimes and shorter maintenance procedures.

Different trends in the mechanical performance of the composite bonded joins are observed with respect to the moisture content level and the adhesive material. Adhesive

selection includes many factors such as adhesive application, type and nature of adherend to be bonded, cure temperature, expected environmental conditions and the stresses that the joint will face during the service. So, for repair joints it is important to perform a careful selection of the adhesive material, keeping in mind the environmental conditions at which the composite structure will face in service. Research is needed to establish whether the effect of pre-bond moisture on repair joints is always detrimental or whether some small percentage of water absorbed in a composite could be tolerated.

1.2 Objective and tasks

The main objective of this work is the analysis of the effect of pre-bond moisture on the fracture toughness of bonded joints under the mode I static and fatigue loading. Taking into consideration this objective, the work has been divided in the following tasks:

1) Investigation of the effect of pre-bond moisture on the fracture toughness of carbon/epoxy composite bonded joints under mode I static load at room temperature. An analysis of the compatibility between different adhesive materials is also performed.

2) Analysis of the effect of pre-bond moisture and post-bond moisture and temperature on the fracture toughness of bonded joints. The same specimen configurations as in task 1 have been considered in this part of the work, but in this case the co-bonded specimens have been wet conditioned and then tested at 80ºC and 120ºC.

3) Design, definition of a test procedure and validation of a multi-fatigue test device for testing multiple specimens at the same time under mode I fatigue loading.

4) Analysis of the pre-bond moisture effects on the fatigue behaviour of adhesive bonded joints for repairs. The device developed in task 3 has been used to perform the fatigue tests.

1.3 Thesis Layout

The thesis consists of seven chapters:

Chapter 1, this chapter, starts with the introduction and the objectives of the work.

Chapter 2 includes a complete state of the art about the effects of moisture and temperature on the performance of bonded joints. The chapter begins with a review about the effects of the environmental factors on bonded joints under different loading conditions. The review continues with a description of the failure modes that are observed in the bonded joints for repairs. And finally, it includes a detailed review of pre-bond moisture effects on static and fatigue loading of bonded joints.

Chapter 3 includes an experimental study of the effect of pre-bond moisture on the fracture toughness at room temperature of adhesive joints under mode I static loading. Three levels of pre-bond moisture are considered: 0%, 0.33% and 1.25%. Apart from that, the study includes a comparative analysis of two adhesive films (F1, F2) used in the repairs. The analysis is performed with the results of static tests and it is followed by a fracture surface analysis using Scanning Electron Microscopy (SEM) and Optical Microscopy (OM) in order to understand the failure mechanisms involved.

Chapter 4 analyses the same materials but at higher test temperatures. Double Cantilever Beam specimens of bonded joints in moisture saturated conditions are tested under mode I loading at 80ºC and 120ºC. An optical microscopy study is performed in order to understand the failure mechanisms.

Chapter 5 describes the design of a multi-fatigue test set up in order to reduce the fatigue testing times. The test set up is used for testing 6 specimens at the same time under mode I DCB fatigue loading. The system also allows to test at different energy release rate percentages and at different load ratios.

Chapter 6 uses the device designed in chapter 5 to study the effect of pre-bond moisture under fatigue loading. Onset and crack growth rate curves are constructed from specimens tested at different energy ratios from 90% to 40%. The compliance calibration method is used to measure the crack length.

The main outcomes and conclusions of the present study are summarized in chapter 7, which also includes a section of future work.

Chapter 2

State of the Art: Adhesive joints between composite materials for structural repairs

2.1 Introduction

As previously stated in chapter 1, the objective of this thesis is the analysis of the effects of the pre-bond moisture in adhesive bonded joints between composite materials for structural repairs. This analysis has been conducted experimentally under static and fatigue loads.

To put the reader in context, a review of the already published work on bonded joints for structural repairs is presented in this chapter. The work is focused on joints between composite materials made with an adhesive or a resin film layer.

The chapter begins with an introduction about the aspects that affect to the performance of the adhesive joints between composite materials, and a general description about bonded joints for repairs. Then, it enters in detail on the effect of the environmental factors and the configuration of the joint on the value of the fracture toughness. Following, there is a description of the failure modes. And finally, a review of the effect of pre-bond moisture on the static and fatigue strength of adhesive joints is included.

2.2 Parameters that affect to the performance of the bonded joint

The application of adhesive bonded joints in structural components made of fibre-reinforced composites has increased significantly in the recent years. This is due to the many advantages over other joining methods such as welding, riveting or bolting. Some of these advantages rely on the high strength/weight ratio, uniformly load transfer through adhesive between the composites, design flexibility, lower fabrication cost and ease of fabrication. However, there are many parameters that have high influence on the performance of the joint. Therefore, aspects like composite bonding methods, surface preparation, adhesive and adherend types, bond line thickness, stacking sequence, curing temperature, surface ply angle, fillet and environmental conditions, must be taken into account during the production process. Examples of studies of the influence of these parameters are provided in references (Matthews et al. 1985, Parker et al. 1983,

Kanerva et al. 2013, Abdelaziz et al. 2006, Song et al. 2010, Kim et al. 2006, Marzi et al. 2011, Zhang et al. 2009, Markatos et al. 2013, Banea et al. 2008).

The bonding method is the most important aspect to take into account when manufacturing a bonded joint. Most of the other parameters depend on it, e.g., the failure process, the failure mode and the joint strength are all influenced by the bonding method (Song et al. 2010, Kim et al. 2006, Markatos et al. 2013).

Composite structures can have bonded joints fabricated by three different processes: secondary bonding, co-bonding and co-curing. Secondary bonding uses a layer of adhesive to bond two pre-cured composite parts. Thus, this type is most similar to metal bonded joints in structural behavior and fabrication method. Co-curing is a process wherein two parts are simultaneously cured. The interface between the two parts may or may not have an adhesive layer. In the co-bonding process one of the detail parts is pre-cured with the mating part being cured simultaneously with the adhesive (Composite material handbook, 2002) A schema of each of these manufacturing processes is shown in figure 2.1. Co-bonding process is the most common process for the repair of composite structures, because in the repair scenario one of the adherends is already cured (the component to be repaired). Repairs by secondary bonding can be also applied. Whatever the manufacturing process, they can be done in an autoclave or out-of-autoclave. For high performance components the curing in autoclave is preferred (high pressures and temperatures), however this is an expensive process and it cannot be used for repairs in-service conditions.

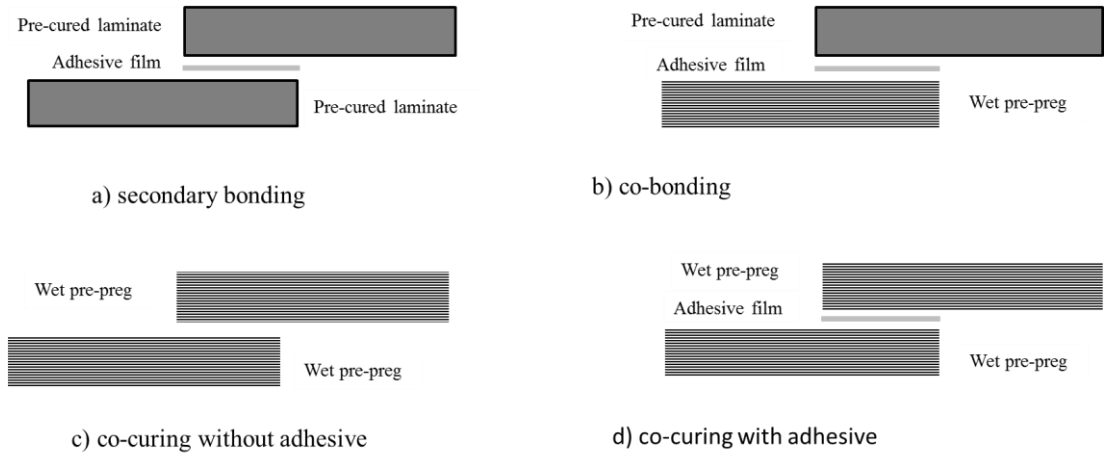

Figure 2.1 Schema of the most common manufacturing bonding processes between composite materials

Surface preparation plays also a very important role and it is directly related to the quality of the bonded joint (Baldan, 2004). This is particularly important in secondary and co-bonding processes. In order to get a strong and durable joint between two different adherends, a surface treatment is necessary prior to bonding. These surface treatments mainly aim to improve specific parameters, such as roughness (Harris et al. 1999), chemical modification (Shanahan et al. 1996), surface free energy (Koh, 2001), etc. To this aim, many different surface treatments are available. From all the available surface treatments techniques, some act through surface roughening such as sanding, grit blasting (Harris et al. 1999), solvent etching (Roizard et al. 2002), plasma (Shanahan et al. 1996, Kim et al. 2002) while others, mainly modify the chemical composition of the surface, such as laser (Crichtlow et al. 1997) or corona discharge (Comyn et al. 1996). Furthermore, owing to its low cost and eases to use, peel ply treatment is one of the most widely spread surface treatments in the composite industry. Peel ply can protect the adhesion surface, during the transport and manufacturing, from environmental degradation (dirt, dust); also it creates a surface roughness pattern and, when removed, leaves a clean surface which leads to the higher strength of adhesive joints (Kanerva et al. 2013, Benard et al. 2005). Figure 2.2 shows the surface roughness pattern on the adherend surface after removing a peel ply. The texture of the peel ply controls the roughness pattern, and the surface is clean and chemically active.

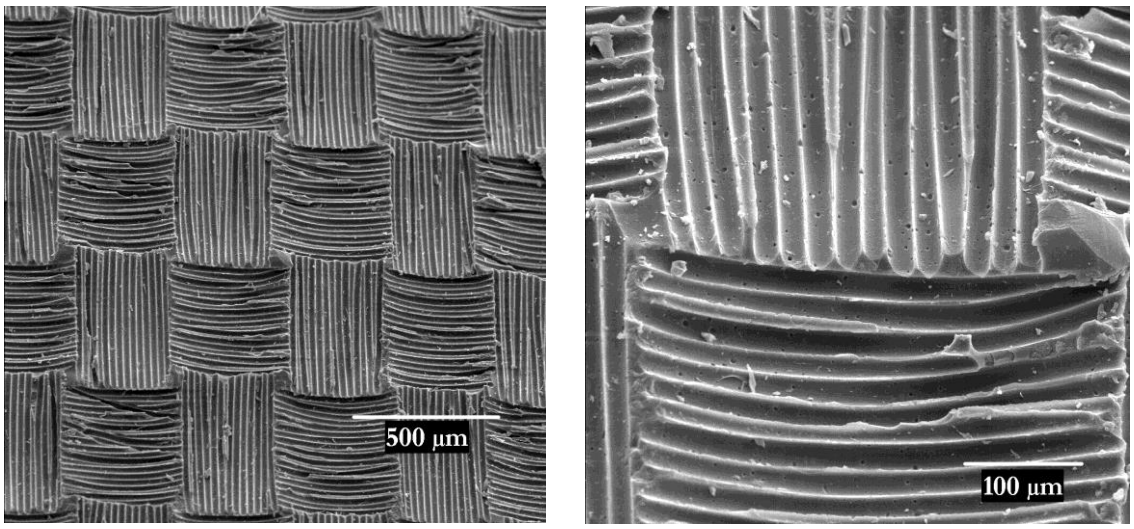

a) Adherend surface at 50x b) Adherend surface at 200x

Figure 2.2 Images of a composite adherend surface after removing a peel ply (Renart 2010).

In relation to the materials, it is well known that the proper selection of the adhesive is necessary for a good joint. There are a wide variety of available adhesive options. And a lot of factors that must be taken into account such as, adhesive application, type and nature of adherend to be bonded, cure temperature, expected environment condition and the stresses that the joint will face during the service. In addition, the bond-line thickness has a significant influence on the static and fatigue behaviour of bonded joints (Sela et al. 1989, Kawashita et al. 2008, Azari et al. 2011, Gefu et al. 2010, Mall et al.1989). It should be optimised in order to get a higher strength. Most researchers found out that a range between 0.2-0.4 mm gives the highest strength. Some other authors reported that the bond thickness should be about 0.125-0.25 mm.

With regards to the adherends, the stacking sequence has a great influence on the fracture properties of bonded joints in composite laminates (Matthews et al. 1985). Cheng (Cheng et al. 2011) found that the failure process of the parent laminate depends on the arrangement of the plies in the patch material. The last but not the least, the joint configuration is also an important part of bond design. A wide variety of joints are available for the designer as discussed by Adams and Wake (Adams et al. 1984). Generally, the joint configurations that have been analysed in the literature are single lap, double lap, step, scarf and butt joints.

With ease fabrication, flexibility in design and wide variety of joint configurations, bonded joints invoke for the repair of damaged composite structures. To improve the performance of a composite bonded repair, one has to take into account various factors such as the material system (patch material and adhesive), surface preparation and curing conditions (temperature, pressure, in or out-of-autoclave) (Caminero et al. 2013, Whittingham et al. 2009). When selecting the material for the preparation of the adhesive joint, it has to be taken into account that the repair will be made in service condition, in other words: out-of-autoclave and in environmental conditions far from the ideal ones.

2.3 Joints for structural repairs

Due to the widespread use of composite components in sectors such as aerospace, automotive or construction there is an increasing need for repair technologies on primary structural components. Common damage arises from accidental impacts, bird strike, hail-stones, lightning strike, etc. (Cheng et al. 2011, Hu et al. 2000). If the

material damage is not extensive, structural repair is the best solution as replacing the entire component is not cost-effective in many cases (Armstrong et al. 2005). However, it is required to follow an exhaustive process to validate the repaired component, and if the component does not fulfil the structural requirements it has to be replaced by a new one. Figure 2.3 summarizes the principal steps to follow for the repair of a damaged structure or component.

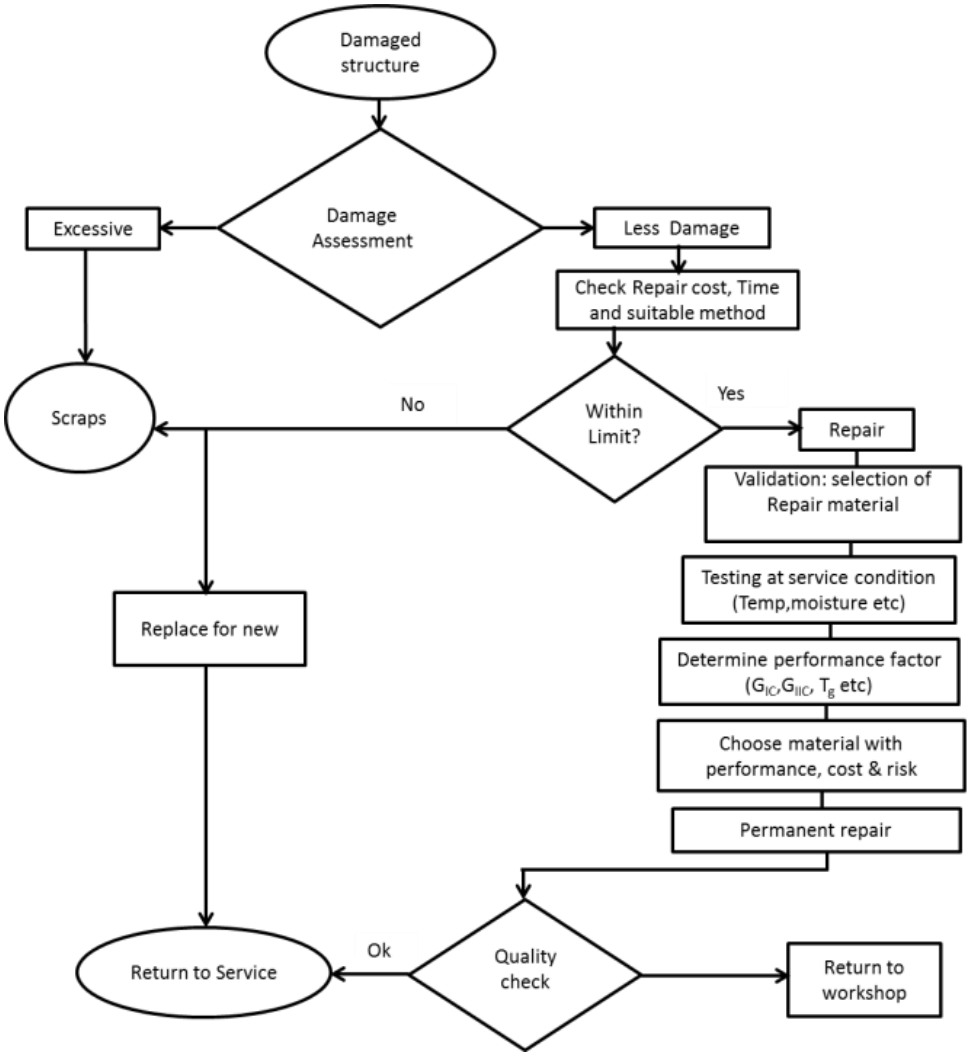

Figure 2.3 Flow chart for the repair of a damaged structure made of composite. The repair is performed with a bonded joint.

There are different bonded repair methods available but patch repairs is the more widely used (Hu et al. 2000). The bonded patch repair method is cost effective and highly damage tolerant in comparison with other conventional repairs made with mechanical fasteners (Cheng et al. 2011). The most common types of repairs carried out with a composite material in aerospace industries are the external bonded patch and the scarf

or stepped joints (Soutic et al. 1997, Found et al. 1995). The performance and quality of the repaired structure using adhesive bonding depends on a certain number of factors such as patch material, adhesive material, bonding method, controlled curing condition and environment conditions (Caminero et al. 2013, Whittingham et al. 2009, Charalambides et al. 1998). Moreover, the time required to fabricate and consolidate a repair patch, which is directly related to the aircraft downtime, will have a significant impact on the associated economical and operational aspects (Wood, 2008).

In order to assure the structural integrity of a repair the following aspects must be considered:

1) Loading conditions: definition of static and fatigue loads, service environmental conditions and thermal stresses. The repair must able to withstand the design limit loads.
2) Failure mode: the type of damage, location and mechanics for growth must be identified.
3) Damage parameters: calculation of parameters such as the stress intensity factor or energy fracture toughness that are used to predict damage growth rates for a given service load and under a certain environment.
4) Test data: Validate the damage growth rates observed in testing with the damage parameter and structural test data for representative repair specimens.
5) Inspection methods: inspection methods must be qualified to ensure that they can detect the damage and that the inspections are conducted often enough to prevent failure.

It is thus essential to have robust, reliable and repeatable structural bonded repair procedures to restore the damage in a composite component. The design should ideally ensure that the strength of the bonded repair is higher than the un-notched strength of the parent adherend so that failure occurs in the parent adherend before the bonded patch fails.

2.4 Environmental factors

Composite structures in service experience environmental threats that are are related to the effect of temperature and moisture absorption. As stated by Vodicka (Vodicka et al. 1997), the environmental factors can change the properties of a composite material, which leads to an effect on the mechanical performance of the joint, which will depend

on various of factors, e.g. specific adherend material used, type of adhesive, exposure conditions (temperature, humidity), exposure time and adherend thickness (Wright et al. 1981).

2.4.1 Effect of post-bond moisture absorption

Composite structures are exposed to different environmental conditions during their service lifetime that can promote the absorption of moisture. The amount of moisture absorbed will depend on the environment and on the polymer acting as composite matrix. It is well known that most of polymeric composites absorb moisture to some extent and their absorption rates and saturation levels are different from each other (Heung et al. 2010, Ameli et al. 2011). Most polymers will absorb atmospheric moisture (the most hydrophilic of these, e.g. nylon, may absorb up to 15 % by weight of water, % w/w) (Choi et al. 2001). Carbon fibre reinforced epoxy composites will typically absorb 0.5-1.0 % w/w of atmospheric moisture. The degree of absorption depends on both matrix and fiber properties, decreasing substantially the absorption rate as the moisture content increases until a saturation point (Kohan et al. 1995).

In composite repairs made with bonded patches, moisture absorbed by the repaired part has been found to have a significant effect on the repair performance (Myhre et al. 1982). Some researchers (Benoit et al. 2012, Garg et al. 1985) observed that mode I delamination toughness (G_{IC}) increases slightly with increased moisture content and temperature, and this effect is most probably the result of matrix plasticisation. In the same direction, Selzer (Selzer et al. 1995) studied three materials (two thermosetting: EP and $EP_{mod,}$ and one thermoplastic: CF/PEEK) exposed to water at different temperatures. He found out that the fully saturated specimens with epoxy matrices exhibited higher values of G_{IC} than the dry specimens. This occurred because the epoxy matrix became soft with the moisture absorption, and the fiber-matrix adhesion poorer, while for the thermoplastic material CF/PEEK the G_{IC} values were not affected by moisture.

On the other hand, the work of Parker (Parker et al. 1983) stated that the strength of CFRP-CFRP joints is degraded under the effect of absorbed moisture, and this reduction is dependent on both the adhesive and the composite adherends. Kinloch (Kinloch et al. 1983) suggested a wide range of degradation mechanisms, including plasticization, hydration, micro cracking of the polymer and fiber-matrix weakening in composite

joints. While Asp (Asp et al. 1998) noticed that, the strain energy release rate in pure mode I is unaffected by changes in moisture content but increases slightly at an elevated temperature.

In pure mode II, most of the authors (Benoit et al. 2012, Selzer et al. 1995, Asp et al. 1998) found out a decreasing trend of the critical strain energy release rate with the moisture content. Selzer (Selzer et al. 1995) studied the moisture effect on three different joint configurations and all of them showed a decrease on G_{IIC} values with an increase of the moisture content. The reduction of the mode II fracture toughness, G_{IIC}, was a result of the weakening of the fiber/matrix interface.

2.4.2 Pre-bond moisture effects

In spite of the fact that structural design procedures take into account the detrimental effect of moisture on the mechanical properties of CFRP, its effect on repairs to damaged structures is unclear. In previously published works, it has been claimed that the presence of absorbed moisture in the adherend may be regarded as essentially the same as pre-bond moisture absorbed by the fresh adhesive; since it will diffuse from the laminate into the adhesive during the heat and cure cycle (Blackman et al.2008).

Few studies have reported on the pre-bond moisture effect on the mechanical properties of the adhesive joints, although most of them found that the presence of moisture in the composite lead to the reduction in joint strength (Blackman et al.2008, Parker 1986, Parker 1989, Armstrong 1996). Sage and Parker (Parker 1986, Sage et al. 1982), attributed the decrease in G_{IC} to voiding, plasticization of the adhesive and a reduction in the interfacial adhesion. Drying the composite substrates before curing the bonded joints was found to prevent the occurrence of voids (Parker 1983). But, for higher moisture contents, drying the specimens at higher temperatures induced a blistering problem (Myhre et al. 1982). A small percentage of pre-bond moisture appears to have no effect and, in some cases, even a positive influence on the fracture toughness. This trend is observed in some adherend-adhesive combinations as illustrated in figure 2.4. For the IM7/977 substrate, there is a small increase on the values of G_{IC} for small percentages of pre-bond moisture (Blackman et al. 2008).

A small amount of pre-bond moisture (0.5% w/w) appears to have little effect on the strength of the repair. However, large amounts of pre-bond moisture, up to 1.3% w/w causes a decrease in the tensile strength. In order to support this idea some results for

certain adhesive joints have been published, claiming that as the moisture level increases, the bond strength increases to some extend too (Parker 1983, Garg et al. 1985, Selzer et al. 1995, Armstrong 1996, Robson et al. 1994, Gao et al. 2001). Matrix ductility (Garg et al. 1985, Asp et al. 1998, Selzer et al.1997), phase separation of the toughening rubber phase (Parker 1983), or an increase of the fibre bridging (Kinloch 1983), are the possible reasons for this increase in the mode I fracture toughness, G_{IC}.

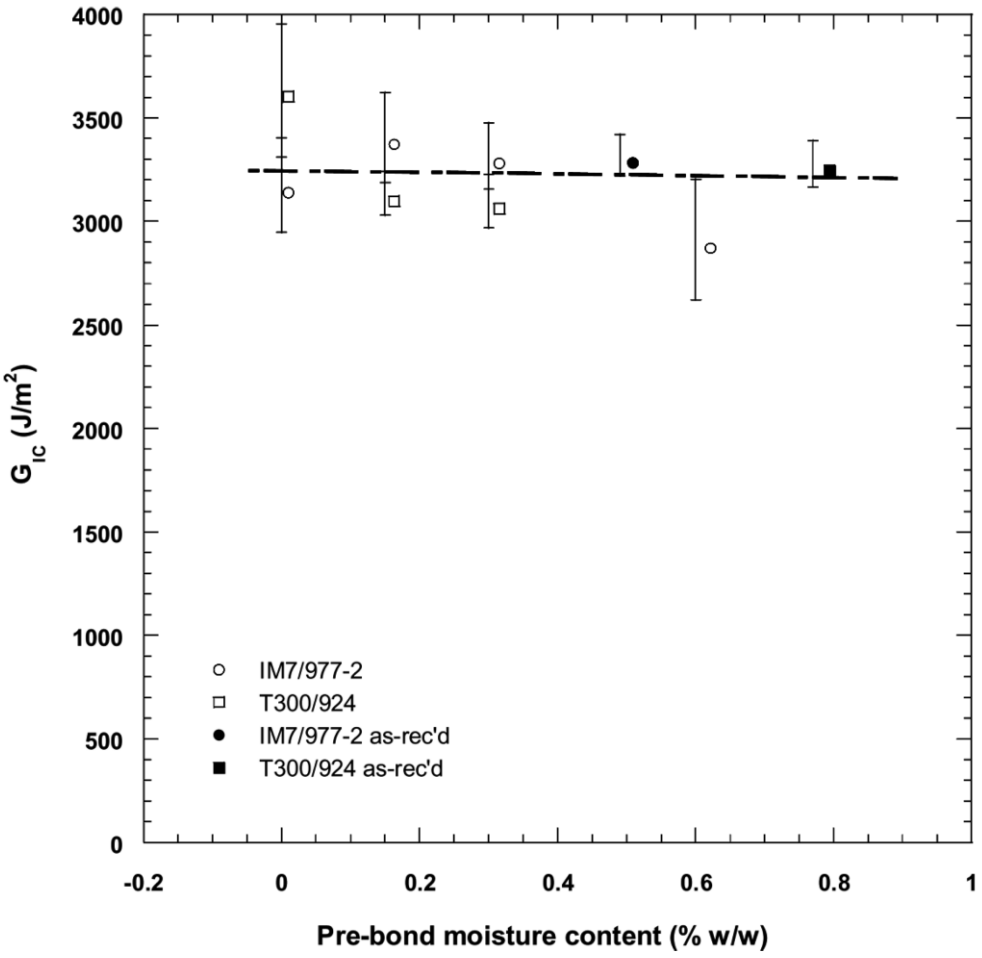

Figure 2.4 Values of G_{IC} against pre-bond moisture content for joints bonded with FM73M adhesive. Data is shown for both T300/924 and IM7/977-2 substrates. (Data points are the mean and error bars the standard deviation of three repeat tests at each condition) (Blackman et al. 2008).

One more possible explanation of this positive effect is that a certain level of embedded moisture may improve the mechanical properties of composites by relieving thermal stresses (Davidson et al. 2009). They are generated by the differences between the thermal expansion coefficients of the fiber and the resin as the matrix cools from the

curing temperature. In the same way, Armstrong (Armstrong, 1986) noticed a positive increase of the fracture energy of bonded joints manufactured with Hysol EA 9394. The energy fracture toughness obtained from specimens first immersed and then dried for a short period of time was higher than in specimens dried by a large amount. The work suggests that, for this adhesive, a small amount of moisture improves the fracture toughness of the bonded joint.

On the contrary, for other adhesives, there is no evidence of a significant change when there is an increase of the pre-bond moisture content up to a certain level; and above this level G_{IC} decreases (Found et al. 1995, Parker 1986, Robson et al. 1994, Selzer et al. 1997, Davidson et al. 2009). Robson (Robson et al, 1994) observed that the flexural strength of the repair joint appears to be unaffected by the pre-bond moisture level. In another work, Parker (Parker, 1986) noticed that strength was adversely affected by the presence of pre-bond moisture in the laminate for three adhesives cured at 120°C. However, the effect on joints cured at 175°C was very small.

From the previously works it can be concluded that, there is no single theory or model with sufficient experimental support to explain the generalized relation between pre-bond moisture and the mechanical properties of joints.

2.4.3 Effect of the temperature

In the last years, there has been a growing requirement, particularly in the aeronautic industry, for the adhesives to withstand high temperatures. It has generally been found that there is an increase in the mode I fracture toughness, G_{IC}, with increasing temperature as shown in figure 2.5 (Garg et al. 1985, Kinloch 1983, Davidson et al. 2009, Akay et al. 1997, Hutapea et al. 1999, Kevin et al. 1997, Thunga et al. 2011, Banea et al. 2011, Aschroft et al. 2001, Kim et al. 2004). An increase of the matrix ductility is the most common explanation for this improvement in the fracture toughness. An increment in the amount of fiber bridging and fiber breakage (Garg et al. 1985, Kinloch et al. 1983, Davidson et al. 2009, Hutapea et al. 1999, Thunga et al. 2011, Coronado et al. 2012) is another explanation. Garg and Ishai (Garg et al. 1985) found an increment of 20% in G_{IC} when testing T300/934 composite specimens in a temperature range from 25°C to 125°C. They stated that it was provoked by the increase in ductility of the matrix. In another work (Hashemi et al. 1990), an improvement up to

80% of the propagation values of G_{IC} was observed in carbon/PEEK specimens, when the temperature was increased from -20°C to 130°C.

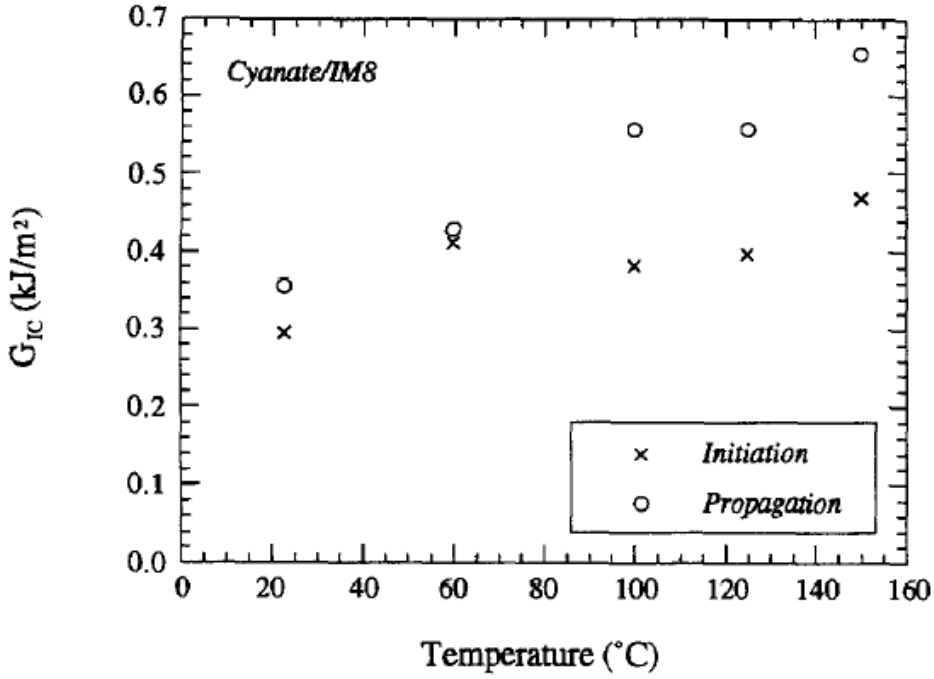

Figure 2.5 Mode I toughness for [0_8/90/0_8] cynate/IM_8 (Kevin et al. 1997).

In very few studies the authors found a different trend. Russel and Street (Russell et al. 1985) found that the initiation values of G_{IC} decreased slightly with an increment of the temperature from -50°C to 100°C, but the propagation values increased with the temperature. The tests were conducted with AS1/3501-6 composite specimens. They suggested that the decrease was likely related to both the residual stress state in the matrix around the fibers and to the fibres constraining the size of the adhesive. Hutapea and Banea (Thunga et al. 2011, Banea et al. 2011) found that if the test temperature is above the T_g, the fracture toughness decreases due to the loss of adhesion between the fibers and the matrix, but below the T_g they obtained an increase in $G_{IC.}$ Melcher and Johnson (Melcher et al. 2007) determined the mode I fracture toughness of an adhesively bonded composite-composite joint under a cryogenic environment. They observed a substantial decrease in the fracture toughness at cryogenic temperatures compared to the tests performed at room temperature.

Pure mode II tests, however, do not exhibit the same trend (Kinloch et al. 1983, Davidson et al. 2009, Kevin et al. 1997). Most of the authors (Cheng et al 2011, Russell et al. 1985) have found a dependence of G_{IIC} with the temperature, but in this case G_{IIC} decreases with the increasing temperature. Kawashaki (Kawashaki et al. 2008) found

that a degradation of the fiber/matrix bond takes place when the temperature increases; this mechanism is responsible for the reduction of the fracture toughness. The effects of temperature on the mode II delamination toughness of CFRP are more limited than in mode I fracture tests. Another work, in which IM8/ITA composite was studied, revealed the same trend for the temperature range from 20°C to 180°C (Cowley et al. 1997). Scanning electron microscopy revealed essentially the same fracture surface over the range of temperatures from -30°C to 120°C, when G_{IIC} decreased (Davis et al. 1987). Chapman (Chapman et al. 1987) found no effect of temperature on G_{IIC} from -50°C to 100°C, but a 20% decrease in G_{IIC} from 100°C to 150°C, which was attributed to have exceeded the material glass transition temperature.

Very few results for the I-II mixed mode behaviour have been published and they are from the same authors that have studied mode I and II. Besides, there is not a clear consensus about the benefits or disadvantages of the temperature on the value of Gc. Russell (Russell et al. 1985) found that the mixed mode initiation toughness values of composite AS1/3501-6 decreased with increasing temperature; having a larger reduction of the total critical energy release rate, Gc, when the ratio of G_{II}/G became higher. On the contrary Hashemi (Hashemi et al. 1990) observed that in propagation toughness of AS4/PEEK at a mixed mode ratio of $G_{II}/G = 0.4$ there was an increment of Gc with increasing temperature. The authors attributed it to an increase of the matrix ductility. And, in other studies (Asp et al. 1998) it was observed that in mixed mode there was no dependence on the temperature.

2.5 Failure Modes

Different failure modes may occur in a bonded composite joint. There are basically 3 main types of failure modes: adhesive failure (at the interface between the adhesive and the adherend), cohesive failure (in the adhesive), and substrate failure (inside one of the adherends) (Edward et al. 2007).

However, in bonded joints for structural applications, due to the materials involved in the joint or used to prepare the surfaces of the adherends, there are more interfaces prone to fail. Figure 2.6 shows the schema of two typical layups of co-bonded joints: one with a pre-cured wet peel-ply and another with a surface treatment resulting from dry peel-ply removal, sanding or grit blasting. In the first case another resin layer is introduced when the wet peel ply is removed from the pre-cured panel.

Therefore, six failure modes must be taken into account for the co-bonded adhesive joints; they are detailed in the internal testing protocol AITM1-0053 from Airbus. The failure modes are: i) inside the pre-cured adherend (delamination); ii) at the interface between the pre-cured panel and the peel ply resin; iii) at the peel-ply adhesive interface; iv) cohesive inside the adhesive; v) at the adhesive co-bonded panel interface (wet-wet interphase) and; vi) inside the co-bonded panel (delamination).

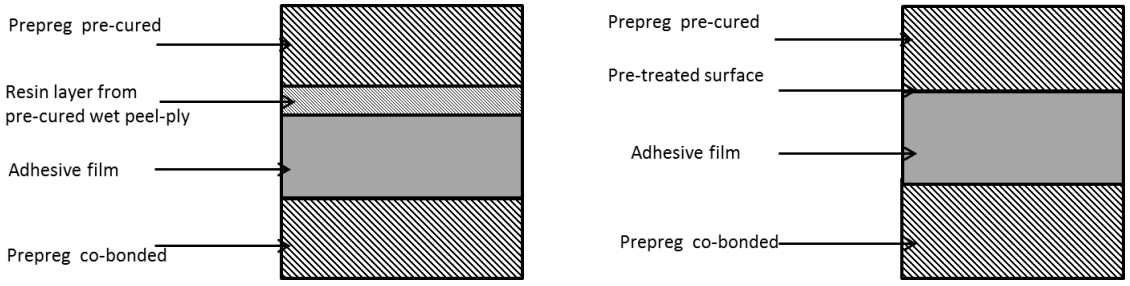

(a) (b)

Figure 2.6 Materials used in a co-bonded adhesive joint: (a) with removal of wet peel-ply (b) with removal of dry peel-ply, sanding or grit blasting.

Many researchers have experimentally investigated which parameters have an effect on the failure mode of composite bonded joints. It has been observed that the failure mode and the strength of the joint are influenced by a lot of variables such as bonding methods, moisture, temperature, type of adhesive, etc. The discussion that is presented next includes only the effects of moisture and temperature.

Temperature and moisture have a high influence on the failure mode of the bonded joint. It is well know that at lower temperature a stable brittle fracture process occurs, whereas at high temperature there is a stable ductile crack growth (Ashcroft et al. 2001). Parker (Parker et al. 1983, Parker et al. 1986) observed that the failure mode changed as the test temperature increased from 20°C to 80°C. The mode I fracture toughness, G_{IC}, increased for both dry and moisturized specimens when tested at a higher temperature, but for moisturized specimens tested at 100°C stick-slip behaviour was observed (Kinloch et al. 1983). Failure mode shifted from the cohesive zone to the adhesive layer with the increase of temperature and moisture content (Parker et al. 1986). Aschroft (Aschroft et al. 2001) noticed that, an increase of temperature caused a change in the locus of failure from predominantly delamination at -50°C to cohesive at 90°C.

The level of moisture content in the joints has an effect on the fracture toughness as well as on the failure mode (Parker et al. 1986, Parker et al. 1990, Armstrong et al. 1996).

Zhang (Zhang et al. 2009) found that in the presence of high levels of humidity the failure shifted from cohesive to an interfacial failure (between adhesive and adherend), which implies that the adhesive/composite interface was weaker than the fiber/matrix one. On the other hand, Hutapea (Hutapea et al. 1999) noticed that the crack grew mostly at the fiber-matrix interface; this behaviour leads to extensive fiber bridging which increase the energy needed to grow the crack.

Knight (Knight et al. 2012) observed that, after a hygrothermal aging conditioning, the failure mode progressed from cohesive to fiber tear (within the top plies of the adherend laminate). Robson (Robson et al. 1994) did not find any change in failure mode with the increase of pre-bond moisture, while Parker (Parker et al.1983) observed a different failure mode with the change of the adhesive. Inspection of the fractured surface revealed that the dry joints failed cohesively in the adhesive layer and that the crack path moved towards the interphase after conditioning (Armstrong 1996, Bowditch 1996). This work stated that joints between adherends with low levels of moisture can lead to a cohesive failure, but the mode of failure can vary depending on the adhesive used.

2.6 Static tests for the characterization of the properties of the adhesive joint

2.6.1 Static test

Double Cantilever Beam (DCB) test is the most widely used method for measuring mode I (opening) fracture toughness (Ashcroft et al. 2001, Blackman et al. 2003, Moura et al. 2008, Chen et al. 2010, ASTM D5528). This is a popular test because of the ease of sample manufacture and testing, coupled with a simple analysis methodology. First, Ripling (Ripling et al. 1964) and Mostovoy (Mostovoy et al. 1967) adapted the DCB test for investigating structural adhesives, and suggested a theory based on a built-in beam which neglected the contribution of the adhesive. Later workers (Ouezdou et al. 1988, Penado 1993, Olsson 1992) modelled the DCB as a beam on an elastic foundation in order to theoretically account for the contribution of the adhesive.

Double Cantilever Beam (DCB) test is widely used in aircraft industry as a peel test to characterize the quality of the adhesive joint between two composite adherends. The bond strength is quantified by means of a unique parameter, the energy fracture toughness (G_{IC}). The principal advantage of this test over other alternative tests is that it

allows testing bonded joints between two rigid adherends. It is routinely applied to any kind of bonded joints: secondary bonded, co-bonded or co-cured. In addition, the same test configuration is used to characterize bonded joints under cyclic loading.

The DCB test was formerly conceived for delamination in composites (ISO 15024, ASTM D5528). Although the scope of the American standard (ASTM D5528) includes the characterization of bonded joints, it does not introduce any refinement in the theory different from that of the delamination tests. In 2009, the International Standard Organization published a specific standard for bonded joints: ISO 25217. It was based on the British standard BS 7991 and the testing protocol developed by Blackman and Kinloch in 2001 (Blackman et al. 2001). But, the data reduction methods to obtain the energy fracture toughness (G_{IC}) are similar to those proposed in the delamination tests.

The DCB test consists of opening the adherends of the bonded joint to cause a propagation of an already existing crack in the specimen mid plane, see figure 2.7. The test is performed under controlled crosshead displacement. The displacement (δ), the load to open the specimen arms (P) and the crack length (a) are recorded during the test.

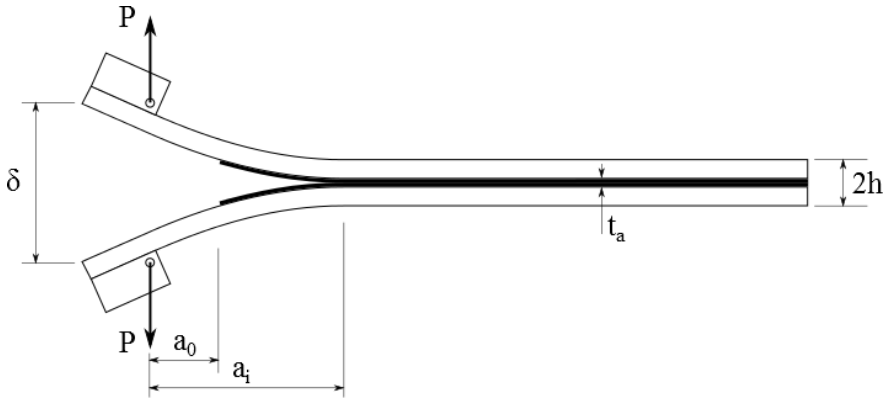

Figure 2.7 Schema of a DCB test of a bonded joint. t_a is the adhesive thickness and 2h the total thickness of the specimen.

The load and displacement are obtained directly from the test machine. The crack length should be obtained from visual observation at the specimen side. According to ISO 25217 the crack length shall be measured at every 1mm from 1 to 10 mm and from 60 to 65 mm, and at every 5 mm from 10 to 60 mm. An artificial crack is created at one of the ends of the specimen by means of the introduction of a Teflon insert in the adhesive mid-plane during the manufacturing. Due to the insert, the crack tip is blunt and does not represent the real shape of a defect that could be created, for example, during an

impact event. Therefore, a short propagation is performed in order to obtain a sharp tip (pre-crack). The propagation test is started from the pre-crack.

Two values of the fracture energy (G_{IC}) are determined: an initiation and a propagation value. Furthermore, there are several methods to determine the initiation values: NL, VIS or 5%/MAX (ISO 25217). Therefore, from each test initiation, values of G_{IC} from the pre-crack and, initiation and propagation values from the propagation test are measured, see figure 2.8.

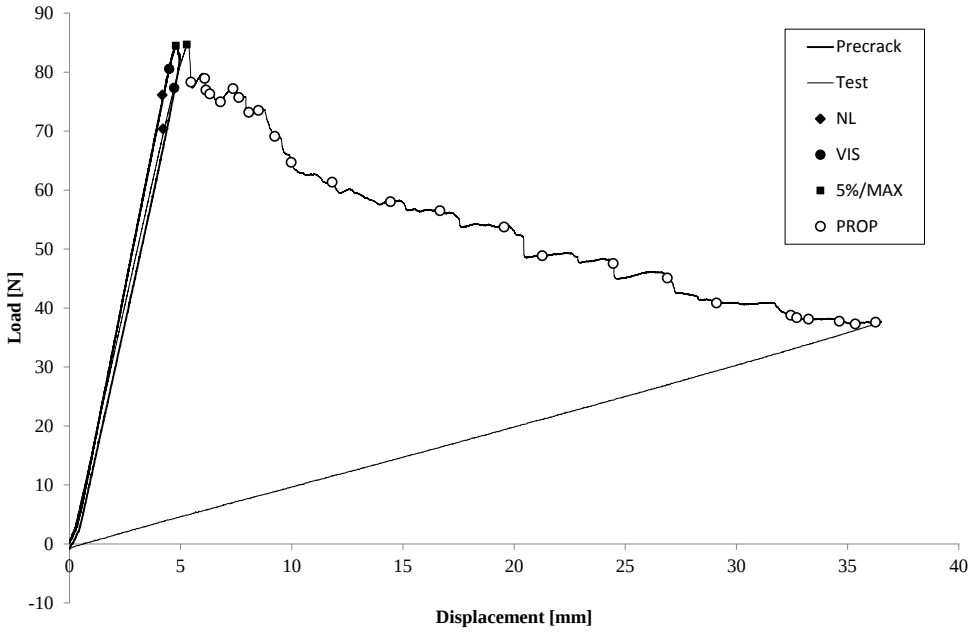

Figure 2.8 Load-displacement curves of a DCB test: pre-crack and propagation test curves including initiation (NL, VIS, 5%/MAX) and propagation (PROP) points.

Apart from this, there are several methods to calculate G_{IC}. All of them are based on the assumptions of Linear Elastic Fracture Mechanics (LEFM). In particular, from the Irwin Kies approach that relates the energy release rate (G_I) to the derivative of the compliance in function of the crack length (dC/da). Among them, it is of specific interest the Modified Beam Theory (MBT) because it is also used in fatigue tests. According to this method, the energy fracture toughness is determined by equation (2.1):

$$G_{IC} = \frac{3P\delta}{2B(a+\Delta)} \tag{2.1}$$

where δ is the total displacement of the specimen arms, P the load, B the specimen width, a the crack length and Δ a crack length correction parameter that is determined

from the linear regression of the cube root of the compliance ($C^{1/3}$) against the crack length (a), see figure 2.9.

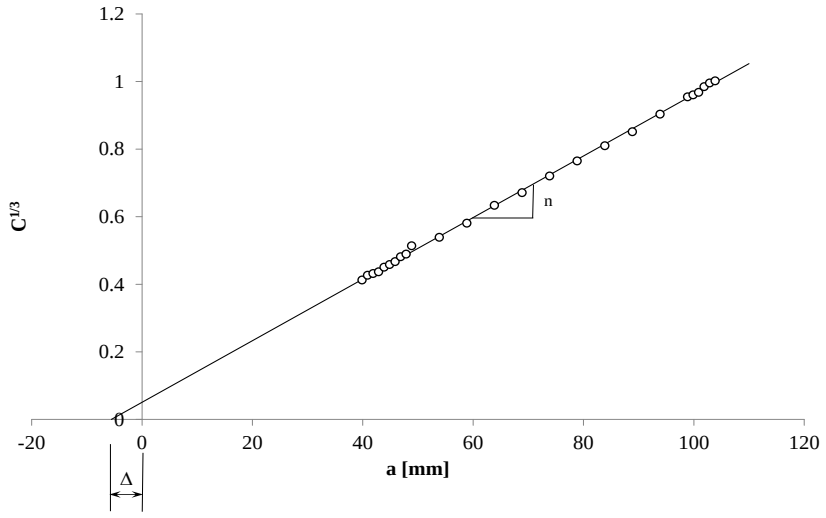

Figure 2.9 Linear regression curve to obtain the crack length correction factor Δ.

2.6.2 Stick-slip effects on adhesive joints

In many cases, when testing bonded joints in mode I, the crack growth does not grow continuously, but proceeds as a succession of rapid growth and arrest phases (Ashcroft et al. 2001). This is commonly referred to stick-slip growth. It can be identified easily by looking at the load-displacement curve, because when the rapid crack growth occurs there is a sudden drop in the force, see figure 2.10. During the arrest phases the load increases linearly according to the specimen stiffness. The stick-slip can occur sporadically in between stages of constant crack propagation (figure 2.10a) or during the entire propagation test (figure 2.10b).

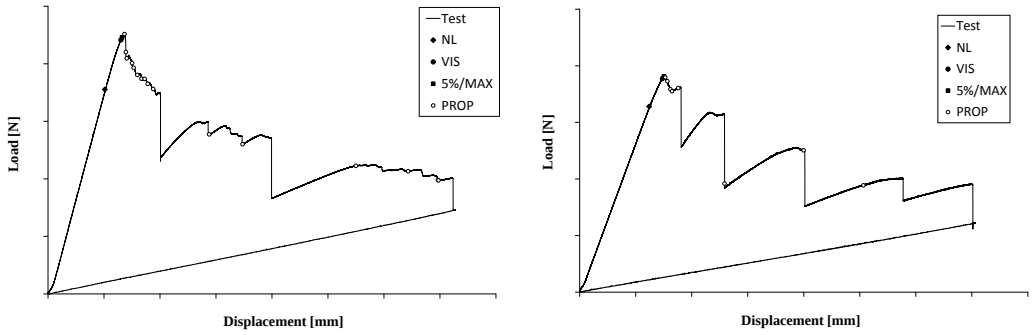

a) b)

Figure 2.10 Load displacement curves of DCB tests: a) continuous propagation with a few regions of stick slip, b) stick slip during the entire test.

The stick-slip propagation can be observed on the specimen fractured surfaces, see figure 2.11. The darker bands correspond to the zones of fast crack growth whereas the lighter zones correspond to constant propagation or arrest phases. If the stick-slip occurs during the entire propagation test, the amplitude of the arrest phases is small, few mm, compared to the size of the fast crack growth regions.

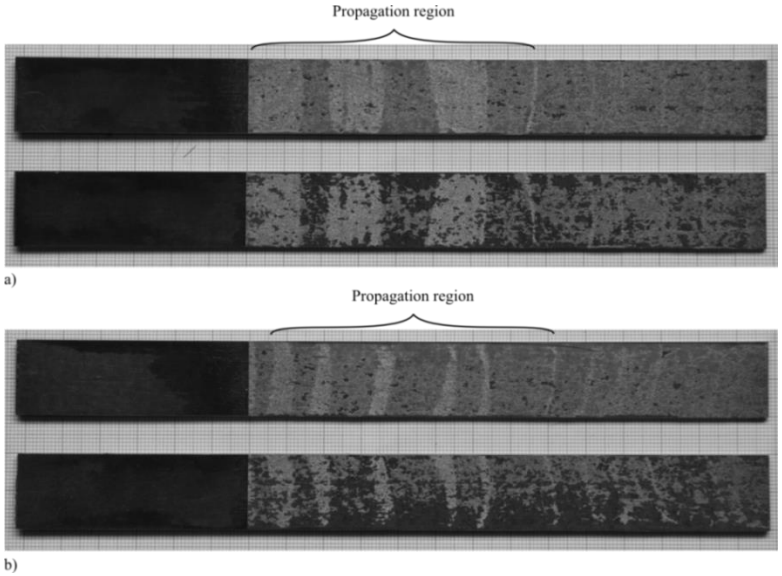

Figure 2.11 Fractured surface of: a) load-displacement curve of figure 2.10a, lighter bands correspond to zones of continuous crack growth; b) load-displacement curve of figure 2.10b, lighter bands correspond to arrest phases.

When stick-slip occurs, two values of the fracture energy are obtained, one from the initiation of the fast crack growth (G_{ICi}) and another from the arrest propagation points (G_{Ia}). Each of them corresponds to the local maximum and minimum peaks of the load-displacement curve. The initiation values are directly related to the bonded joint fracture properties. On the contrary, the arrest values include dynamic effects and should not be used for the assessment of the quality of the adhesive joint.

Standard ISO 25217 suggests the calculation of both initiation (G_{ICi}) and arrest (G_{Ia}) values with the Simple Beam Theory (SBT) method. The values of crack length to calculate G_{ICi} can be measured from the arrest bands of the fractured surface. However, in some cases, they are difficult to observe (i.e. bonded joints with a resin layer and woven fabric adherends). In this case it is preferable to video-record the crack front with an optical device during the test, and measure the value of the force and displacement at the initiation of fast crack propagation. An alternative and a simpler way to calculate G_{IC} is the area method. The fracture energy is obtained from the ratio between the area

under the load-displacement curve and the fractured surface (specimen width multiplied by the crack extension). This method has the advantage that the crack has to be measured only at the beginning and at the end of the propagation. However, in situations of crack growth with stick-slip behaviour, due to the jumps in the load-displacement curve, a region of the curve is underestimated, resulting in a conservative value of G_{IC}.

2.7 Fatigue loading

Fatigue loading is the major source of failure in which a structure can fail at a small percentage of the quasi-static strength. Therefore fatigue analysis and fatigue strength prediction are highly demanded in order to simulate the bonded joint. To reach an accurate prediction of the fatigue life of a component is a challenge, due to the complex nature of fatigue crack initiation and propagation, the geometry of the bonded joint and the material behaviour under loading and unloading regimes (Jen et al. 2012, Sarfaraz et al. 2011, Gao et al. 2011, Khalili et al. 2008).

Repair operations in composite aircraft structures should guarantee that the resulting parts maintain the structural integrity of the pristine component. This includes the static strength, damage tolerance and fatigue durability. The bonded joint between the structure and the patch is the most critical part of the repair and its fatigue behaviour has to be investigated. For fatigue damage two approaches have been used extensively: onset and crack growth tests.

2.7.1 Onset tests

The onset tests account for the initiation of the crack growth. A series of samples are tested at different load levels under a constant force or displacement amplitude, until the crack starts to propagate. At this point, the test is stopped, the number of cycles (N) measured, and the value of G_{Imax} estimated. A plot is made of G_{Imax} against the number of cycles. These curves are called onset curves and they have been adopted from the S-N or Whöler curves for fatigue in metals. A schematic onset curve is shown in figure 2.12.

A lower load level requires a higher number of cycles until the onset of propagation. In most cases, there is a level of energy release rate at which the crack does not propagate,

even for a large number of cycles. This value is the onset threshold (G_{Ith}). A load below this value is considered to have an infinite fatigue life.

In mode I fracture tests there are different methods to determine the number of cycles until the onset of propagation. The ASTM D6115 standard recommends 3 criteria: 2 based on the increment of the compliance in the specimen arms (1% and 5%) and a visual method (VIS).

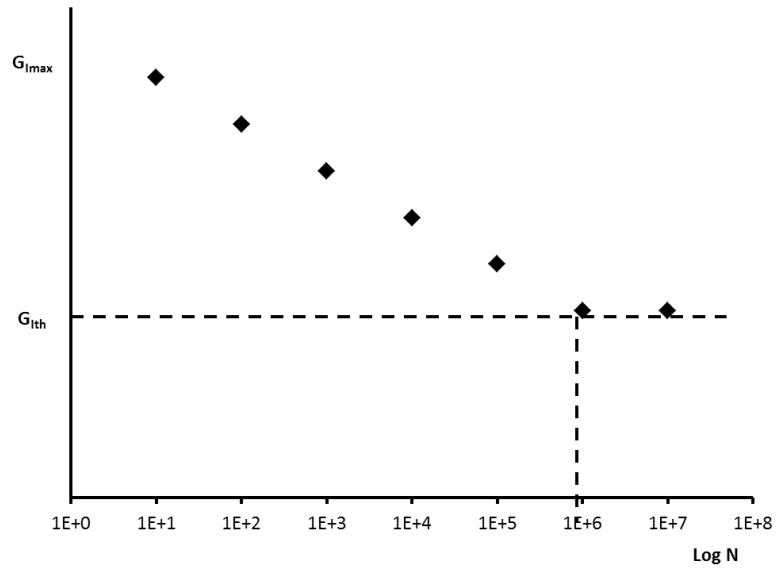

Figure 2.12 Onset curves of G_{Imax} against the number of cycles (N) represented in logarithmic scale. G_{Ith} is the onset threshold value.

The methods based on the compliance compare the actual value to the initial one obtained at N=1 cycles. When the compliance has increased a certain amount, 1% or 5%, it is considered that the crack has started to propagate. The normalized procedures require stopping the test periodically to carry out static tests on the linear zone of the material in order to evaluate the specimen compliance (Argüelles et al. 2008, Argüelles et al. 2011, Brunner et al. 2013). The accuracy on the determination of the onset point depends on the frequency of the stops, which makes the results of the compliance curve scattered.

An alternative method is by optical visualization of the onset of crack propagation (ASTM D6115, Arguelles et al. 2008). This method also requires the technician intervention or/and sophisticated devices to monitor the crack. Besides, it has been demonstrated that it does not predict the real position of the crack front inside the

specimen (Sans et al. 2013). Therefore, the method based on the compliance is the most extended among the authors (Arguelles et al. 2008, Vinciquerra et al. 2004).

In order to reduce the scattering of the results, new methods based on the real-time monitoring of the compliance have been developed (Renart et al. 2014). In this case, the compliance is recorded at every cycle, and a continuous curve of C against N is obtained. With this method, the increase in the compliance can be estimated with the precision of 1 cycle. Figure 2.13 shows the clear difference between the compliance calibration by the ASTM D6115 method and the real time monitoring of the compliance.

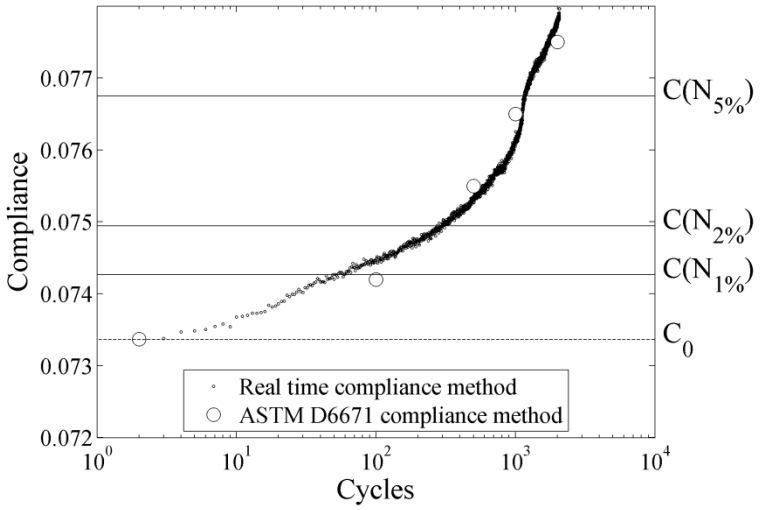

Figure 2.13 Compliance increase versus the number of cycles using the standard ASTM D6115 and real time compliance monitoring method.

To calculate the mode I energy release rate, the CBT (Corrected Beam Theory) data reduction method is used (ASTM D6115), like in the static tests. In this case, the value of G_{Imax} is obtained from the maximum force at cycle N = 1, because it is supposed that the crack does not propagate during the test.

2.7.2. Crack growth rate curves

The crack growth rate fatigue tests are used to measure the evolution of the size of a defect once it has started to propagate. In bonded joints and at a coupon level, a crack is propagated at the adhesive layer under a cyclic loading.

A common fatigue crack propagation curve is a logarithmic plot of the crack growth rate (da/dN) against the maximum strain energy release rate (G_{max}). The curve is defined

by the three regions, as shown in figure 2.14: a) threshold region, below which no crack advance takes place; b) a linear crack growth region, which is well described by the Paris law and; c) a fast crack growth region, where catastrophic failure takes place when the fracture toughness G_C is reached.

In order to construct the crack growth rate curve, the most important task is to monitor the crack growth during the fatigue test. Continuous monitoring of the crack requires an automatic measuring system. There are many methods which can be used to automatize the measurement of the crack front, e.g. strain gauges (Ogasawara et al. 2007), acoustic emission (Roberts et al. 2003), Digital Image Correlation (DIC) (Vanlanduit et al. 2009), Fiber Bragg Grating (FBG) sensors (Sans et al. 2013) and compliance based methods (Renart et al. 2014). Among them, the compliance based methods are the simplest ones, due to their applicability under various environmental conditions, easiness of implementation and economical cost.

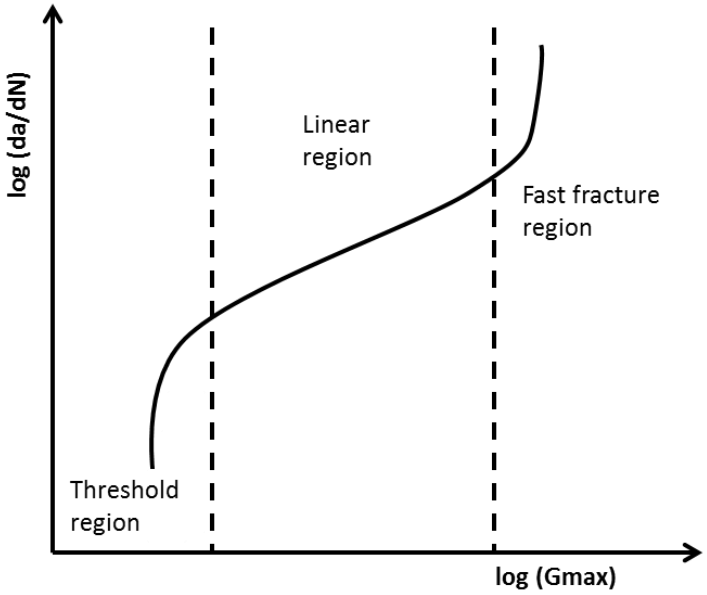

Figure 2.14 Fatigue crack propagation curve

Obtaining both the onset and crack growth rate curves requires long testing times and it is also labour intensive. The threshold limit is an important property of the material, and the number of cycles to reach it may be different depending on the material. In any case a large amount of cycles is required; and in most cases it is not clear when it stops or when it will stop. Like in onset tests, the threshold value is in most cases imposed by the

user. Generally 1 million to 10 million cycles are typical values to reach the threshold level (Rodrigo et al. 2009).

Even for the lower number of cycles, 1 million, it takes several days/weeks to test a batch of specimens at the typical frequency of 5 Hz. With increasing the test frequency the fatigue test period can be reduced. However, it provokes problems such as hysteric heating (Lang et al. 1987), or incorrect response of the involved materials (Johnson et al. 1989). These problems may be significant, especially in polymer materials. In metallic components, the test frequency can be increased without any effect on the results, but the behaviour of the organic matrix composite material is very sensitive to high frequencies. To test multiple specimens in a single station is an optimal solution, in order to reduce the fatigue time instead of increasing the frequency of the test.

2.7.3 Influence of environmental effects on fatigue tests

Environmental factors play an important role in predicting the fatigue life of the composite structure. The presence of aggressive environments (low or high temperature and/or high humidity levels) affects the behaviour of structural joints under fatigue. Knowledge about the material resistance to interlaminar fracture and fatigue is essential to establish design allowable and damage tolerance guidelines for structures.

It is known that moisture absorption results in varying degrees of plasticization, strength loss and increase of ductility of some epoxy adhesives. However, the effect of moisture on the fatigue and fracture properties of bonded joints employing these adhesives is still not fully understood. In addition, since adhesive joints are systems comprised by two adherends, an adhesive, and the interphase regions, the performance of all components may strongly affect to the performance of the joint as a whole. Thus, knowledge of the behavior of an adhesive joint exposed to various environments must be supplemented by knowledge of the behavior of the specific bonded systems.

An adhesive joint loses its strength and fatigue resistance when exposed to hostile environmental conditions such as high humidity and/or high temperature. Most of the works related to this topic (Degrieck et al. 2001, Ferreira et al. 2007, Johnson et al. 1998) noticed that the moisture absorbed by the composite, in general, has a negative influence on the fatigue life of the joint. Ferreira et al. (Ferreira et al. 2007) conducted a study comparing the fatigue resistance of glass fiber reinforced (GFR) thermoplastic composites. They used dry specimens and specimens immersed in water. They observed

that the fatigue strength and tensile static resistance of the specimens immersed in water were lower than the dry specimens. Johson and Butkus (Johnson et al. 1998) found that mode I fracture toughness and fatigue crack growth threshold were significantly reduced upon an exposure to a high temperature and high humidity aircraft service environment. Charalambides et al. (Charalambides et al. 1998) investigated the performance of carbon fiber/epoxy repair joints bonded using an epoxy film adhesive under static and fatigue loading. They immersed the repair joints in distilled water at 50°C for periods of up to 16 months, and they evaluated the effect of the hot/wet environment on the static and fatigue strengths. They found that fatigue behaviour of the repair joints was significantly lower to that of the parent material. Gao (Gao et al. 2001) conducted experimental and theoretical studies to determine the fatigue lifetime of anisotropic conductive adhesive films under different testing conditions, including hygrothermal aging and thermal cycling. They concluded that the fatigue lifetime decreased with increasing the hygrothermal aging time. Ashcroft (Ashcroft et al. 2000) investigated the effects of environments and fatigue loading on the performance of bonded composite joints. They found that adhesively bonded composite joints can be significantly affected by the service environments, depending on the joint type and the material used. A significant reduction in fatigue strength was observed when immersion time increased, and when the water temperature exceeded the glass transition temperature of the adhesive (Ferreira et al. 2002). Shaw and Liao (Shaw et al. 2001) studied unidirectional glass fiber reinforced and glass carbon fiber reinforced epoxy matrix composites under tension-tension fatigue in air and in distilled water at 25°C. Cycling loading in water resulted in a shorter fatigue life for both glass and hybrid samples when compared to the samples tested in air. Mosaki (Mosaki et al. 1989) investigated the moisture-conditioned specimens for a 914C laminate, and found out that the growth rate in water was 300 times faster than that for specimens with prior immersion. The threshold value was reduced to about 65%.

Increasing the aging times accelerates the degradation of the threshold values, and this is related to the loss of the rubber toughening mechanism as shown in figure 2.15.

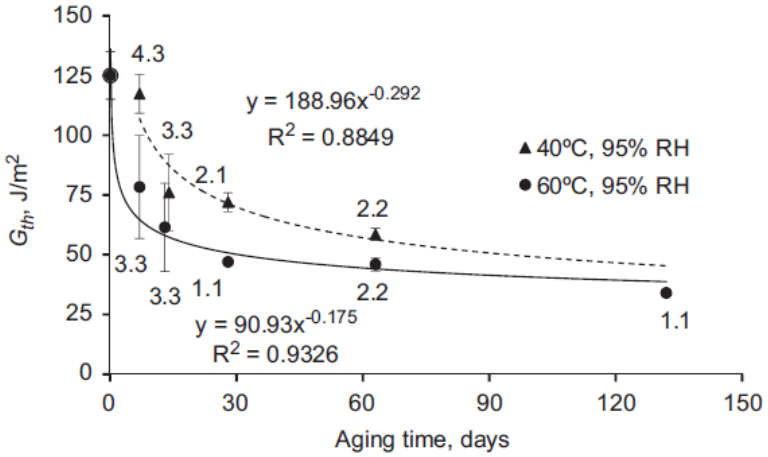

Figure 2.15 Fatigue threshold vs. aging time for specimens aged under 40°C-95% RH and 60°C-95% RH environments (Datla et al. 2011).

The effect of temperature on the fatigue performance of bonded joints has been studied also by some authors. Ashcroft and Shaw (Ashcroft et al. 2002) compared the results of quasi-static and fatigue tests in un-cracked lap joints. They conducted the tests on epoxy bonded CFRP joints at -50°C, 22°C and 90°C. They pointed out that temperature has a significant effect on the locus of failure, and that the fracture toughness increases. Ashcroft (Ashcroft et al. 2001) studied the environment and pre-conditioning effects on fatigue loading of bonded composite joints. They tested CFRP/epoxy double lap joints at the temperature ranges experienced by a jet aircraft. They found that as temperature increased the fatigue resistance decreased. This phenomenon was more pronounced in presence of high humidity levels. An increase in temperature was found to provoke higher stiffness degradation, aggravated by the addition of humidity. Shorter fatigue life was observed at higher temperatures and also they noticed that the mode of failure was shifted from cohesive to interfacial in presence of high humidity (Zhang et al. 2009).

Chapter 3

Pre-bond moisture effect on adhesive film joints at room temperature (RT)

3.1 Introduction

Composite structures in service experience environmental and mechanical threats. The main environmental threats are related to the effect of temperature and moisture absorption, as they can affect the strength of composite structures and reduce their lifetime. Therefore, moisture absorption should be taken into account during the structure design. In composite bonded joints, as those used for repairs, the amount of moisture uptake in the adherends, which might have an influence on the final performance of the joint, depends on a number of factors, e.g. specific adherend material used, exposure condition (temperature, humidity), exposure time and skin thickness (Wright 1981). In order to reduce the amount of moisture, the adherends are dried before curing the adhesive joint.

Very few studies have been reported on the pre-bond moisture effect on the mechanical properties of the adhesive joints. Most of authors (Blackman et al. 2008, Parker 1983, Parker 1986, Parker 1990, Armstrong 1996, Sage at al. 1982) found that the presence of moisture in the composite leads to the reduction in joint strength. However, some authors noticed that low levels of moisture can improve the joint strength or produce no effect, so complete drying is not necessary (Myhre et al. 1982, Robson et al. 1994, Selzer et al. 1995, Gao et al. 2001). A proper selection of the adhesive material and drying procedures to assure a low level of moisture would give positive influence on the performance of adhesive joints.

The objective of this chapter is to characterize the effect of pre-bond moisture on the Mode I interlaminar fracture behaviour of composite repairs, by using Double Cantilever Beam specimens. In order to attain the pre-bond moisture, the adherends were immersed in water at 70°C for 336 hrs. Then, two drying processes of 1 h and 24 h were used before curing the bonded joints. Scanning Electron Microscopy (SEM) and Optical Microscopy studies were performed to understand the failure mechanisms.

3.2 Experimental Details

3.2.1 Materials and Methods

In order to determine the effect of pre-bond moisture on the fracture behaviour of bonded composites joints, an experimental study was carried out with two different adhesive films, denoted as F1 and F2. The adhesives were epoxy films with an embedded carrier. The name and the properties are not revealed for confidential reasons. One of the adherends (a $[0, 90]_n$ plain weave carbon fabric epoxy prepreg) was previously cured in an autoclave at 180°C and 700 kPa of applied pressure. The CFRP substrates were immersed in distilled water at a constant temperature of 70°C for 336±12 hour to promote moisture uptake. After that, the substrates were dried in an air circulated oven at a constant temperature of 80°C, for 1 hour and for 24 hours. The weight measurements of two adherend material coupons were used to calculate the moisture uptake and loss (% in weight) during the substrate conditioning steps prior to the bonding operation. The coupons were periodically removed from the chamber, wiped with tissue paper and then weighed. Weighing was performed on an analytical balance with an accuracy of 0.1 mg.

Surface preparation of the tool side of the pre-cured substrates was done immediately after drying and consisted of sanding and cleaning with a solvent, followed by a water break test and then, a brief drying using a hot air gun for at least 1 minute at an air temperature of 70ºC maximum. The bonded joints with the pre-cured panel, the adhesive films (F1 and F2) and the fresh repair prepreg plies (plain weave carbon fabric epoxy prepreg) were cured at 120°C under vacuum pressure simply to reproduce those "in-field" conditions normally used in repair procedures. Curing process time and temperature were selected according to the manufacturer's indications. A Teflon insert was placed between the adherends so that an initial pre-crack of 60 mm was obtained. The dimensions of the panels were 350×300 mm. The specimens for Double Cantilever Beam fracture toughness tests, according to ISO15024, were 25 mm in width and 150 mm in total length. The nominal thickness of panels was 3 mm. Pre-cured panels were inspected by c-scan. The bonded joints were also inspected by C-scan to check that no flaws (zones with porosity or non-bonded areas) were present in the bond line. The results of the inspections were acceptable according to the acceptance criteria specified (18 dB of maximum attenuation).

The adhesive thickness in each panel was measured by means of optical microscopy. The edges of all specimens were abraded with an emery paper. Specimens were wiped with alcohol to remove any dust particle before observation. Fluorescence Optical Microscope (Leica brand, DMR-XA) was used to distinguish the resins in the pre-cured and the co-bonded adherends from the adhesive film (figure 3.1).

All specimens were observed at a 10x magnification using a blue filter (Band pass filter BP 450-490 nm) under a fluorescence light radiation. 20 single optical images were taken for each sample. "Canon Stitch" software was used to obtain a mosaic image by composing all the single images of each specimen. Quartz software was used to measure the adhesive thickness in each mosaic image. The adhesive thickness of the joints measured at the thinnest zones was around 90 µm. Maximum adhesive thickness was found to be around 195 µm.

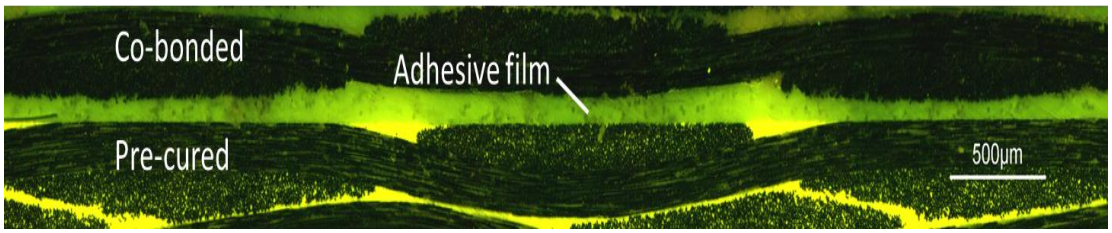

Figure 3.1 Fluorescence optical inspection of the edge of the specimen from which the adhesive thickness was measured.

3.2.2 Mechanical Testing

A universal testing machine, MTS Insight with a 1 kN load cell, at a crosshead rate of 5 mm/min was used for the DCB tests. Tests were performed at room temperature (RT) in a laboratory controlled environment (23±2°C, 50±5% RH) at the University of Girona (ISO 17025 accredited). Batches of six specimens were tested at each condition. The crack length during propagation was monitored optically at the specimen's edge by means of a long distance microscope Questar QM100. Values of load, displacement, and crack length were measured simultaneously for crack initiation and crack propagation data, according to ISO 15024 standard. The data was analyzed to determine the fracture energy G_{IC} using several methods: Corrected Beam Theory, Modified Compliance Calibration and Area Method for crack onset and propagation.

The fracture surfaces of all specimens were examined. The transverse cross section and longitudinal section (figure 3.2) of fractured specimens were analysed using a Fluorescence Optical Microscope (as explained above) and SEM, respectively. The schematic sketch in figure 3.3 shows the sample preparation process for Optical Microscope and SEM observation of fractured specimens. The sample preparation stages for Optical Microscope observation involved cutting, embedding and polishing, while a gold coating was applied to increase the imaging capability of samples for SEM observation.

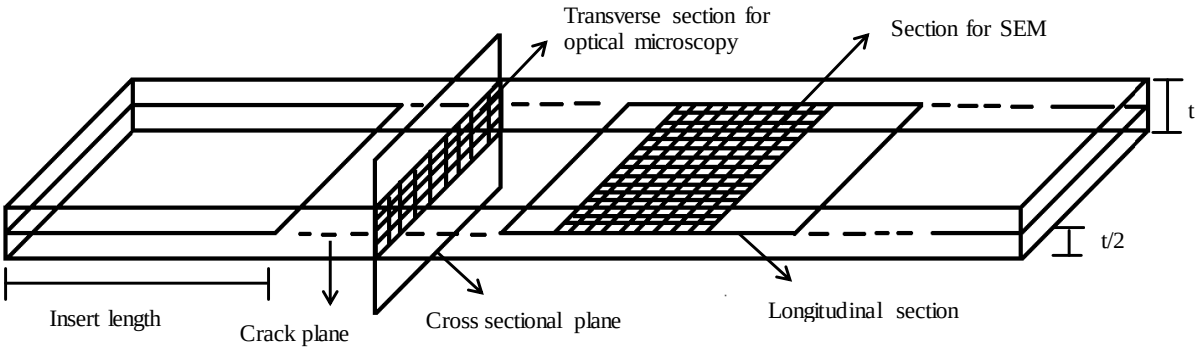

Figure 3.2 Configuration of DCB specimen and extraction of samples for microscopy inspections.

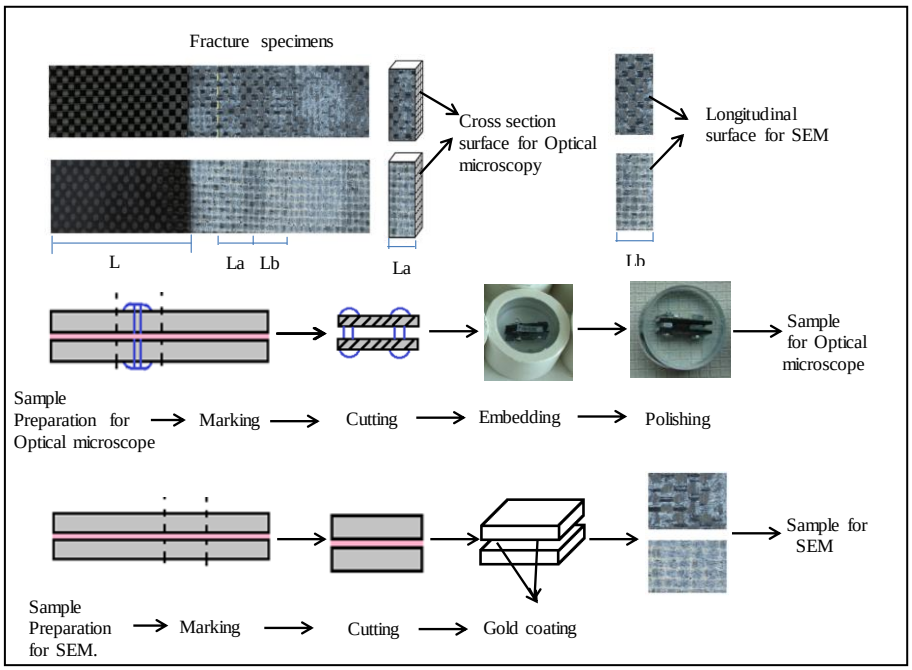

Figure 3.3 Sample preparation process for Optical Microscope and SEM.

3.3 Results

3.3.1 Moisture absorption

The moisture absorption and desorption of the CFRP substrate as a function of time is shown in figure 3.4. The immersion temperature (70ºC) and time (336 h) were selected because it was well-known that they cause a quick moisture uptake for the pre-cured adherend material used in this study, leading to a situation close to equilibrium. The moisture substrate uptake, caused by this immersion process, was 1.6%. The choice of the drying conditions, in turn, obeyed the practical considerations of real repair operations. Drying for 24±0.5 hours at 80±5ºC is known to notably reduce the moisture content, although it does not remove it completely. It is a compromise between an acceptable reduction of moisture and an acceptable duration of a repair intervention. The aim of the short drying cycle (1 hour at 80±5 ºC) was to investigate the tolerance of the different types of bonding agents to the cure in the presence of a considerable amount of moisture in the substrate. Assessing the feasibility of a reduced repair time was the final goal of this study. The moisture content before bonding was 1.25% and 0.33%, for the 1 hour and 24 hour drying at 80°C, respectively.

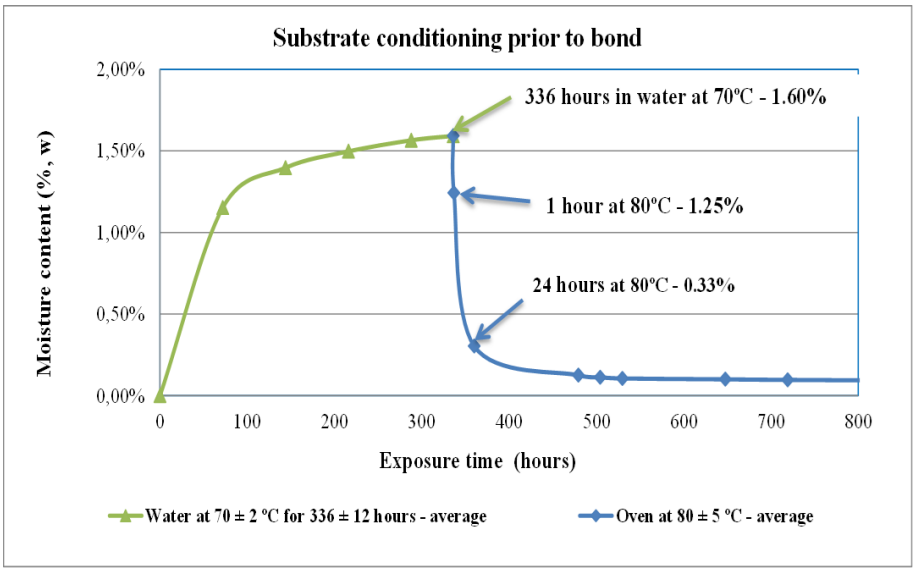

Figure 3.4 Average moisture content in the substrate as a function of the exposure time during the immersion in water at 70±2 ºC for 336±12 hours and subsequent drying in an oven at 80±5ºC.

3.3.2 Load-displacement behaviour

Typical load-displacement curves for the specimens with different moisture contents before bonding are shown in figure 3.5. It can be seen that, for joints with adherends without pre-bond moisture conditioning, the curve is linearly increasing until onset of fracture from which the load suddenly drops and again increases, and fracture evolves repeating this pattern. The alternating dropping and increasing of load corresponds to alternating phases of very fast crack growth with crack arrest periods. That is, growth was not continuous, but instead proceeded as a succession of rapid growth and arrest phases; this is commonly referred to "stick-slip" behaviour of growth and this behaviour observed for both the adhesive film joints. This behaviour was not so markedly observed in the specimens with pre-bond moisture (1.25% and 0.33%) for both the adhesive films (F1, F2) joints.

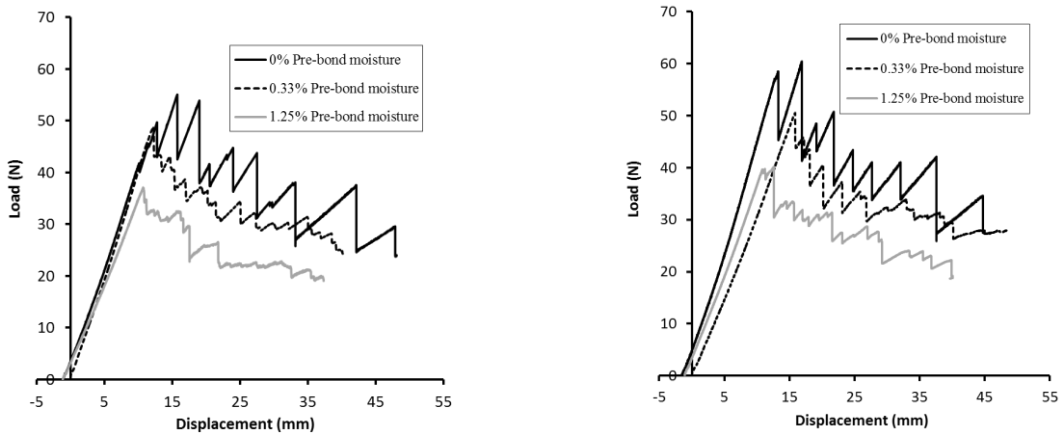

(a) Adhesive film, F1 (b) Adhesive film, F2

Figure 3.5 Load-displacement curve of Mode I DCB tests (a) Adhesive film, F1 (b) Adhesive film, F2.

3.3.3 Failure mode

Figure 3.6a shows the failure mode of a specimen without pre-bond moisture conditioning. The crack initiated at the interphase, however, an additional crack appeared in the composite laminate in the pre-cured adherend. This failure mode with multiple cracks was not observed in the specimens with pre-bond moisture content (1.25% and 0.33%). In those samples the waviness associated to the fabric reinforcement was observed as shown in figure 3.6b.

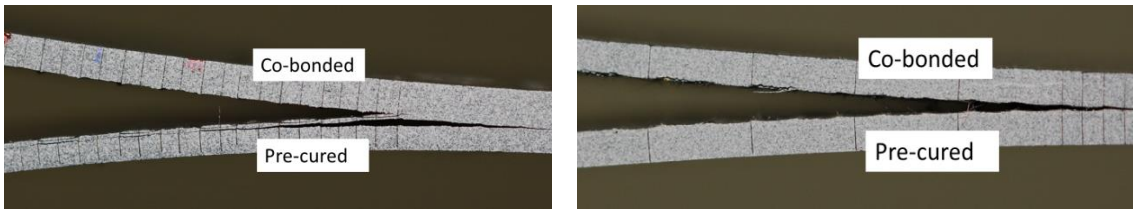

(a) (b)

Figure 3.6 Edge view of the bonded joints (a) without pre-bond moisture, where a double crack is clearly seen and (b) with pre-bond moisture.

3.3.4 Toughness Results (G_{IC})

According to ISO 15024, the values of crack initiation were determined from both the insert film and from the mode I pre-crack generated in a preliminary test. Nonlinear (NL), visual (VIS) and the maximum load or 5% increment in compliance (Max/5%) were measured. Thus for each of the six adhesive joints investigated, the six values of initiation were deduced i.e. three values from the insert and three values from the mode I pre-crack. For brevity, only the results obtained using the Corrected Beam Theory (CBT) method are presented here (figures 3.7a to d).

The values of G_{IC} onset from the insert film were lower than the values from the pre-crack for both adhesive films (figure 3.7). The onset values from the insert exhibited noticeable differences between methods (NL, VIS and MAX/5%). Instead, theses different methods provided similar results in the tests over pre-cracked specimens.

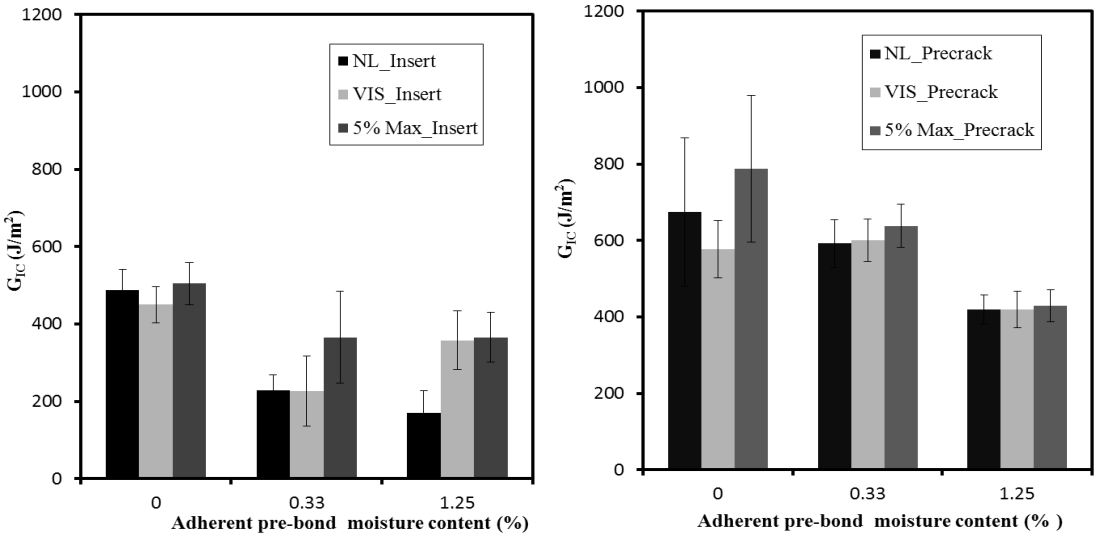

(a) (b)

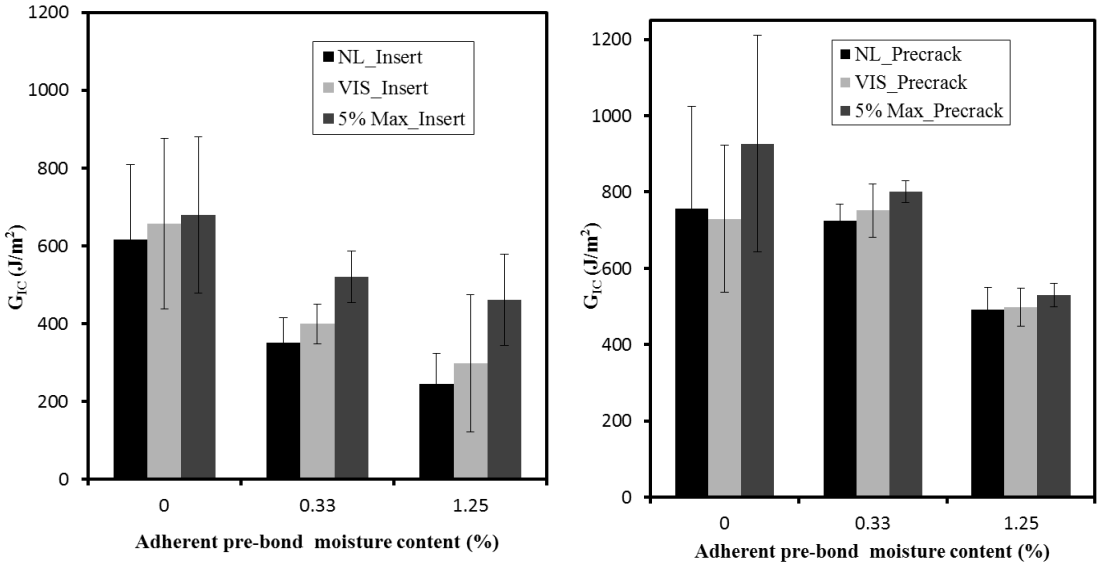

(c) (d)

Figure 3.7 (a-b) Initiation values of G_{IC} measured from (a) insert and (b) pre-crack, versus pre-bond moisture content for joints bonded using an Adhesive F1; (c-d) for bonded joints with Adhesive F2. The height of the columns represents the mean values and the error bars the standard deviation for each batch of six specimens

Mean propagation values of G_{IC} calculated using the CBT method, are shown in table 3.1. The fracture toughness values for the joints without pre-bond moisture were higher than the joints with pre-bond moisture for both bonding agents (F1, F2). It should be reminded, however, that a multiplicity of cracks was observed during testing for the joints without pre-bond moisture. In this case the crack growth energy results from the contribution of every propagating crack, leading to larger values than those found if a single crack was propagating. Hence the mean propagation G_{IC} value measured for the joint without pre-bond moisture should be taken as a reference for comparison with the joints with pre-bond moisture only with caution. It should be mentioned that both adhesive film joints showed a significant (50%) increase in fracture toughness when the pre-bond moisture content was 0.33% in the substrate compared to 1.25%. Approximately a 20-25% difference in fracture toughness, $G_{IC,}$ was observed in between the joints with different adhesive films for all moisture conditions (the adhesive F2 with higher G_{IC} than F1).

Substrate Conditioning	Pre-bond moisture content (%)	Test condition	G_{IC} (J/m^2)
Adhesive film (F1)			
Non-preconditioned	0.00	RT/ambient	790±32
Immersion+24hr drying	0.33	RT/ambient	629±58
Immersion+1hr drying	1.25	RT/ambient	409±23
Adhesive film (F2)			
Non-preconditioned	0.00	RT/ambient	804±102
Immersion+24hr drying	0.33	RT/ambient	751±59
Immersion+1hr drying	1.25	RT/ambient	495±38

Table.3.1 Mean propagation values of fracture toughness (G_{IC}) resulting from the CBT data reduction method for the bonded joints with and without pre-bond moisture.

3.3.5 Fracture Surface analysis

3.3.5.1 Visual inspection of the fractured surfaces

The failure surface of the specimens was inspected visually and recorded by macrophotography. In figures 3.8 and 3.9, the starter crack formed by the PTFE insert can be seen at the left hand end of the specimen, with crack growth running from left to right. The adherends appearing on top of the images are the co-bonded adherends (repair patches) and those appearing at the bottom are the pre-cured substrates.

The co-bonded adherend is completely covered by the adhesive film as shown in figure 3.8a, for the specimen without pre-bond moisture. Figure 3.8b corresponds to the failure surface of a joint manufactured using adhesive film F1 with pre-bond moisture of 0.33%. It shows that most of the adhesive film remained attached to the pre-cured adherend and some adhesive film remain on the co-bonded, it indicate cohesive failure also occurred. The contribution of cohesive failure decreased as the moisture content in substrates increased to 1.25 % as shown in figure 3.8c. Adhesive F2 showed the same behaviour (refer to figure 3.9).

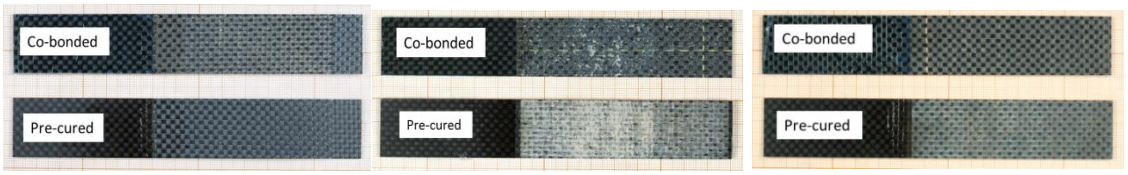

(a) F1, 790 J/m^2 (0.0%) (b) F1, 629 J/ m^2 (0.33%) (c) F1, 409 J/m^2 (1.25%)

Figure 3.8 Fractured surfaces of joints with different pre-bond moisture bonded with adhesive film, F1.

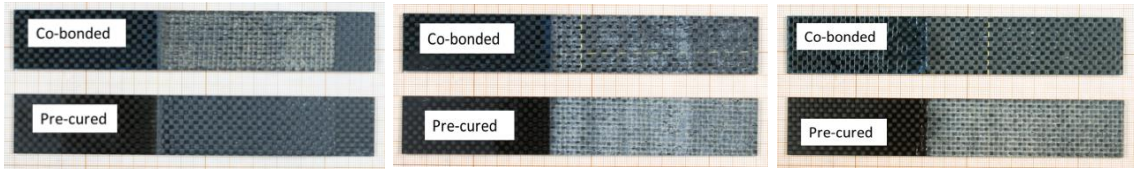

(a) F2, 804 J/ m^2 (0.0%) (b) F2, 751 J/ m^2 (0.33%) (c) F2, 495 J/ m^2 (1.25%)

Figure 3.9 Fractured surfaces of joints with different pre-bond moisture bonded with adhesive film, F2.

3.3.5.2 Optical and Scanning Electron Microscope

All optical micrographs were taken at approximately 7 mm from the tip of the insert. Optical micrographs corresponding to the specimens with pre-bond moisture content 1.25% and 0.33% are shown in figures 3.10 and 3.11 respectively (pre-cured adherend at the bottom of the image and co-bonded on top). It is clearly seen that the joint failed near the co-bonded adherend and that some carbon fibres were pulled out from the co-bonded adherend and remained attached to the adhesive film, figure 3.10a. The same fracture trends with a slightly increased contribution of cohesive failure of the adhesive, also occurred for the joint with 0.33% pre-bond moisture, figure 3.10b. The same fracture occurs for the adhesive film, F2 joints in both pre-bond moisture conditioned as shown in figure 3.11.

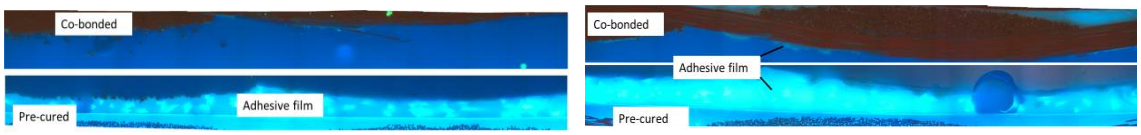

(a) F1, 1.25% (b) F1, 0.33%

Figure 3.10 Optical micrographs of the transverse cross section of tested bonded joints with adhesive film F1 (a) pre-bond moisture content of 1.25% (b) 0.33% (Pre-cured adherend at the bottom and co-bonded on top).

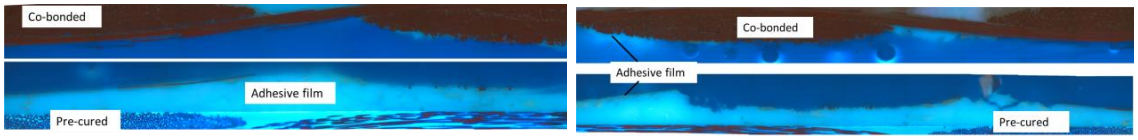

(a) F2, 1.25% (b) F2, 0.33%

Figure 3.11 Optical micrographs of the transverse cross section of tested bonded joints with adhesive film F2 (a) pre-bond moisture content of 1.25% (b) 0.33% (Pre-cured adherend at the bottom and co-bonded on top).

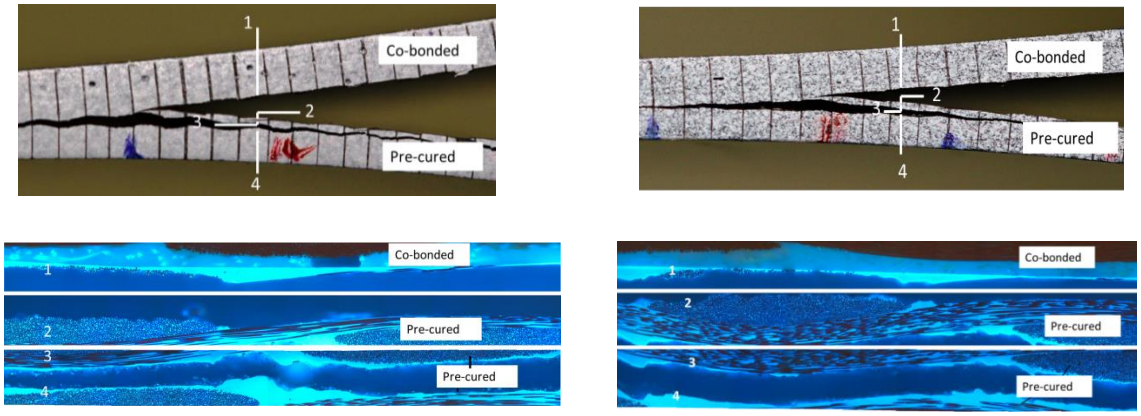

(a) F1, 0% (b) F2, 0%

Figure 3.12 Optical micrographs of the transverse cross section of tested bonded joints without pre-bond moisture (0.0%) (a) adhesive film F1 (b) adhesive film F2 (Pre-cured adherend at the bottom and co-bonded on top)

The joint with 0% pre-bond moisture failed in the pre-cured adherend; either in the interphase (location 1 and 2) or interlaminar (location3 and 4) as shown in figure 3.12a. It seems that the resin from the pre-cured adherend was weaker than the joint between the adhesive film and the co-bonded repair prepreg. The most important fact to remark

that there is a dramatic change in the failure mode from the samples without pre-bond moisture to the ones with pre-bond moisture. The adhesive F2 showed same failure mode (refer to figure 3.12b).

All SEM micrographs were taken at approximately 12 mm from the pre-crack tip. In all SEM images (figures 3.13 and 3.14), the crack was growing from bottom to top and the Teflon insert was below the bottom edge of the SEM photographs. In figures 3.13 and 3.14 SEM photographs are presented to compare the occurrence of fiber bridging, matrix plastic deformation, fiber imprints and micro cracks between 1.25% and 0.33% pre-bond moisture specimens. In figure 3.13 it is readily seen that the 1.25% pre-bond moisture specimen exhibits numerous detached fibres appearing on the fractured surface of the co-bonded panel. Using higher magnification figure 3.13b the fracture surface on the co-bonded side consisted of matrix with exposed fibers whereas the fracture surface on the adhesive side (pre-cured) consisted of adhesive with imprints of the fibers from the opposite fracture surface. This observation suggests that fibers were pulled away from the bonding with the adhesive indicating a weaker adhesion between both. No noticeable plastic deformation of the adhesive can be identified in figure 3.13b, reinforcing the idea of a weak adhesion between the co-bonded panel and the adhesive.

On the other hand, the fracture surface of the 0.33% pre-bond moisture specimen figure 3.13d shows a rougher surface, and some indications of matrix plastic deformation taking place. The adhesive film remained attached to both the adherends, co-bonded and pre-cured, as show in figure 3.13d, indicating that cohesive failure of the adhesive occurred. Some broken fibres, indicating the occurrence of fiber bridging could also be identified (figure 3.13d). No significant differences were observed in the surface features between the joints with different adhesive films for both pre-bond moisture conditions (see figure 3.14).

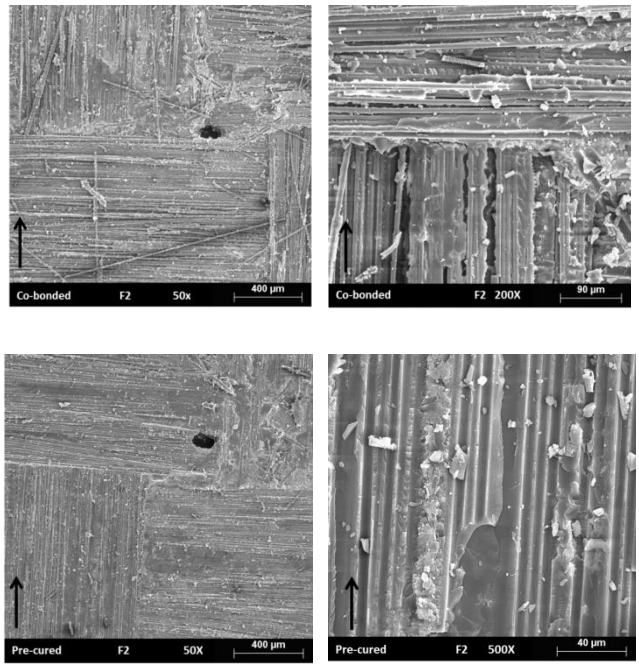

1.25% pre-bond moisture

(a) (b)

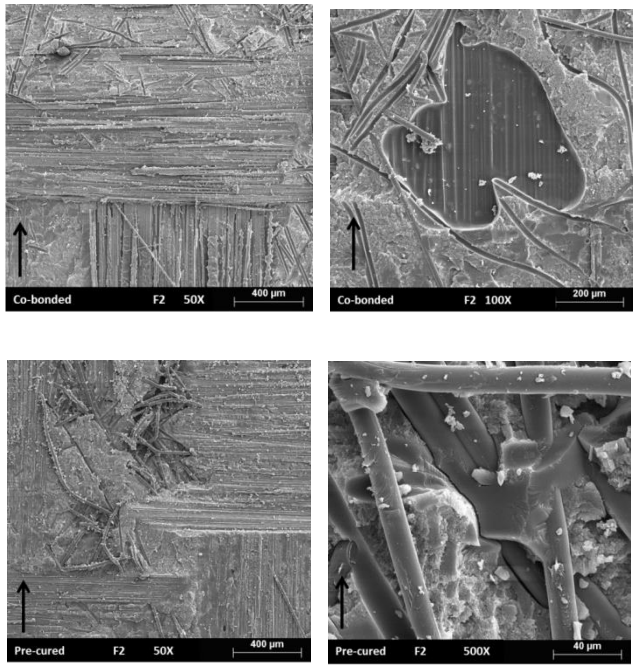

0.33% pre-bond moisture

(c) (d)

Figure 3.13 SEM micrograph of fracture surfaces of bonded joints with adhesive F2 (Top image is co-bonded panel and bottom image is pre-cured panel).The direction of the crack growth is indicated with a black arrow located at the bottom left corner of each picture.

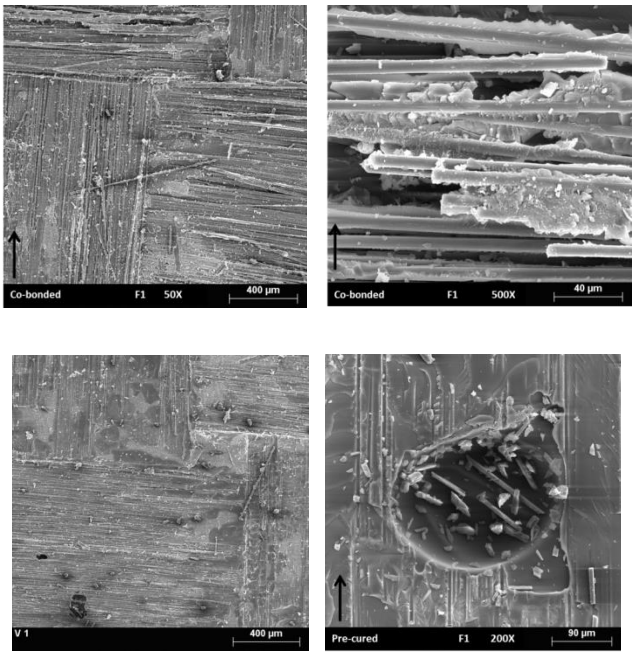

1.25% pre-bond moisture

(a) (b)

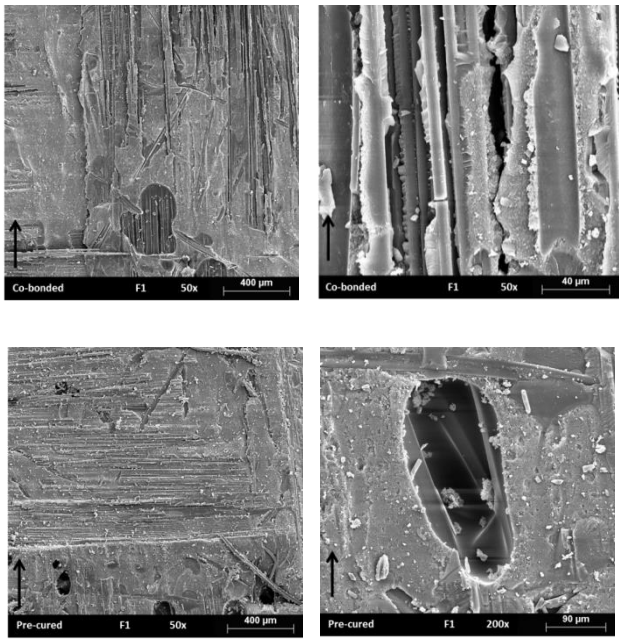

0.33% pre-bond moisture

(c) (d)

Figure 3.14 SEM micrograph of fracture surfaces of bonded joints with adhesive F1 (Top image is co-bonded panel and bottom image is pre-cured panel). The direction of the crack growth is indicated with a black arrow located at the bottom left corner of each picture.

3.4 Discussion

Multiple cracks in different planes were observed for the bonded joints without pre-bond moisture for both adhesive films, while the joints with pre-bond moisture conditioning of the substrate did not exhibit multiple cracks. Cracks tend to progress through the path that requires less energy. The presence of multiple cracks is an indication that the interlaminar interface in the pre-cured adherend is weaker (in terms of fracture toughness) than the interface corresponding to the adhesive film or to the adhesive film and the co-bonded repair prepreg. Therefore, the multiple crack propagation is an indication of a strong bond interface (the crack prefers to move to other weaker interfaces). The fact that the specimens with pre-bond moisture did not exhibit it evidences that the bond interface is not as strong as it was in the non-conditioned specimens.

The fracture toughness, G_{IC} increased almost 50% with the decrease in pre-bond moisture from 1.25% to 0.33%. This G_{IC} propagation value increase was probably due to the matrix deformation and cohesive failure of the adhesive as deduced from the SEM studies. 0.33% pre-bond moisture was obtained by increasing the drying time to 24 hour before bonding. As Armstrong (Armstrong et al. 1996) reported, drying of composite shows a positive effect on the fracture toughness. In contrast to the findings of Robson (Robson et al. 1994) this work evidences that even pre-bond moisture below 0.5% has an effect on the bond quality, as suggested by the different behaviour between 0.33% specimens and non-preconditioned joints.

Both adhesive film joints showed mixed failure, wet-wet failure (between the co-bonded adherend and the adhesive) and cohesive failure. Some light fibre tearing was also evidenced in the co-bonded adherend. When pre-bond moisture content decreased from 1.25% to 0.33% the cohesive failure component increased, which was reflected in an increase on the fracture toughness. The interphase which seems to be more affected by the presence of pre-bond moisture is the interphase between the adhesive and the co-bonded adherend (the “wet-wet” interface during the bonding process) indicating that water diffusion from the pre-bonded adherend, through the adhesive, during curing plays a crucial role.

The results suggest that further drying, beyond 24 hours, would increase the contribution of the cohesive mode of failure, leading to bonded joints with better mechanical performance. However, repair procedure requirements in terms of duration of the operation will counterbalance this drive for long drying processes. These findings highlight the importance of establishing proper drying procedures in repair operations.

3.5 Conclusions

Co-bonded joints with adhesive films acting as bonding agents for in service repair conditions have been produced. The effect of the moisture uptake of the pre-cured adherend on the performance of the joint has been analysed. For that purpose, the pre-cured adherend has been soaked in water for 336 hours at 70ºC and then dried for 1h or for 24 h. Fracture toughness onset and propagation in mode I has been taken as an indicator of the joint quality.

Joints with non-conditioned adherends exhibited multiple interlaminar cracks in the pre-cured adherend in addition to the insert plane indicating that the interlaminar interface in the pre-cured adherend is weaker (in terms of fracture toughness) than any of the interfaces in the bondline. However, the presence of pre-bond moisture in the pre-cured adherend produced a remarkable change in the failure mode, with the crack propagating in the interface between the adhesive film and the co-bonded adherend. This wet-wet failure was more evident in the samples with high pre-bond moisture content (1.25%). Samples with less pre-bond moisture (0.33%) exhibited a slightly increased contribution of cohesive failure.

These facts resulted in the fracture toughness decreasing with the pre-bond moisture content. Drying for 24 hours lead to a fracture toughness increment of 50% in comparison to the samples dried for 1 hour. This was correlated to a larger contribution of the cohesive mode of failure as revealed by the SEM study. Even the 24 hours drying operation did not lead to a recovery of the properties found in the specimens without pre-bond conditioning. These results indicate that a more exhaustive drying process on the repair substrate might avoid the detrimental effect of pre-bond moisture. However, while enlarging significantly the drying time might not be practical for repair operations, increasing the drying temperature might be a suitable approach provided any detrimental effect in the resin is prevented.

Even though both studied adhesives, F1 and F2, presented the same failure pattern, the fracture toughness of the adhesive film F2 was almost 20% higher than the adhesive F1 for all moisture conditions. This fact indicates that even if pre-bond moisture content has a strong effect on the bond quality, a careful choice of the adhesive should not be disregarded.

Chapter 4

Pre-bond moisture effect on adhesive film joints tested at high temperatures

4.1 Introduction

The non-mechanical hygroscopic variation is considered to be closely related to the long term durability and short term static strength of composite structures, especially when the water absorption is accompanied with high variation of temperature. The aerospace industry pays attention to high temperature/humidity environments due to their deleterious effect on material properties. In the last years, there has been a growing requirement, particularly in the aeronautic industry, for adhesives to withstand high temperatures. These adhesives have to maintain their mechanical properties at the intended service temperature and to maintain their structural integrity. Design of the bonded repair must consider the temperature and humidity environment that the component will experience during the service period.

The study reported here examines the hygrothermal effects on repairs with moisture content in the substrate before co-bonding the repair laminate. The focus of this research is the characterization of hygrothermal (temperature, pre-bond and post-bond moisture) effects on the mode-I interlaminar fracture behaviour of a repaired composite by means of DCB static tests.

In order to apply the pre-bond moisture, the adherends were immersed in distilled water at 70°C for 336 hrs and then dried for 1 hr and 24 hr at 80°C. Before testing the specimens, they were conditioned at 70º C and 85% of relative humidity (RH) until saturation. Then, these wet specimens were tested at 80°C and 120°C. An analysis of the fracture surface morphology is performed in order to determine the failure mode.

4.2 Experimental Details

4.2.1 Material

Two different adhesive film joints denoted by F1 and F2 were used to manufacture bonded joints between carbon fibre reinforced adherends. The adhesives were epoxy

films with an embedded carrier. Substrate panels of a woven cross-ply $[0, 90]_n$ epoxy pre-preg were pre-cured in autoclave at 175°C and 700 kPa of applied pressure. The bonded joints with the pre-cured panel, the adhesive films (F1 and F2) and the fresh repair prepreg plies were cured in an oven under vacuum pressure. Time and temperature of the curing process was selected according to the manufacturer indications. A Teflon insert was placed between the adherends so that an initial pre-crack of 60 mm was obtained.

Panels with a nominal thickness of 3 mm were obtained; and by cutting them, specimens for DCB tests of 25 mm wide and 150 mm long (according to the recommendations of ISO 15024). The specimens were grouped in batches of six samples. Pre-cured panels were inspected by C-scan. The bonded joints were also inspected by C-scan to check that no flaws were present in the bond line (zones with porosity or non-bonded areas). The results of the inspections were acceptable according to the acceptance criteria specified (18 dB of maximum attenuation).

4.2.2 Conditioning

Before performing the co-bonded joint, the CFRP substrates were immersed in distilled water at constant temperature of 70°C for 336±12 hours to promote moisture uptake. During the process they were periodically removed from the chamber and wiped with a tissue paper and then weighed. Weighing was performed on a balance with an accuracy of 0.1mg. After that, the substrates were dried in an air circulated oven at constant temperature of 80°C for 1 hour and 24 hours.

The specimens were categorized into two groups: with and without substrate condition (pre-bond moisture). All specimens were put in climatic chamber at 70°C/85% RH condition for moisture saturation. Moisture content was monitored in accordance with ASTM D5229 standard. Specimens were removed from the climatic chamber after moisture equilibrium for testing.

4.2.3 Adhesive thickness

The bond line thickness in each panel was measured with an optical microscope. The edges of all specimens were polished with fine graded sandpaper. A Fluorescence Optical Microscope (Leica, DMR-XA) was used to take the measurements of the bond

line thickness. With the fluorescence technique it was possible to distinguish the adhesive layer between the resins of the co-bonded adherend. The maximum bond line thickness was found to be around 195 µm and the minimum was around 90 µm for both adhesives.

4.2.4 Mechanical Testing

A universal testing machine, MTS Insight with a 1 kN load cell was used for the DCB tests. The tests were performed at a crosshead rate of 5 mm/min according to the recommendations of ISO 15024 standard. The specimens, previously conditioned at 70°C/85% RH, were tested at 80°C and 120°C in a climatic chamber adapted to the testing machine. The tests were conducted in a laboratory controlled environment (23± 2°C, 50±5 RH) of the University of Girona. The crack length during the propagation was monitored optically at the specimen's edge by means of a long distance microscope Questar QM100. Values of load, displacement, and crack length were measured simultaneously for crack initiation and crack propagation data. The data was analysed to determine the fracture toughness energy G_{IC} for onset and propagation using several data reduction methods: Corrected Beam Theory, Modified Compliance Calibration and Area Method. All the tested specimens were examined with an optical microscope at the specimen's side like it was done in chapter 3.

4.3 Results and discussion

4.3.1 Moisture absorption

The moisture absorbed by the substrate at 70°C during 336 hr was 1.6%. Then it was dried for 1 hr and 24 hr at 80°C. The final moisture content in substrate before bonding, defined also as pre-bond moisture level in the composite substrates, was 1.25% and 0.33%.

After manufacturing the specimens, they were conditioned at 70ºC/85% RH. The moisture content at saturation for specimens without pre-bond moisture condition was found to be approximately 1.2% and 1.1% for F1 and F2 adhesive joints respectively. For the specimens with 1.25% moisture it was 1.03% and 1.1% for F1 and F2 bonded joints, while the moisture absorbed was around 1.2% and 1.4% for F1 and F2 bonded joints with 0.33% pre-bond moisture in the substrate. The moisture content at saturation

for the specimens without pre-bond moisture was lower than the one of the specimens with pre-bond moisture. Significant differences in moisture absorption levels occurred for the joints with different pre-bond moisture levels see figure 4.1. Final values, corrected for zero weight by means of a third traveller of each class dried to equilibrium, are shown in table 4.1.

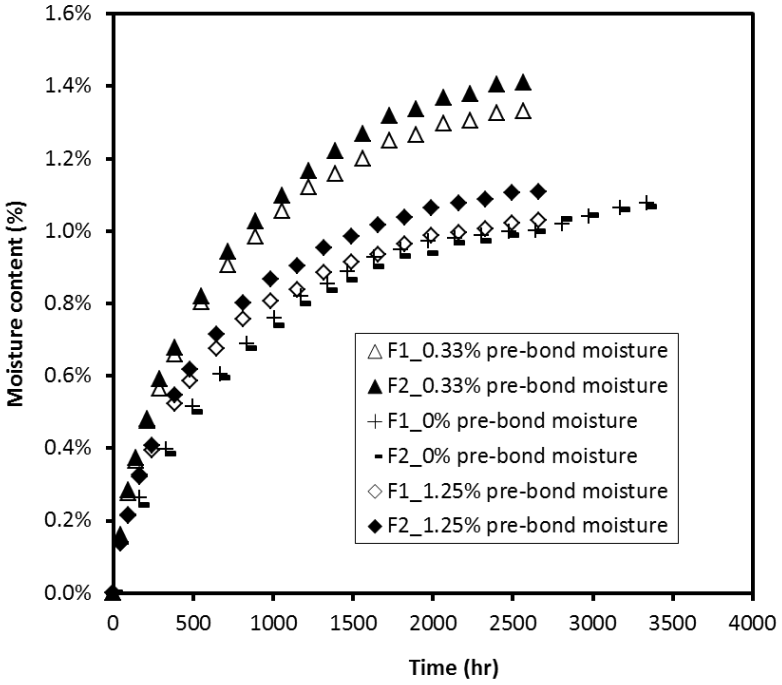

Figure 4.1 Average moisture content in the bonded joint specimens before testing, as a function of the exposure at 70°C/85% RH.

Co-bonded specimens	**Weight gain (70°C/85%RH)**		drying at 50ºC for 72 hr +70ºC for 72 + 90ºC equilibrium	
	Traveller 1	**Traveller 2**	**Traveller 3**	Final value prior to test
Reference sample (F1)	1,2	1,2	0,2	1,4
Reference sample (F2)	1,2	1,2	0,3	1,5
Pre-bond moisture 1 hr (F1)	1,0	1,0	0,6	1,7
Pre-bond moisture 1 hr (F2)	1,1	1,1	0,6	1,7
Pre-bond moisture 24 hr (F1)	1,2	1,4	0,5	1,7
Pre-bond moisture 24 hr (F2)	1,4	1,4	0,5	1,9

Table 4.1 Average moisture content in the bonded joint specimens before testing, as a function of the exposure at 70ºC/85% RH. Values corrected for zero weight with traveller 3.

4.3.2 Load-displacement behaviour

Figure 4.2 shows typical load-displacement curves of DCB tests performed at 80ºC and 120ºC. The figure also includes the results of specimens prepared with different pre-bond moisture conditions. The load level increases as the test temperature increases from 80°C to 120°C for the adhesive film F1 joints. Stick-slip failure mode is observed for the higher (1.25%) pre-bond moisture specimen at 120°C for both adhesive films, while at lowest pre-bond moisture level it does not occur. The bonded joints with adhesive F2 show more stick-slip behaviour than the joints made of F1 adhesive.

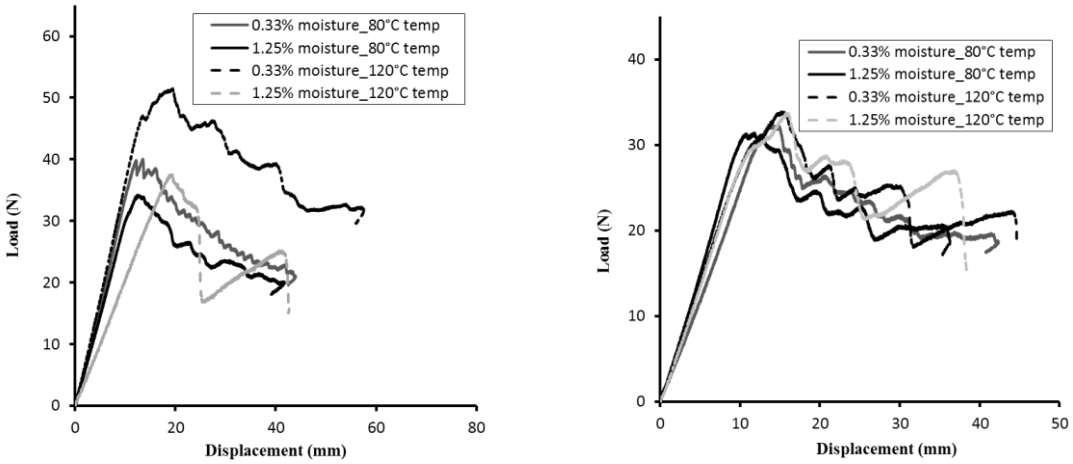

(a) (b)

Figure 4.2 Load - displacement curve of mode I DCB tests at 80°C and 120°C (a) bonded joints with adhesive film F1 and (b) adhesive F2.

4.3.3 Fracture toughness results (G_{IC})

Figure 4.3 shows the results of the mode I fracture toughness of the NL point (G_{IC}^{NL}) in function of the temperature and the pre-bond moisture. Two results are provided: directly from the insert and after a pre-crack, according to the recommendations of ISO 15024 standards. The values of the energy fracture toughness are determined with the CBT data reduction method. The discrete symbols correspond to the mean value of the G_{IC} at nonlinear (NL) load points, and "error bars" to the standard deviation for each batch of six specimens. The tests performed at 120ºC with specimens without pre-bond

moisture are considered not comparable to the rest because the failure was not in the adhesive. Therefore, these results are not included in figure 4.3.

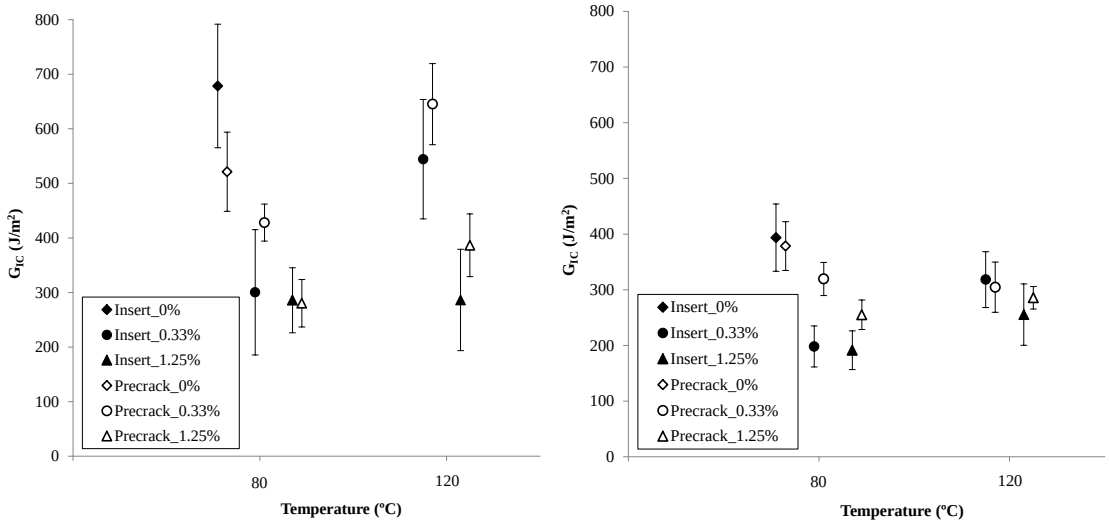

Figure 4.3 Initiation values of G_{IC}^{NL} measured from the mode I insert and pre-crack for bonded joints with (a) adhesive film F1 and; (b) adhesive film F2.

From the results of the initiation values it is observed that the pre-bond moisture has a negative effect on the energy fracture toughness. G_{IC} decreases when the pre-bond moisture increases from 0.33% to 1.25%. This occurs for both adhesives and temperatures. The same trend is observed for the dry specimens tested at 80ºC. They have higher values of G_{IC} than specimens with pre-bond moisture. This decrease is more accentuated for adhesive F1 than for F2. However, the joints with adhesive F1 give as result higher absolute values of G_{IC} than the ones with adhesive F2.

In relation to the temperature, there is an increment of GIC in the joints with F1 adhesive when the test temperature increases from 80ºC to 120ºC. The only exception if for the specimens with 1.25% pre-bond moisture tested from the insert, in which G_{IC} remains almost the same. The specimens with adhesive F2 do not exhibit this clear trend, e.g. for the specimens with 1.25% pre-bond moisture there is a small increase in G_{IC} with respect to the temperature; on the contrary, for the specimens with 0.33% pre-bond moisture the value of G_{IC} increases for the specimens tested from the insert, but decreases if they are tested from the pre-crack.

The results of the propagation values of are presented in table 4.2. Like in figure 4.3, the table includes the results of the tests performed at 80ºC and 120ºC with the specimens manufactured at different pre-bond moisture conditions.

Substrate conditioning *	Test condition	G_{IC} (J/m^2) from tests at 80ºC	G_{IC} (J/m^2) from tests at 120ºC
Adhesive film F1			
a	Wet (70°C/85 %RH)	718	**
b	Wet (70°C/85 %RH)	440	524
c	Wet (70°C/85 %RH)	554	1005
Adhesive film F2			
a	Wet (70°C/85 %RH)	566	**
b	Wet (70°C/85 %RH)	336	443
c	Wet (70°C/85 %RH)	391	457

Table.4.2 Mean fracture toughness propagation values obtained from CBT data reduction method.

* Substrate conditioning:

a) Non-conditioned, weight gain 0.0%

b) Immersion in water at 70 °C + dried at 80°C for 1 hr, weight change 1.25%

c) Immersion in water at 70 °C + dried at 80°C for 24 hr, weight change 0.33%

** The crack propagation occurred at the adherends instead of at the adhesive.

For both adhesive films, F1 and F2, the fracture toughness of the bonded joints increases with the increase of the temperature. This increase on the fracture toughness is independent on the pre-bond moisture condition. At 80°C, the joints with 0% pre-bond moisture exhibited higher fracture toughness, $G_{IC,}$ than the joints with pre-bond moisture (0.33% and 1.25%). As previously commented, for the 0% pre-bond moisture specimens tested at 120°C the crack front deviated from the adhesive layer to the co-cured laminate. These results were not comparable to the rest and were removed from table 4.2.

For specimens tested at 80ºC and 120ºC, the fracture toughness increases as the pre-bond moisture level decreased from 1.25% to 0.33%. But increment in G_{IC} is different depending on the adhesive film used. For the joints with adhesive film F1 tested at 80ºC

this increment is around 20%. At 120°C the increment is about the double for the adhesive film. For the joints with adhesive film F2 the increase in G_{IC} is bigger in the tests at 80ºC (about a 30%) than in the specimens tested at 120º (about a 16%). This tendency is totally opposed to the results obtained from the initiation values.

4.3.4 Fracture surface analysis

4.3.4.1 Visual fracture surface

Once the tests were finished, the specimens were opened and their fracture surfaces were inspected by optical methods. In all the pictures of the fractured surfaces, the adherends appearing on the top are the co-bonded laminate and the adherends at the bottom are the pre-cured substrates.

Figures 4.4 and 4.5 show the failure surface of 6 wet specimens tested at 80°C (2 adhesive films, F1 and F2, and 3 pre-bond moisture conditions, 0%, 0.33% and 1.25%). The surface shows cohesive failure of the adhesive to be the dominant failure mode for the adhesive film F1 joint with 0% pre-bond moisture at 80°C, figure 4.4a. A complete cohesive failure surface for the adhesive film F2 joints tested at same temperature was also observed, see figure 4.5a.

The pre-cured surface is completely covered with the adhesive film for the 0.33% and 1.25% pre-bond moisture specimens tested at 80ºC, as shown in figures 4.4 and 4.5. Only a few white spots (adhesive film) are observed on the co-cured part of joints with 0.33% pre-bond moisture.

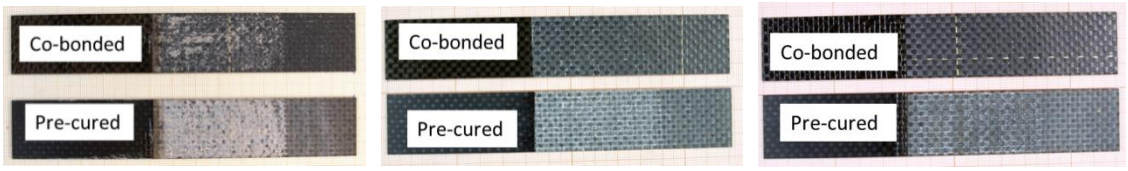

(a) (b) (c)

Figure 4.4 Fracture surfaces of bonded joints with adhesive film F1 with different pre-bond moisture contents: (a) 0 %; (b) 0.33%; and (c) 1.25%, tested at 80°C.

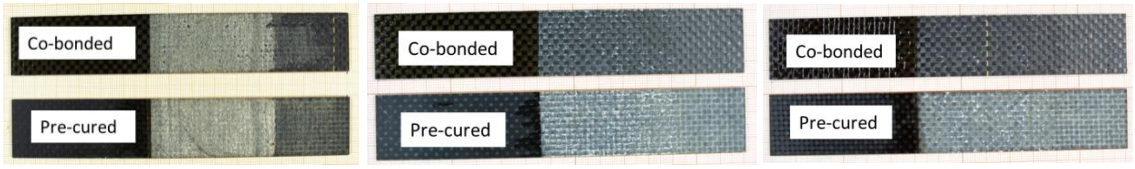

(a) (b) (c)

Figure 4.5 Fracture surfaces of bonded joints with adhesive film F2 with different pre-bond moisture contents: (a) 0 %; (b) 0.33%; and (c) 1.25%, tested at 80°C.

At temperatures of 120°C there is a failure at the outer surface of the co-cured panel for the joints without pre-bond moisture, see figure 4.6. In those tests there is no crack propagation, the specimen arm breaks before propagation starts. When increasing the pre-bond moisture from 0% to 0.33% or 1.25%, the failure mode is located at the bonded joint.

For bonded joints tested at 120ºC with F1 adhesive and 0.33% pre-bond moisture the pre-cured panel is covered with adhesive. These adhesive joints exhibit the same failure type than the ones tested at 80ºC. When increasing the pre-bond moisture some black and white strips appear on the pre-cured panel (see figure 4.7b). They indicate a stick-slip failure mode, also observed in the load-displacement curves (figure 4.2). The same failure pattern is observed in adhesive F2 bonded joints, see figure 4.8.

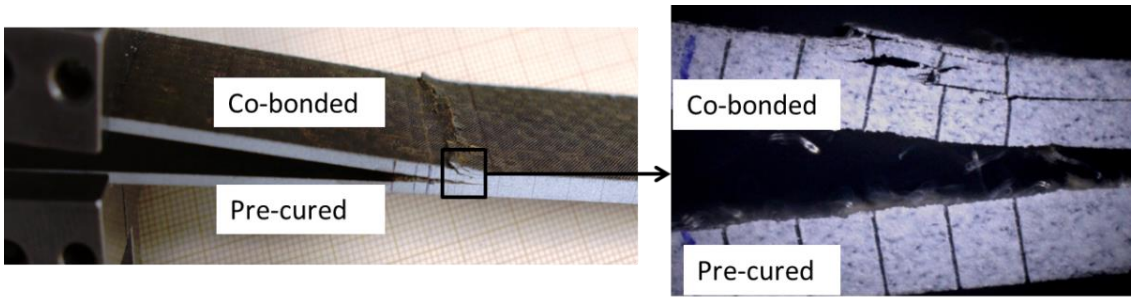

Figure 4.6 Fracture surface of bonded joints with 0% pre-bond moisture tested at 120°C.

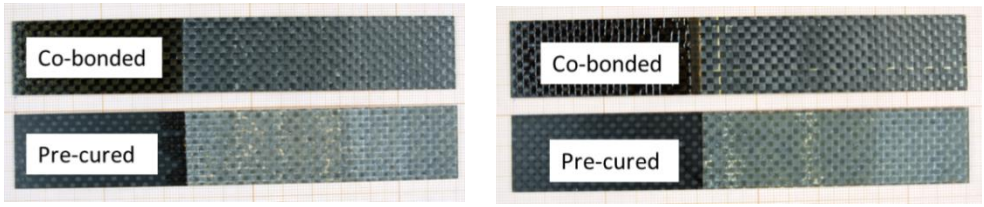

(a) (b)

Figure 4.7 Fracture surfaces of bonded joints of adhesive film F1 with different pre-bond moisture content (a) 0.33%; and (b) 1.25%, tested at 120°C.

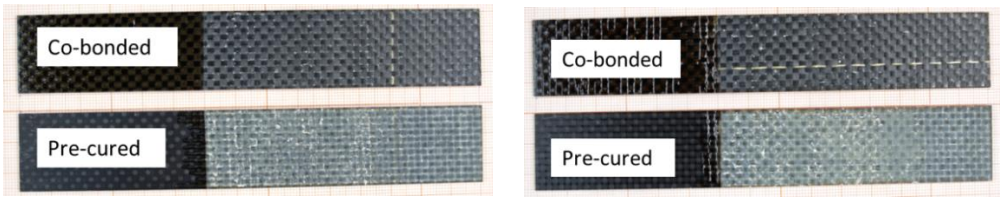

(a) (b)

Figure 4.8 Fracture surfaces of bonded joints of adhesive film F2 with different pre-bond moisture content (a) 0.33%; and (b) 1.25%, tested at 120°C.

4.3.4.2. Optical microscopy

All optical micrographs were taken at approximately 7 mm from the insert tip. Both, the top (co-bonded panel) and the bottom (pre-cured adherend) halves of the open specimens were observed at the same distance from the pre-crack length. The images are plot in figures 4.9 to 4.12. Figures 4.9 and 4.10 show the transverse cross sections of specimens tested at 80ºC. The sections of specimens tested at 120ºC are shown in figures 4.11 and 4.12.

It is clearly shown in figures 4.9a and 4.10a that there is adhesive film in both substrates (co-cured and pre-cured panels) in the joints with 0% pre-bond moisture. This means that a complete cohesive failure occurred. For the specimens with pre-bond moisture tested at 80ºC the adhesive remains on the pre-cured panel, thus the failure at the co-cured interlayer is the dominant mode of failure, see figures 4.9b and 4.9c, and figures 4.10b and 4.10c.

For the joins with pre-bond moisture, the failure mode remains same when the test temperatures increase from 80ºC to 120ºC, see figures 4.11 and 4.12. The failure occurs at the interface with the co-bonded panel. Finally, for the 0% pre-bond moisture

specimens tested at 120ºC, the failure occurs at the outer surfaces, as described in the previous section.

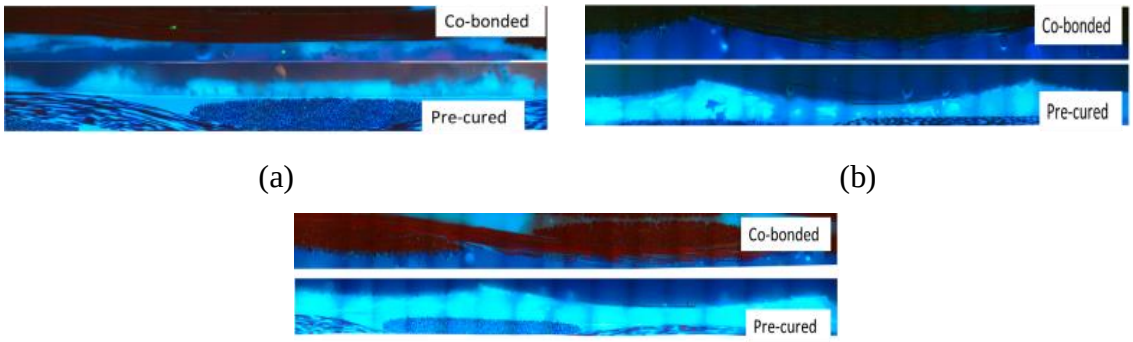

(a) (b)

(c)

Figure 4.9 Optical image of the transverse cross section of bonded joints with adhesive film F1 and with different pre-bond moisture conditions: (a) 0 %; (b) 0.33%; and (c) 1.25%. Specimens tested at 80°C.

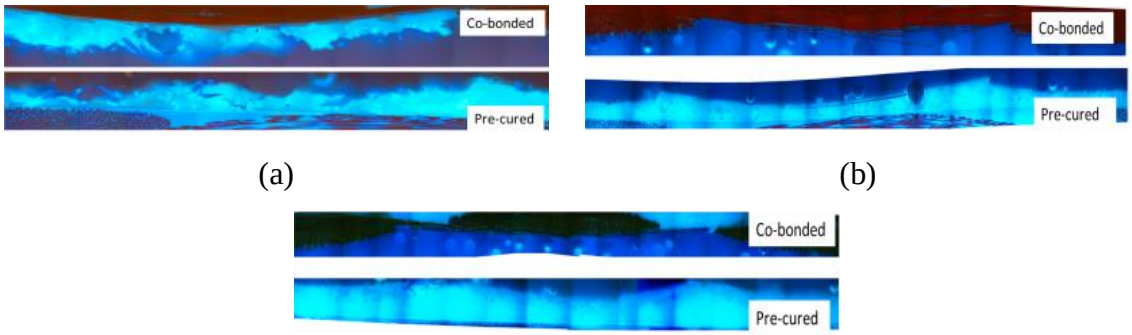

(a) (b)

(c)

Figure 4.10 Optical image of the transverse cross section of bonded joints with adhesive film F2 and with different pre-bond moisture conditions: (a) 0 %; (b) 0.33%; and (c) 1.25%. Specimens tested at 80°C.

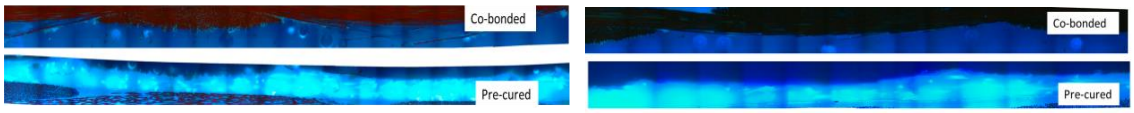

(a) (b)

Figure 4.11 Optical image of the transverse cross section of bonded joints with adhesive film F1 and with different pre-bond moisture conditions: (a) 0.33%; and (b) 1.25%. Specimens tested at 120°C.

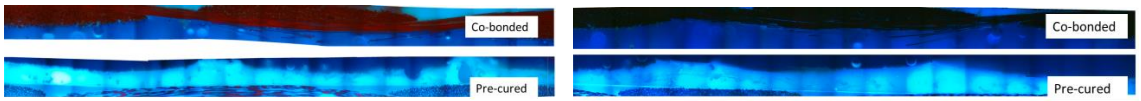

(a) (b)

Figure 4.12 Optical image of the transverse cross section of bonded joints with adhesive film F2 and with different pre-bond moisture conditions: (a) 0.33%; and (b) 1.25%. Specimens tested at 120°C.

4.4 Discussions

As a general trend, when the specimens are tested at room temperature there is a decrease in the fracture toughness with increasing pre-bond moisture level, independently of the adhesive film used (F1 and F2), as indicated in chapter 3. In those specimens with a lower pre-bond moisture level (up to 0.33%) the decrease in G_{IC} is smaller, a loss of about 15% being recorded. After this level, the energy fracture toughness of the repaired joints fall more, up to a 40%, when a pre-bond moisture level in the pre-cured surface is of 1.25%. When the specimens are tested at 80ºC the behaviour is similar with regards to the fracture toughness values. 0% pre-bond moisture conditioned joints exhibit higher fracture toughness compared to the 1.25% and 0.33% pre-bond moisture joints when tested at 80°C. Cohesive failure occurs in the co-bonded specimens tested at 80ºC with 0%pre-bond moisture and this is a possible explanation for the increment in the fracture toughness. The specimens with pre-bond moisture presented a wet-wet failure in the interface between the co-bonded adherend and the adhesive films.

But at higher temperature (120°C) the failure occurs at the outer surface of the co-cured panel in those specimens without pre-bond moisture with multiple cracks that grow away from the bond line with pre-bond moisture the failure occurs again in the wet-wet interface. At higher test temperatures, 80°C and 120°C almost no difference in the fracture toughness G_{IC} is observed between the different pre-bond moisture levels (0.33% and 1.25%) for adhesive film joints (F2) whilst a clear dependency on the temperature is observed for F1 adhesive joints, where the fracture toughness increases significantly.

4.5 Conclusions

DCB mode I tests have been used to determine the influence of pre-bond moisture and temperature on the fracture toughness (G_{IC}) of bonded joints manufactured with two different adhesive films (F1, F2) and subjected to post-bond wet conditioning.

In the specimens tested at 80ºC and 120ºC, the mode I the fracture toughness, G_{IC}, increases with increasing the temperature in all adhesive film joints, this occurs independently of pre-bond moisture conditioning. This increase might be produced by an increment of the matrix deformation.

There are no significant differences in fracture toughness between the different pre-bond moisture levels for the adhesive film joints F2, when tested at 80°C and 120°C. On the contrary F1 adhesives increase the value of G_{IC} with the temperature. It implies that for the latter adhesive the temperature has a major positive influence on G_{IC} than the negative effect of the pre-bond moisture when tested at high temperatures

At 120ºC and for the specimens without pre-bond moisture, the co-bonded adherend appears to be the weakest part of the specimen, where multiple cracks appear away from the bond line.

In the presence of pre-bond moisture, the interface between the co-bonded adherend and the adhesive films weakened in the wet specimens tested at both 80ºC and 120ºC. The adhesive films remained bonded in all cases to the pre-cured adherend. This wet-wet failure has also been observed in the specimens with pre-bond moisture tested at room temperature (see chapter 3).

These results indicate the need of a careful and detailed characterization of the bonded joints, paying attention not only to the fracture toughness values but also to the failure mode. For the repair systems studied here the presence of pre-bond moisture has a dramatic effect on the failure mode, moving it from the adherends themselves or the bulk adhesive films to the wet-wet interface in all cases, whatever the subsequent aging of the bonded joint and the test temperature. To avoid this failure mode, the removal of moisture from the pre-cured adherend appears to be essential.

Once the impact of the pre-bond moisture has been eliminated by the proper drying process, careful choice of the adhesive and the repair pre-preg and consideration of the operating conditions and in-service temperature should not be ignored, as evidenced by

the comparison of the different behaviour of the bonded joints with F1 and F2 at room temperature/as received versus 80ºC/wet and 120ºC/wet.

Chapter 5

Multiple specimen methodology for onset and crack growth determination under fatigue loading of DCB specimens

5.1. Introduction

The majority of the structural components are subjected to dynamic loads during the service life. Fatigue loading may cause a structure to fail at a load levels that are just a small percentage of the quasi-static strength. Therefore, the fatigue lifetime prediction of the components is of high interest for the scientific community and for the industry. Fatigue behaviour of adhesive joints between CFRP laminates is a challenge, mainly due to the complicated nature of fatigue crack initiation and propagation, the geometry of bonded joints, and the complex material behaviour under loading and unloading regimes, etc. (Khalili et al. 2008, Sarfaraz et al. 2011, Gao et al. 2011, Jen 2012).

In composite materials, much attention has been devoted to the fatigue behaviour of interlaminar cracks (Hojo et al. 1994, Cvithkovich et al. 1998, Hojo et al. 2006, Turon et al. 2007, Argüelles et al. 2008). In this case, the fatigue life is divided in 2 phases: onset and crack propagation.

There are different methods to determine the number of cycles (N) to reach the crack propagation onset. ASTM D6115 suggests 3 criteria: two based on a 1% or 5% increase of the compliance compared to the initial value ($N = 1$), and another method based on the visual observation of the crack initiation. However, normalized procedures to obtain the onset point require stopping the test periodically, and to carry out static tests on the linear zone of the material in order to evaluate the specimen's compliance (Argüelles et al. 2008, Argüelles et al. 2011, Brunner et al. 2013). The accuracy on the determination of the onset point depends on the frequency of test stops, and requires the continuous intervention of the technician. This is costly and leads to scattered results. A continuous monitoring of the compliance or the crack length could help to reduce this scattering.

A common way to present the fatigue crack propagation curve for adhesively bonded joints is by means of the logarithmic plot of the crack growth rate (da/dN) against the maximum strain energy release rate (G_{max}). The crack propagation curve is defined by

the three regions as shown in figure 5.1: (I) a region of crack arrest below which no crack advance takes place (defined by the crack growth rate threshold, G_{th}), (II) a linear region which is well described by the Paris law (defined by the slope n), and (III) a fast or unstable crack growth region, where catastrophic failure takes place when the fracture toughness G_C is reached.

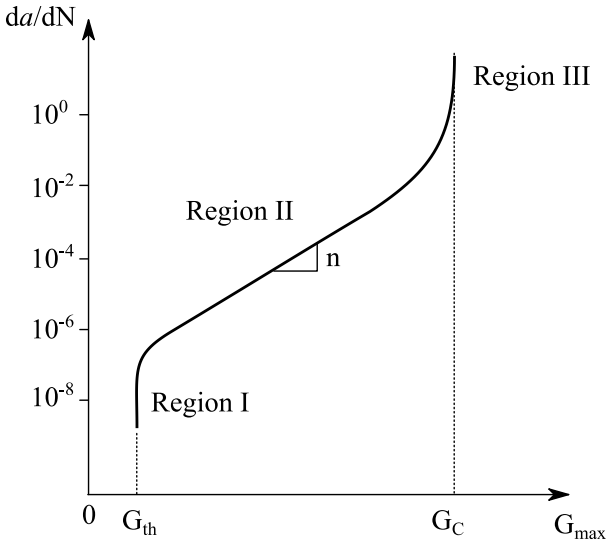

Figure 5.1 Fatigue crack propagation curve. Region I: region of crack arrest which is defined by the crack growth rate threshold (G_{th}). Region II: linear growth described by the Paris law (slope n). Region III: fast or unstable crack growth region defined by the fracture toughness (G_C).

In order to construct the crack growth rate curve the most important parameter to monitor is the crack growth. An automatic system is desirable. There are many possible methods: e.g. strain gauges (Ogasawara et al. 2007), acoustic emission systems (Roberts and Talebzadeh 2003), Digital Image Correlation (DIC) (Vanlanduit et al. 2009) or Fibre Bragg Grating sensors (Sans et al. 2012). However, all of them require complex devices and test set-ups. An alternative method that does not require additional equipment is to estimate the crack length by means of the compliance. A calibration of crack length vs. compliance is necessary (Renart et al. 2014).

Whichever the result to be obtained, onset or crack growth rate, a very long period of fatigue testing is usually required, i.e. the number of cycles to reach the threshold value may be different depending on the materials, but generally a range from 1 to 10 million cycles is considered (Krause and Mathis 1988). By increasing the test frequency the fatigue test period could be reduced. However, it may cause problems such as hysteric

heating (Lang and Manson 1987). In metallic components, the test frequency can be increased beyond 10 Hz, but the organic matrix of CFRP laminates is very sensitive to frequency, and heating problems may arise if the frequency increases beyond those levels. The alternative to overcome this problem is to test a number of specimens simultaneously.

The aim of this work is to implement a test methodology to investigate onset and crack growth rate curves of multiple specimens, simultaneously, in a single universal testing machine. The method must be capable to test the specimens at different levels of load and at different energy release rates. This paper presents the step by step approach of testing multiple specimens in the devised multi-fatigue test set up, and the corresponding data reduction procedures.

This methodology has been implemented for mode I Double Cantilever Beam (DCB) fatigue tests. This chapter also includes the results (onset and crack growth rate curves) for a batch of 6 adhesive joints between composite adherends for repair purposes.

5.2 Methodology

In this section, the design of a multiple-specimen fatigue test device is described, as well as the experimental methodology to obtain the onset and crack growth rate curves. In order to reduce the scattering in the onset curves, a method to continuously record the specimen compliance has been implemented. By means of this methodology and the compliance calibration, a continuous curve of the crack growth rate has been obtained.

5.2.1. Test rig design

The test rig is designed to fit in a universal servo-hydraulic testing machine. In this work it has been mounted on a MTS 858. In this equipment, the actuator is located on the top and the load cell on the bottom of the frame. The machine also incorporates an alignment system between the load cell and the load frame.

The test rig comprises two circular steel plates, 198 mm in diameter and 34 mm thick, which are attached to the actuator and to the load cell by a M12 screw. The plates allow assembling fixtures for different tests, e.g. DCB, 3ENF or ELS, see figure 5.2. For mode I DCB tests, 6 specimens can be tested at the same time (in a hexagonal

distribution) whereas for mode II (3ENF or ELS) there is only room available for 4 assemblies.

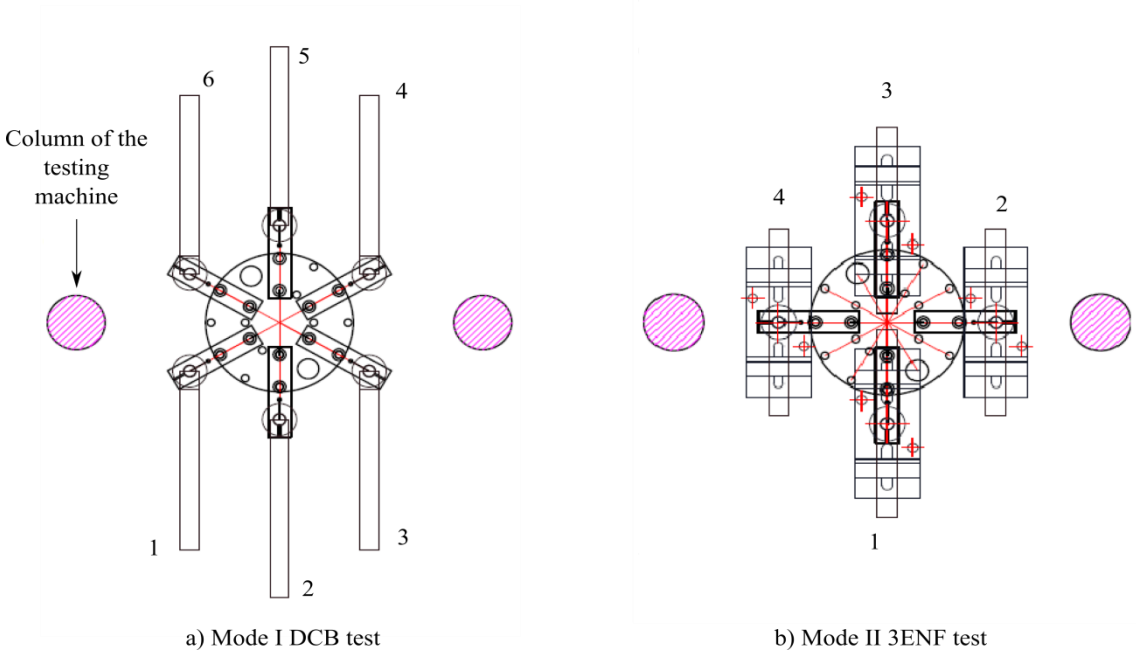

a) Mode I DCB test b) Mode II 3ENF test

Figure 5.2 Specimen distribution and identification for Mode I DCB (a) and mode II 3ENF(b) fracture tests.

In order to align the plates, each has two open holes of 28 mm of diameter. The alignment is done by introducing two cylindrical bars in the holes. Once aligned, the plates are fastened to the actuator and to the load cell.

For the mode I case, 6 steel hand-rails have been attached to each plate. The end of each hand-rail has been machined to act as a clamp, where a cylindrical support is attached. This clamping system allows the rotation of the supports to align the top and bottom specimen fixtures. The system has been designed to be stiff enough to support loads up to 5 kN in any of the arms without deflecting significantly.

Over each of the bottom cylindrical supports a load cell of 1.25 kN has been attached. At the same time, each load cell is connected to an adaptor. The adaptor is the component that connects to the clamping system by means of an articulated joint. Another set of 6 cylindrical supports and adaptors has been attached to the upper hand rails. In addition to the rotation, this set allows the vertical displacement, which is controlled by means of a knob located at the end of each upper support. In this way, the zero force can be set individually for each specimen and also the displacement ratio can

be controlled. Schemas of the device and the detail of one of the test arms are shown in figure 5.3.

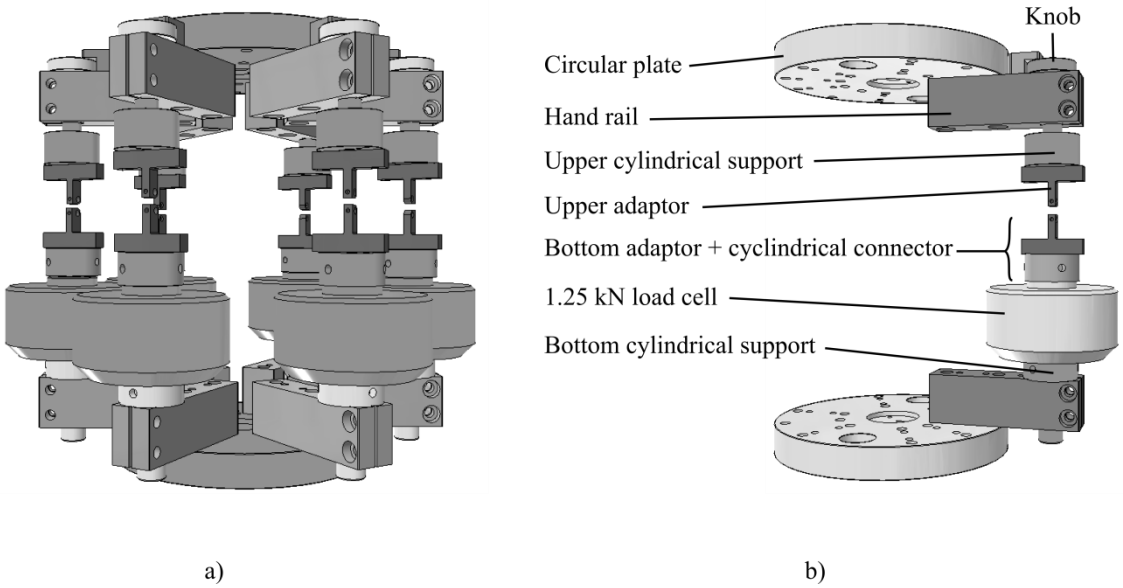

Figure 5.3 Drawing of the multi-fatigue test device (a) and detail of one of the arms (b)

5.2.1.1. Specimen fixture system

In order to have more flexibility in clamping the specimen, a mechanical hinge is used. The fixture system is an evolution of the design presented by the same authors in 2011 (Renart et al. 2011). The mechanism has been proved to be equivalent to the traditional fixture systems defined by the mode I DCB standards (ASTM D5528, ISO 15024, ISO 25217).

The mechanism to fix the specimen works in the same way than in the previous design previously published: a holding grip in the shape of a dovetail. However, the point of rotation has been moved to one of the corners (the closest to the crack front) in order to minimize the stiffening effects induced by the fixture system. Thus, having a mechanical fixture that behaves as a hinge, see figure 5.4.

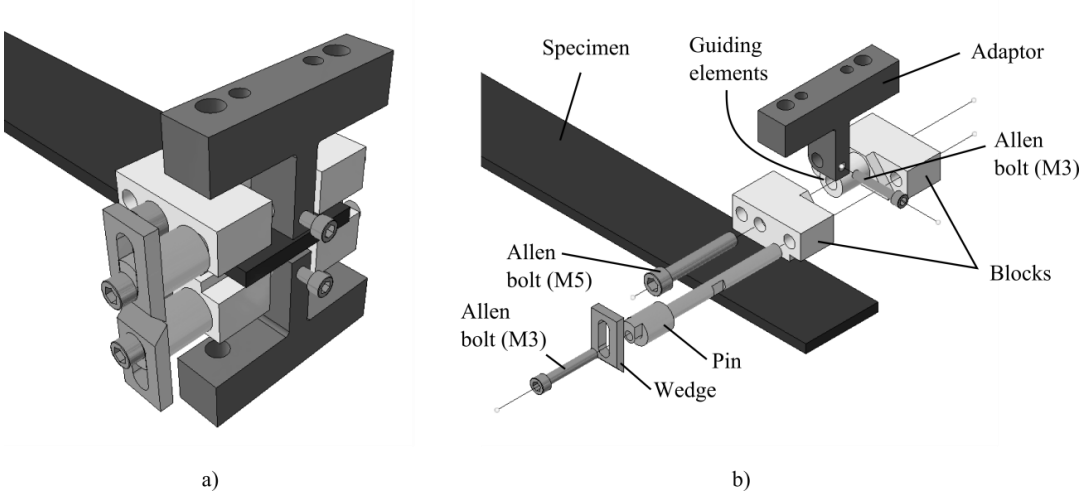

Figure 5.4 Specimen fixture system (a) and breakdown of the mechanism (b)

The pins that articulate the joint between the fixture system and the adaptors have also been redesigned. In order to prevent their release during a cyclic test, they have been fixed to the adaptor with a M3 screw. The pin ends have been machined to allocate a wedge. With this system it is possible to take displacement measurements from an external device, a clip-on-gage extensometer. Figure 5.5 shows the test rig with 6 specimens and the extensometer attached to one of them.

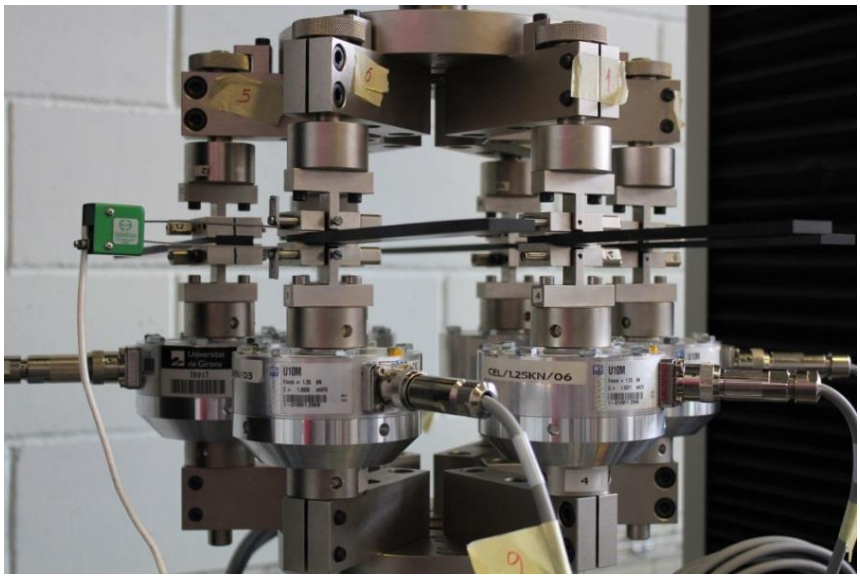

Figure 5.5 Multi-fatigue test devices with 6 specimens and the clip-on-gage extensometer attached in one of them to measure the displacement.

5.2.2. Data acquisition system

The DCB fatigue tests were performed at a loading frequency of 5 Hz and with constant displacement amplitude. During the test, the time, the crosshead displacement, the displacement from the clip on gage extensometer, and the force measured by each load cell were acquired continuously at a frequency of 100 Hz, thus having about 20 data points per cycle. The data acquisition was performed with an external system from HBM (model Quantum MX1615).

On the other hand, the number of cycles and the maximum and minimum crosshead displacement and force applied by the machine were recorded internally at every cycle. These data was synchronized with those from the external acquisition system. This was done with the aim to compare the loads measured in each specimen to the total load applied by the piston.

5.2.3. Determination of the crack length

Monitoring the specimen crack length is essential to obtain the crack growth rate curve (da/dN). It has been found in the literature that the monitoring of the crack length by optical methods is used by a part of the scientific community (Martin et al. 1990, Hojo et al. 2006, Argüelles et al 2008, Kenane et al. 2011, Stelzer et al. 2012, Brunner et al. 2013). However, this method has some drawbacks, such as the reliability of the measurement if taken at the specimen side (Brunner et al. 2009, Sans et al. 2013), and that it requires the use of an optical device capable to provide images with a high magnification and good resolution. It becomes especially difficult when the crack growth is very small, or if this system is pretended to be mounted on a multi-fatigue test rig. The number of devices and the amount of data to be processed make this option unfeasible for industrial purposes.

An alternative method consists on estimating the crack length through the specimen compliance (C). Taking into account the beam theory approach there is a relationship between the compliance (C) and the crack length (a):

$$\mathrm{C}^{1/3} = \mathrm{m} \cdot (\mathrm{a} + \Delta) \tag{5.1}$$

Where Δthe crack length correction is factor, and m is the slope of the curve.

By means of equation (5.1) the evolution of the crack length against the number of cycles can be estimated from the curve of $C(N)$. If the compliance is measured continuously during the test, a continuous curve for $a(N)$ is obtained.

This method, however, requires performing some additional tests at different crack lengths to obtain the relationship between C and a (compliance calibration). Those tests consist of loading and unloading the specimen at a known crack length and measuring the compliance. They can be obtained before or after the fatigue test and they could be static (1 loading cycle) or cyclic (short-cycle fatigue tests) (Renart et al. 2014).

In this work a static compliance calibration was performed. It was done after pre-cracking the specimens and before the fatigue tests. From the pre-crack tests the displacement (δ), the load (F_p) and the crack length (a_p) of the last propagation point were obtained. To perform the compliance calibration, the specimen was loaded and unloaded at different crack lengths: from $a_p - 2$ mm to $a_p - 10$ mm, decrementing the crack length each time by 2 mm. This was possible by sliding the fixtures along the specimen edge to the convenient position. In order to avoid the crack propagation during the compliance calibration tests, the maximum load was set to a 90% of F_p. The curves of the pre-crack test and the calibrations of the compliance for a theoretical test are shown in figure 5.6.

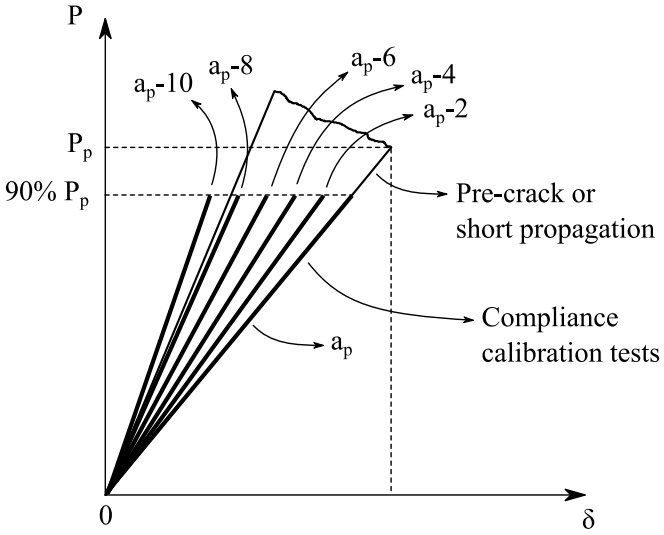

Figure 5.6 Theoretical curves of the pre-crack test and the compliance calibrations

The calibrations were performed individually. The same mechanical clamping system than in the fatigue tests was used.

5.2.4 Test setup

The multi-fatigue device allows testing 6 specimens in to mode I DCB fatigue loading. The specimens are mounted on the fixture in outward direction to avoid interference between them, see figure 5.2a. Despite being subjected to the same displacement range ($\Delta\delta = \delta_{max} - \delta_{min}$), each of them can be tested at a different percentage of energy release rate ($\%ERR$) and/or at a different load level (R).

5.2.4.1 Loading level

The percentage of the energy release rate is obtained by adjusting the initial crack length, a_0, of each specimen. In order to determine this value, the following data is required: the average value of the energy fracture toughness from the static testing campaign, $[G_{IC}]_{av}$, and the crack length correction factor, Δ, of each specimen (obtained from the compliance calibration tests). The percentage of the energy release rate is estimated as:

$$\%ERR = \frac{G_{Imax}}{[G_{IC}]_{av}} \tag{5.2}$$

Being G_{Imax} the maximum level of the energy release rate applied to the fatigue test, which is described by the following equation (ASTM D6115):

$$G_{Imax} = \frac{3P_{max}\delta_{max}}{2B(a+\Delta)} \tag{5.3}$$

Where B is the specimen width, P_{max} and δ_{max} are the maximum cyclic load and displacement respectively (P_{max} obtained at the beginning of the test), a is the crack length and Δ the crack length correction factor.

Expressed in terms of the compliance ($C = \delta_{max}/P_{max}$), equation (5.3) becomes:

$$G_{Imax} = \frac{3\delta_{max}^2}{2BC(a+\Delta)} \tag{5.4}$$

Considering the relationship between the compliance and the crack length, defined in equation (5.1), and isolating the crack length in equation (5.4), we obtain an expression of the initial crack length (a_0) in function of G_{Imax} and the maximum displacement (δ_{max}) at the beginning of the test.

$$a_0 = \left(\frac{3\delta_{max}^2}{2Bm^3G_{Imax}}\right)^{1/4} - \Delta \quad (5.5)$$

Therefore, for an imposed value of the maximum displacement, it is possible to test at different levels of the maximum energy release rate by changing the initial crack length of each specimen (a_0).

This method is valid under two assumptions. The first one is related to the crack length: it was seen that a larger initial crack length causes larger crack propagations (Sans et al. 2013); in this work it is considered that the differences of crack propagation on the specimens will not affect to the results. The second assumption is related to the formulation: the equations are based on a Linear Elastic Fracture Mechanics approach, i.e. a linear relationship between δ_{max} and P_{max} is considered.

It is worth to be mentioned that, due to the fact that the initial value of G_{Imax} is estimated from the average values of the static testing campaign, the test will not be performed at the exact percentage of initial energy release rate. Therefore, G_{Imax} (and thus the $\%ERR$) must be recalculated after the fatigue test with the measured values of P_{max}, δ_{max} and a_0 obtained from each specimen at the beginning of the test. These discrepancy may be attributed to the differences between the crack length measurement at the specimen edge and the real crack length to be accounted in the calculation.

5.2.4.2 Displacement ratio

R is the ratio between the minimum (P_{min}) and peek (P_{max}) loads of the fatigue test. For linear elasticity and small deflections it is identical to the displacement ratio (ASTM D6115):

$$R = \frac{\delta_{min}}{\delta_{max}} \quad (5.6)$$

For the multi-fatigue test, the displacement ratio applied by the machine is identical for all the specimens. However, it is possible to add an additional displacement to each specimen by the rotation of the knob located at the top part of the test fixture, see figure 5.3. This additional displacement can be settled before the test and it can be measured and controlled by a COD attached to the rotation pin between the specimen fixture and the adaptor, see figure 5.7.

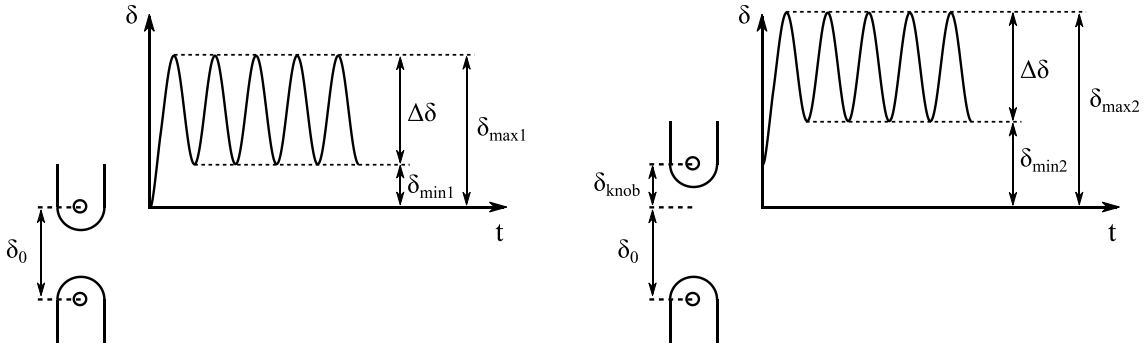

a) no additional displacement

b) additional displacement δ_{knob}

Figure 5.7 Procedure to modify the load ratio (R) by applying an additional displacement with the knob: a) $R_1 = \delta_{min1}/\delta_{max1}$ *and b)* $R_2 = \delta_{min2}/\delta_{max2}$.

The displacement amplitude will be the same but the values of δ_{min} and δ_{max} will change, thus having a different value of R. Table 5.1 summarizes the values of a and δ_{knob} to be applied to the specimens to test at different levels of %ERR and R. The maximum and minimum values of the displacement are the same in all cases, 5 and 0.5 mm respectively. For the calculation, the specimens considered are 25 mm wide, the static energy fracture toughness $G_{IC} = 650\, J/m^2$, and the compliance calibration tests are represented by $m = 0.01$ and $\Delta = 4\, mm$.

R	%ERR	a [mm]	δ_{knob} [mm]	G_{Imax} [J/m²]	G_{Imin} [J/m²]
0.1	30	48.66	0.00	195	19.5
	50	42.35		325	32.5
	70	38.61		455	45.5
	90	36.02		585	58.5
0.3	30	48.66	1.43	195	58.5
	50	42.35		325	97.5
	70	38.61		455	136.5
	90	36.02		585	175.5
0.5	30	48.66	4.00	195	97.5
	50	42.35		325	162.5
	70	38.61		455	227.5
	90	36.02		585	292.5

Table 5.1 Values of the initial crack length of the specimen and the displacement to be applied to the knob in order to test at different levels of the energy release rate and at different ratios of R. Specimen properties considered: width of 25 mm, energy fracture toughness $G_{IC} = 650\, J/m^2$*, and compliance calibration curve* $C^{1/3} = 0.01(a + 4)$

5.2.5 Analysis of the data

The outputs from the experiment are the number of cycles, the displacement applied by the piston and the load measured by each load cell. The frequency of the data acquisition system is much higher than the frequency of the test, 100 Hz and 5 Hz respectively. Therefore about 20 measurements per cycle are collected.

5.2.5.1 Calculation of the dynamic compliance

An average value of the dynamic compliance is estimated every 20 acquired measurements by means of the linear regression of the load-displacement curve within the displacement levels δ_{min} and δ_{max}, see figure 5.8. With this method, the effects of the non-linearities or initial offsets in the results are minimized.

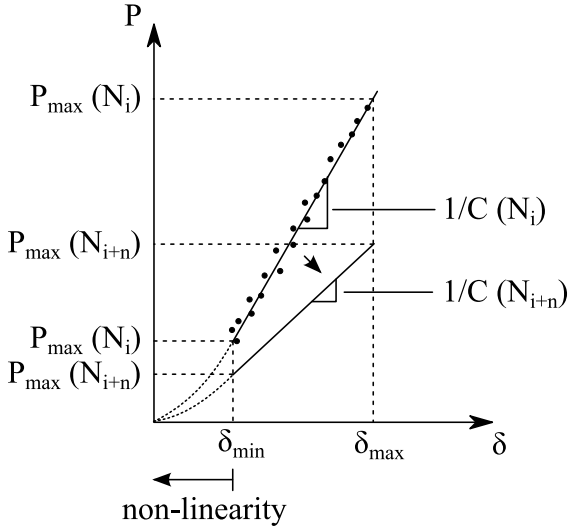

Figure 5.8 Determination of the compliance value from the linear regression of the load-displacement values of one fatigue cycle (20 data points). Comparison between 2 values of the compliance obtained at different number of cycles ($N_{i+n} > N_i$).

As the number of cycles increases the crack extends, and consequently, the stiffness of the specimen decreases. This is traduced in an increase of the compliance against the number of cycles. In DCB fracture tests at constant displacement the compliance tends to stabilize to a certain value, see figure 5.9. This occurs when the crack propagation arrests.

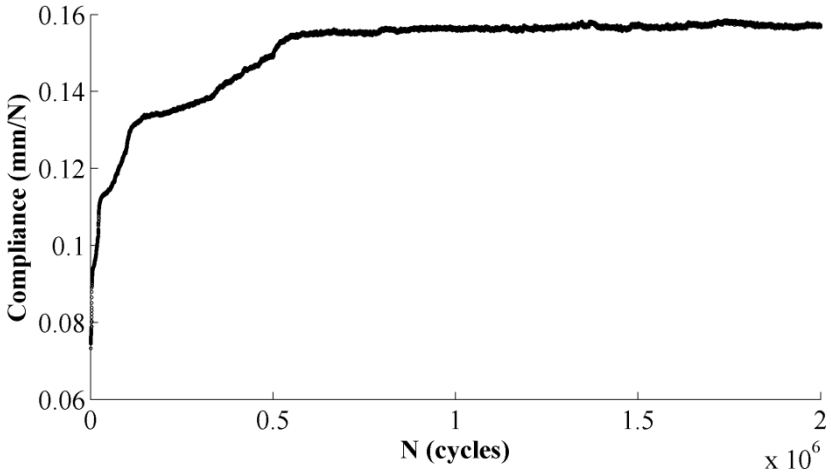

Figure 5.9 Curve of the compliance against the number of cycles of a DCB test: specimen T6DR03 of table 5.4.

5.2.5.2 Determination of the crack growth rate

By means of the linear relationship between $C^{1/3}$ and a expressed in equation (5.1), a continuous curve of a against the number of cycles is estimated from $C(N)$ curve.

The crack growth rate (da/dN) is obtained by the derivative of $a(N)$ curve with respect to the number of cycles. A common methodology is to use a 7-point average method to perform the derivative (Stelzer et al. 2014, ASTM E647). However this methodology can induce large sources of error when being applied to curves with a lot of points because the compliance scatter is bigger than the horizontal distance between the data points.

In this work the derivative has been performed by linear regressions of bigger groups of points. From the experimental results it is observed that in the first cycles there is a large increase of the compliance (and also of the crack length), whereas during the last cycles there is almost no increase of the compliance neither crack growth, see figure 5.9. I.e. in the beginning of the test the compliance increases rapidly in a few cycles, therefore groups with a very few data points need to be used to capture this change; on the other hand the change in compliance is almost imperceptible at a large number of cycles and large groups of points are required. Therefore, the set of points to be fitted must increase as the number of cycles does. The way in which the points are grouped is obtained from the curve of the compliance against the number of cycles.

First of all the data points have been adjusted to a potential curve such as:

$$C = c_1 N^{c_2} + c_3 \tag{5.7}$$

Where c_1, c_2 and c_3 are the adjustment parameters. This fitting is only used to determine the length of the collection of points to be eventually fitted by means of a linear regression to get da/dN. It is worth to be mentioned here that the $C(N)$ curve has an asymptotic behaviour, i.e. it should be adjusted with an exponential curve such as $C = c_1(1 - c_2 e^{-c_3 N})$. However it has been proved that, in this case, potential curves provide better adjustments, especially in the initial set of data points, and they offers the best distribution of the group of points.

Once determined the adjustment coefficients, equation (5.7) is differentiated and a new curve of dC/dN against the number of cycles is obtained, see figure 5.10.

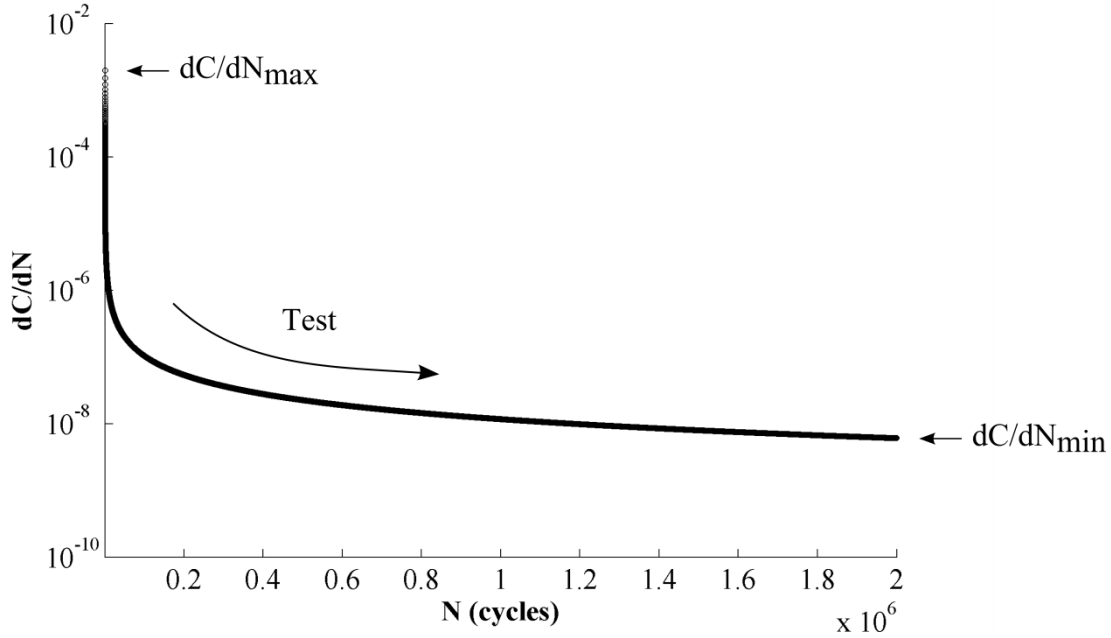

Figure 5.10 Curve of dC/dN against the number of cycles obtained from the derivative of the potential law $C = c_1 N^{c_2} + c_3$ ($c_1 = 0.1047$, $c_2 = 0.0534$ and $c_3 = -0.0651$): specimen T6DR03. dC/dN is represented in logarithmic scale for a better plot of the curve. The arrow indicates the evolution of the test (increase of the compliance).

Next, a relationship between the grouping of points and dC/dN is obtained. The size of the group is delimited by the number of cycles, therefore the parameter is referred to as ΔN. It has been experimentally observed that an asymptotic relationship between ΔN

and dC/dN is required in order to represent a curve of da/dN with small scatter. In this relationship, the size of the group is inversely related to the value of dC/dN, see figure 5.11, and it can be represented with the following equation:

$$\Delta N = \frac{c_4}{\frac{dC}{dN} + c_5} \tag{5.8}$$

Where c_4 and c_5 are adjustment coefficients that can be determined by delimiting the size of the groups (i.e. by defining the values of ΔN_{min} and ΔN_{max}):

$$c_4 = \Delta N_{min}\left(\left(\frac{dC}{dN}\right)_{max} + c_5\right) \tag{5.9}$$

$$c_5 = \frac{\Delta N_{min}(dC/dN)_{max} - \Delta N_{max}(dC/dN)_{min}}{\Delta N_{max} - \Delta N_{min}} \tag{5.10}$$

The values of dC/dN_{max} and dC/dN_{min} are delimited by the results of equation (5.7). It has been observed that the values of $\Delta N_{min} = 2$ and $\Delta N_{max} = 2000$ provided a good grouping of the points, i.e. a number of points enough to represent a continuous curve with low scatter.

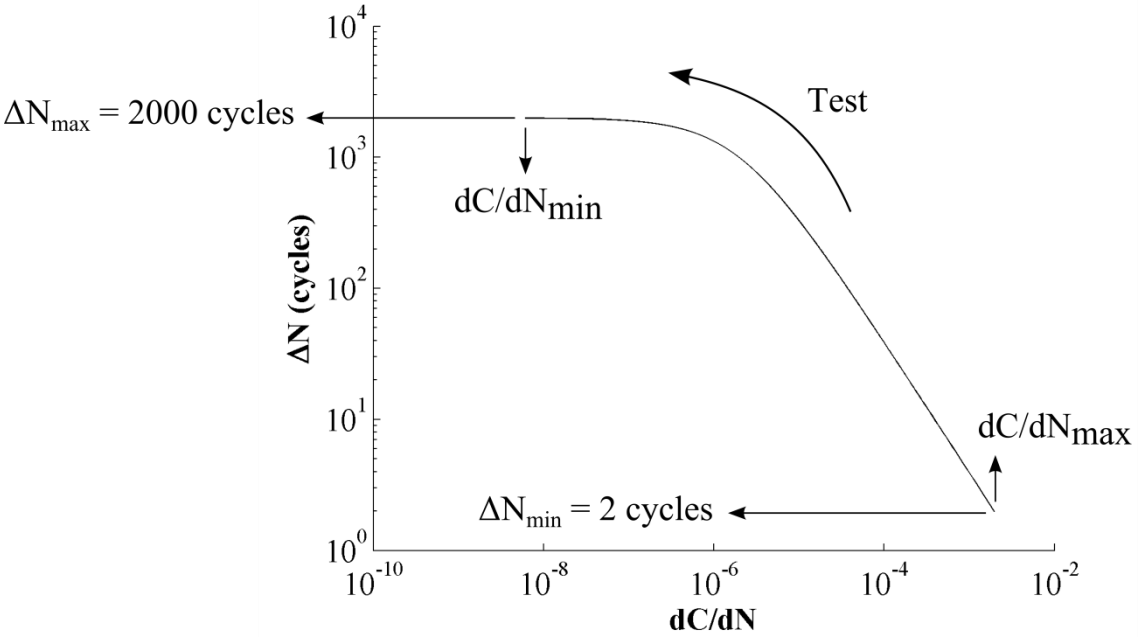

Figure 5.11 Curve of ΔN against dC/dN represented by equation (8), $c_4 = 3.957 \cdot 10^{-3}$ and $c_5 = 1.972 \cdot 10^{-6}$, specimen T6DR03. The curve is represented in log-log scale for a better plot. The arrow indicates the evolution of the test (increase of the compliance).

Finally, the data of $a(N)$ curve is grouped in the same intervals of ΔN_i, and a linear regression is performed at this intervals to obtain the crack growth rate, da/dN against the number of cycles, N.

5.2.5.3 Determination of G_{Imax}

For each cycle, the maximum value of the mode I energy release rate (G_{Imax}) is determined according to the Corrected Beam Theory data reduction method (ASTM D6671), see equation (5.3). One value of G_{Imax} is obtained for each cycle. However, in order to relate this parameter to the crack growth rate, the value of G_{Imax} is averaged for each group of pointsΔN_i.

5.3 Experimental validation

An initial test campaign to validate the multi-fatigue test device and the procedure was carried out. The validations consisted on providing evidence that the displacements were properly applied to the specimens and that the load was correctly measured. In relation to the displacement, it was verified that the deflection did not change during the fatigue test (after a large amount of cycles) due to plays between the components. In relation to the force, it was verified that the total force measured by the machine corresponded to the sum of the forces measured in each specimen.

These tests were performed in a MTS 858 servo-hydraulic testing machine. The frequency was 5 Hz and load ratio for all the specimen was set to R = 0.1. Constant displacement amplitude was applied during all test, the maximum displacement was set to 5.8 mm and the minimum to 0.58 mm. The tests were stopped after 2.5 million cycles.

The specimens tested where composite coupons with the following dimensions: 200 mm long, 25 mm wide and 6 mm thick. A Teflon insert was located at one of the specimen ends in order to create an artificial crack. The length of the insert was 60 mm. The specimens were made of AS4/8552. These tests were run in a controlled environment (23±3ºC and 50±5% RH).

5.3.1 Displacement verification

The displacement of each specimen was measured by connecting an external clip-on-gage extensometer to the pin of the clamping system, see figure 5.5. The displacement acquired from the extensometer was compared to the crosshead displacement applied by the testing machine.

The measurements were performed every certain number of cycles. The procedure consisted of stopping the fatigue test, clamping a clip-on-gage extensometer in one of the specimens, and then performing a short 500 cycle fatigue test without removing the rest of the specimens. For this specimen, the maximum and minimum values of the displacement were averaged and compared to those measured by the crosshead. The process was repeated for the rest of the specimens and, once finished, the fatigue test continued until the next measurement. The displacement verification was done for the specimens located at positions 1, 3, 4 and 6 of figure 5.2a. The values of the maximum displacement and the amplitudes of each of the measurements are listed in table 5.2.

N (cycles)		$2.35 \cdot 10^4$	$2.85 \cdot 10^5$	$7.5 \cdot 10^5$	$1.55 \cdot 10^6$	$2 \cdot 10^6$
Crosshead	δ_{max} (mm)	5.74	5.74	5.74	5.74	5.74
	$\Delta\delta$ (mm)	5.11	5.11	5.11	5.11	5.11
Specimen 1	δ_{max} (mm)	5.77	5.60	5.72	5.71	5.73
	$\Delta\delta$ (mm)	5.11	5.06	5.04	5.02	5.02
Specimen 3	δ_{max} (mm)	5.73	5.57	5.57	5.57	5.58
	$\Delta\delta$ (mm)	5.10	5.10	5.11	5.11	5.11
Specimen 4	δ_{max} (mm)	5.77	5.55	5.55	5.53	5.53
	$\Delta\delta$ (mm)	5.06	5.05	5.06	5.06	5.06
Specimen 6	δ_{max} (mm)	5.75	5.58	5.59	5.58	5.58
	$\Delta\delta$ (mm)	5.11	5.11	5.12	5.12	5.11

Table 5.2 Values of the maximum displacement (δ_{max}) and the displacement amplitude ($\Delta\delta$) measured by the crosshead and the external clip-on-gage extensometer. The external measurements were taken on the specimens located at positions 1, 3, 4 and 6 of the test device.

From the results of table 5.2 it is observed that the displacements measured with the clip-on-gage extensometer are very similar to the displacement imposed by the crosshead. The error is less than 4% in all of the cases. The same occurs with the displacement amplitude, being the error less than 2%. It is also observed that the

maximum displacement measured by the extensometer decreases during the first measurements and then it keeps constant during the rest of the test; the amplitude keeps constant during the whole test. This change on the maximum displacement may be attributed to a thermal effect. During the first two hours there is a heating of the hydraulic oil that expands the length of the actuator (Renart et al. 2014).

5.3.2 Load verification

Each load cell measures a different maximum load that depends on the specimen (dimensions and material), the energy release rate level (initial crack length) and the load ratio (R=$\delta_{min}/\delta_{max}$). The total load applied by the machine should be the sum of the loads of all the load cells. The difference between them should be as small as possible, which means that the load applied is fully transferred to the specimen and not lost by friction effects.

This comparison was performed at the same number of cycles than the displacement verification. The results are shown in table 5.3. The difference between the total load and the sum of each load cell was less than 0.5%. Therefore, it can be assured that all the force applied to the device was transferred to the specimens.

N (cycles)	$2.35\cdot10^4$	$2.85\cdot10^5$	$7.5\cdot10^5$	$1.55\cdot10^6$	$2\cdot10^6$
Specimen 1	60.75	55.15	53.28	52.17	51.48
Specimen 2	54.50	49.14	47.45	46.22	45.83
Specimen 3	52.85	48.47	46.71	45.59	45.06
Specimen 4	59.37	54.40	52.80	51.63	51.18
Specimen 5	59.81	53.59	51.91	50.60	49.77
Specimen 6	59.80	55.00	53.29	52.19	51.64
Σ specimens	347.08	315.75	305.42	298.40	294.96
Piston	346.34	314.84	305.83	299.06	296.03
Error	-0.21%	-0.29%	0.13%	0.22%	0.36%

Table 5.3 Comparison between the sum of maximum loads (P_{max}) measured by each load cell and the force applied by the piston.

5.4 Example results and discussion

Once the multi-fatigue test device was validated, a batch of six specimens was tested. As results, the onset and crack growth rate curves were obtained.

The specimens tested were co-bonded joints between composite adherends. The pre-cured panel was a carbon fibre [0/90] fabric. The "wet" layup was another carbon fibre [0/90] fabric. As bonding agent, an adhesive film was used. The total stacking sequence was ($[0/90]_7$/Adh/$[0/90]_7$), being Adh the adhesive layer. The layup on the left corresponds to the pre-cured panel and the sequence on the right to the "wet" layup. The stacking sequence was chosen to have a total specimen thickness of 3 mm. The rest of the dimensions were 150 mm long and 25 mm wide. In order to create an artificial crack, a Teflon insert was placed at one of the ends in the specimen mid-plane. The thickness and the material of this insert fulfilled the requirements of the AITM1-0053 test procedure from Airbus. The specimens were pre-cracked before the fatigue test.

The tests were run in a MTS 858 (Bionix) servo-hydraulic machine in which the multiple fatigue test device was mounted. The multiple fatigue tests were performed at 5 Hz and the run-out was set to 2.5 million cycles. The same load ratio was applied to all the specimens, $R = 0.1$, by imposing the same displacement range for all the specimens: $\delta_{max} = 5\ mm$ and $\delta_{min} = 0.5\ mm$. Each specimen was tested at a different percentage of energy release rate (%ERR): from 40% to 90% increasing it by 10%. The set-up for each specimen is summarized in table 5.4.

Specimen	R	% ERR	δ_{max} (mm)	δ_{min} (mm)	Δ [mm]	m	$[G_{IC}]_{av}$ [J/m^2]	B [mm]	a [mm]	G_{Imax} [J/m^2]
T6DR03	0.10	90	5.0	0.5	0.88073	0.01067	682.04	25.11	36.5	613.83
T6DR05		80			3.40638	0.01067		25.05	35.5	545.63
T6DR07		70			1.39003	0.01078		25.10	38.5	477.43
T6DR02		60			2.40700	0.01014		25.09	41.0	409.22
T6DR04		50			2.29263	0.01075		25.04	41.0	341.02
T6DR06		40			0.16017	0.01076		25.13	45.5	272.82

Table 5.4 Initial crack length (a) of each specimen to reach the desired level of the energy release rate (%ERR) to be applied to the test. δ_{max} and δ_{min} are the maximum and minimum displacements applied to the specimens, Δ and m are the correction parameters obtained from the compliance calibration, $[G_{IC}]_{av}$ is the average value of

the energy fracture toughness from the static tests, B is the specimen width and G_{Imax} the energy release rate applied to each test.

In order to calculate the level of energy release rate to be applied, the specimen width (B), the values of Δ and m from the compliance calibration and the average value of the mode I energy fracture toughness ($[G_{IC}]_{av}$) from the static tests were used. G_{Imax} is the estimated initial maximum value of energy release rate applied to the test.

5.4.1 Onset curve

Only methods based on the increase of the compliance have been used to represent the onset curves. Three criteria have been taken into account: a 1% and a 5% increase of the compliance, as it is required in standard ASTM D6671, and an intermediate value, a 2% increase.

The increase of the compliance is measured from the curve of the compliance against the number of cycles. For the specimen T6DR03 this curve is shown in figure 5.12.

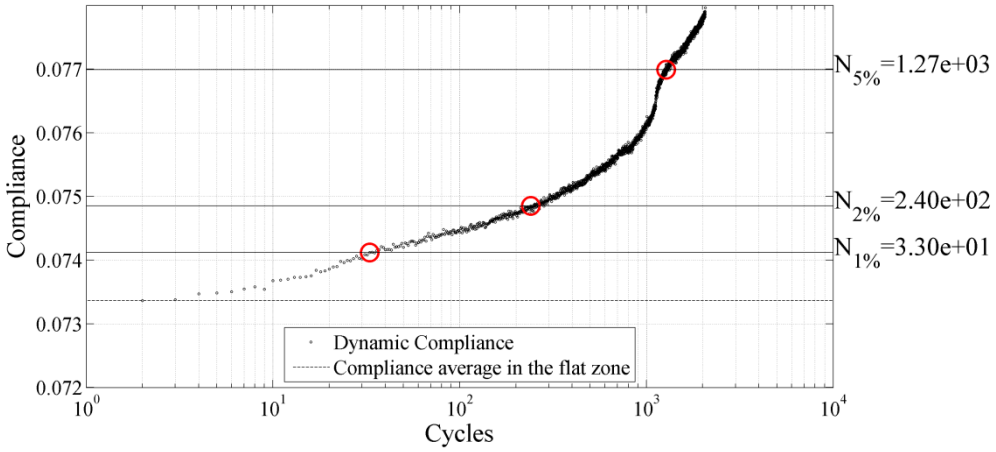

Figure 5.12 Curve of the compliance against the number of cycles of specimen T6DR03 ($\%ERR = 90\%$, $R = 0.1$). The curve indicates the number of cycles for which the compliance increases a 1%, 2% and 5%. The compliance at N = 2 cycles has been taken as the reference value.

The results of the six specimens tested in the multiple fatigue test device are summarized in table 5.5. The value of G_{Imax} obtained from the test data (equation (5.3)) and the recalculated percentage of the energy release rate that has been applied ($G_{Imax}/[G_{IC}]_{av}$) are also included.

Specimen	R	Initially set by the user		$[G_{IC}]_{av}$ (J/m^2)	Re-calculated from the test data	Onset of propagation (cycles)		
		% ERR	G_{Imax} (J/m^2)		$G_{Imax}/[G_{IC}]_{av}$ (%)	$N^{1\%}$	$N^{2\%}$	$N^{5\%}$
T6DR03	0.1	90	521.77	682.0	77	33	240	1270
T6DR05		80	480.96		71	93	199	1457
T6DR07		70	407.49		60	121	335	1852
T6DR02		60	286.48		42	12963	97510	151084
T6DR04		50	281.58		41	4129	12951	1259492
T6DR06		40	203.93		30	> 2500000	> 2500000	> 2500000

Table 5.5 Number of cycles at which the compliance increases at 1%, 2% and 5%. The table includes the percentage of energy release rate (%ERR) and the value of G_{Imax} imposed in each test, and the percentage of the energy release rate recalculated from the test data with equation (5.3) ($G_{Imax}/[G_{IC}]_{av}$).

The onset curve obtained with the three criteria is shown in figure 5.13.

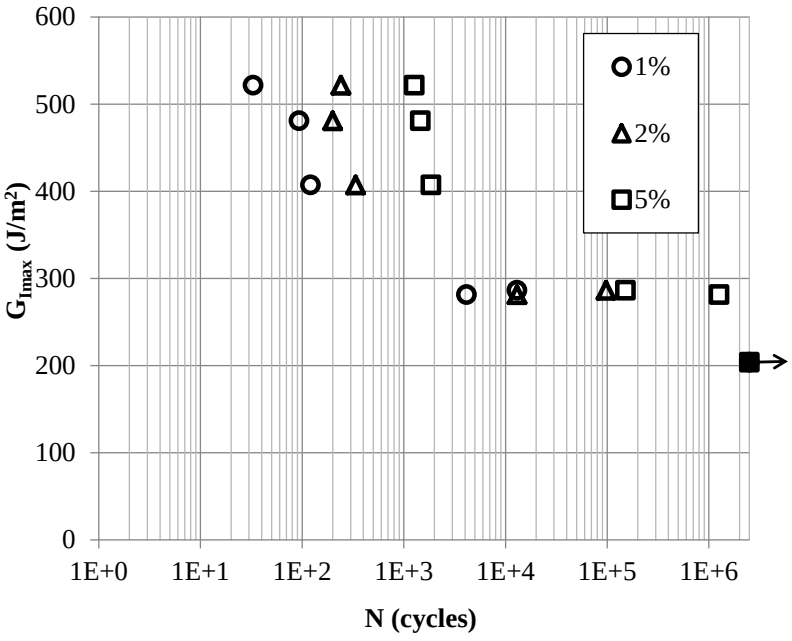

Figure 5.13 Onset propagation curve including the three criteria based on the 1%, 2% and 5% increase of the compliance. At %ERR = 30% the crack did not propagate and the test was run out after 2.5 million cycles. This is indicated with a black point and an arrow.

In most of the specimens, as the %ERR increase; the number of cycles that is required to reach the onset of crack propagation decreases, as expected. However the 1% and 2% criteria have some points in which this tendency is not satisfied. This occurs with the specimen with the highest percentages of ERR, where the onset occurs at a very few number of cycles; and also between specimens with similar ratios of $G_{Imax}/[G_{IC}]_{av}$. In both cases the results could be influenced by the material properties.

According to the 2% and 5% onset criteria, in specimen T6DR06 the propagation did not occur even after 2.5 million cycles. It was considered that the crack would not propagate beyond this point.

From the comparison between the criteria, it is observed that there is a lot of difference in the number of cycles at which the onset of the propagation occurs. In some cases this difference is larger than a decade (e.g. specimen T6DR04). In all the tests the 1% is the more conservative criterion, whereas the 5% is the less restrictive. In most of the tests the 1% increase of the compliance is reached after a very few number of cycles (for example: N = 33 for specimen T6DR03), therefore a methodology to continuously record the compliance during the test is essential to obtain the data for this criterion. On the other hand the 5% criterion is the less restrictive but provides a robust incremental relationship between the energy release rate applied and the number of cycles at which the onset of propagation occurs. The authors consider this criterion the best option for comparison purposes.

Finally, there is a difference between the expected percentage of ERR and the value obtained from the test (ratio $G_{Imax}/[G_{IC}]_{av}$). The latter is always smaller than the initial imposed value. These differences may be attributed to errors in the measurement of the crack length. Due to the meniscus shape of the crack front, what is measured at the specimen sides does not correspond to the real crack length. In any case, a direct relationship between the applied percentage of ERR and the measured values has been obtained.

5.4.2 Crack growth rate curve

The crack growth rate curves of each of the 6 specimens are represented in figure 5.14. They are shown in descending order according to the level of energy release rate applied to the test.

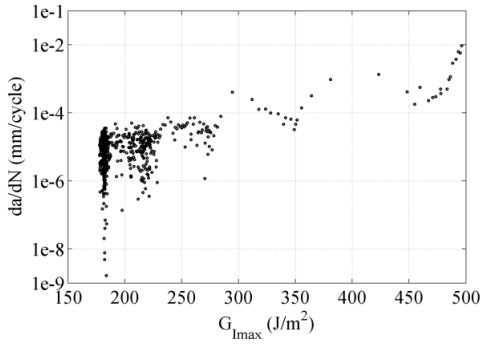

a) T6DR03 (%$ERR = 90\%$)

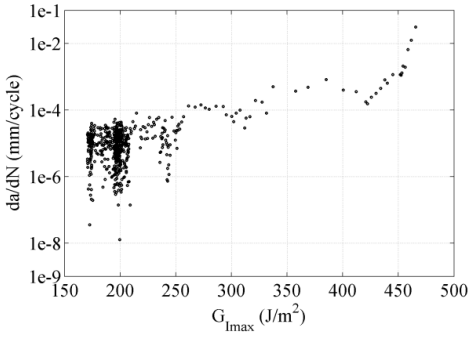

b) Specimen T6DR05 (%$ERR = 80\%$)

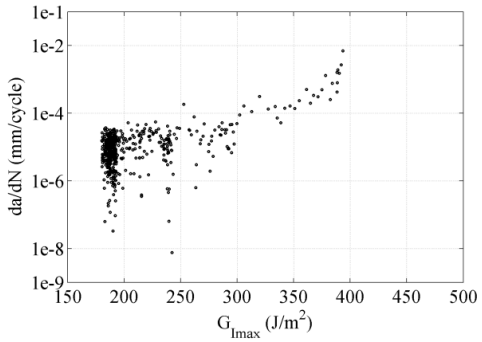

c) T6DR07 (%$ERR = 70\%$)

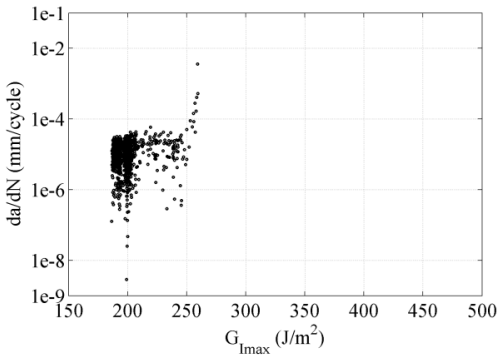

d) T6DR02 (%$ERR = 60\%$)

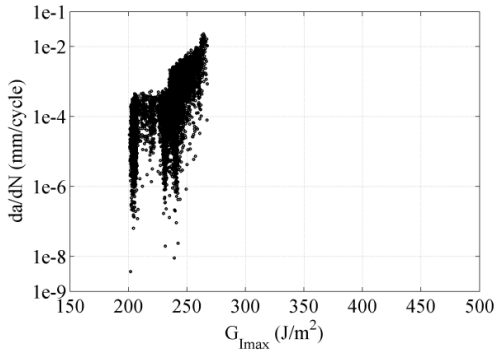

e) T6DR04 (%$ERR = 50\%$)

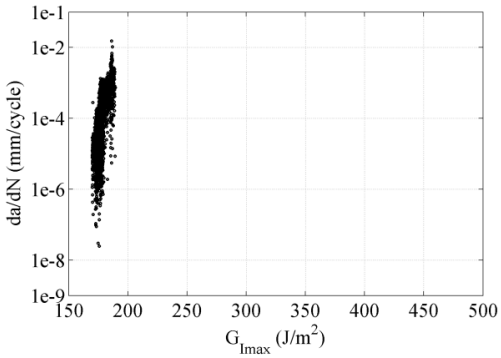

f) T6DR06 (%$ERR = 40\%$)

Figure 5.14 Individual crack growth rate curves of each specimen (%ERR refers to the percentage of energy release rate applied to the test)

Following the methodology described in this chapter it is possible to obtain an almost continuous representation of the crack growth rate along to 6 decades (from values of 10^{-2} to 10^{-8}). The curves with the highest values of ERR start at higher levels of G_{Imax}. The three regions shown in figure 5.1 are clearly visible. However regions II (linear region) and III (fast crack growth regions) do not correspond with what was initially expected. In region II the crack growth does not propagate in a steady state manner but it advances in jumps. In relation to region III, in all the specimens (even in those tested at the lowest percentages of ERR: 40%, 50% or 60%) there is a region of fast crack propagation. This is clearly shown in figure 5.15 where all the curves are represented in a single figure. In region III the values of G_{Imax} are much more small than those that cause a fast crack grow. This initial region may be attributed to a change of the state of the crack front during the fatigue test.

All the details belonging to the results of the fatigue test curves are discussed in detail in chapter 6 together with the results of all the adhesive joint configurations.

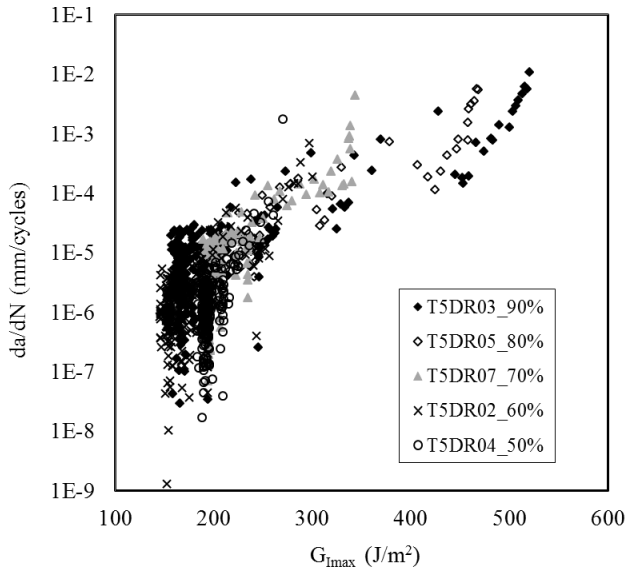

Figure 5.15 Fatigue crack growth rate curve versus the maximum strain energy release rate (G_{Imax}) of all the six specimens.

In relation to the results of figure 5.15 it is observed that all the curves represent the same behaviour. The specimens with the highest values of energy release rate are capable to reproduce almost the whole curve, whereas the specimens with the lower percentages only reproduce the last part (region of crack arrest and a part of the linear

region represented by the Paris law). In any case the continuity of the curve is clearly observed.

Regarding to the threshold values there are significant differences within the specimens. From the visual inspection before and after the tests these may be attributed to the shape of the crack front. This topic is discussed in detail in chapter 6.

5.5 Conclusions

A method for multiple-fatigue testing under displacement control has been developed. The design and the test procedures have been adapted to DCB fatigue tests, although other interlaminar tests can be implemented. The device allows testing at different levels of energy release rate and load ratios. This is achieved by clamping the specimen at different crack lengths and by the adjustment of the initial displacement applied to the specimen. The method also allows the continuous monitoring of the compliance during the test, thus, providing continuous curves of the evolution of the compliance against the number of cycles and continuous crack growth rate curves. The precision of the method is 1 cycle. The crack length is estimated from an independent compliance calibration.

The device has been verified by means of displacement and force measurements. The displacement measured in each specimen has been compared to the displacement applied by the testing machine. This verification has been performed during a 2.5 million cycle real test. Errors less than 4% were obtained, indicating that the device is stiff enough to transmit the displacement from the machine to the specimen. On the other hand, the force measured by each load cell has been compared to the total force applied by the machine. Errors of less than 1% were obtained, indicating that all the force applied is transmitted to the specimen, and that there is no loss of force due to friction between the subcomponents.

Finally an experimental test campaign has been conducted in order to obtain results of the onset of propagation and crack growth rate curves. A full onset curve was obtained from the six specimens with ratios of $G_{Imax}/[G_{IC}]_{av}$ from 40% to 80%. Different criteria for the determination of the onset point were considered, all of them based on the increase of the compliance: 1%, 2% and 5%. Large differences between the onset cycles predicted by each criterion were obtained, being 1% the most restrictive and 5%

the less one. The continuous monitoring of the compliance allowed determining the onset number of cycles for the specimens with the higher values of ERR. This occurred at a very few number of cycles (N = 33 cycles for specimen T6DR03). The criterion of 5% was proven to provide the most robust relationship between the energy release rate applied and the onset number of cycles. Therefore the 5% onset criterion was considered at this stage for comparative evaluation of the different adhesive joint configurations.

In relation to the fatigue crack growth rate, continuous curves of da/dN against G_{Imax} were obtained. The curves covered almost the full range of the crack growth rate (more than 8 decades, from 10^{-1} to 10^{-8}). A continuity in the results between specimens tested at different %ERR was obtained.

From the results of the testing campaign it is clearly demonstrated that the device is capable to test 6 specimens in one run and to provide results of onset and crack growth rate curves with the same level of precision than a single station. This makes this device especially useful for large fatigue testing campaigns.

Chapter 6

Effect of pre-bond moisture in co-bonded joints under fatigue loads

6.1 Introduction

Composite structures in service experience damage that comes from accidental impacts, mechanical stresses, environmental factors (moisture and temperature), etc. (Hu et al 2000; Cheng et al. 2011). Structural maintenance and repair is the most feasible solution, as replacing the entire component is not cost effective in many cases (Armstrong et al. 2005). Repair operations in composite aircraft structures should guarantee that the resulting parts maintain the structural integrity of the pristine component. This includes the static strength, damage tolerance and fatigue durability. The bonded joint between the structure and the patch is the most critical part of the repair and the evaluation of its behaviour under fatigue loading is very relevant. In fatigue loading, a structure may fail at small percentage of the static strength. Therefore, fatigue analysis and fatigue strength predication are highly required especially for the case of fail-safe or damage tolerance design. This behaviour is characterized by the onset and crack growth rate curves.

In the revision of the state of the art (chapter 2) and in the subsequent chapters (3 and 4), it has been seen that the environmental effects have high importance on the behaviour of adhesive joints under quasi-static loading. This also occurs in fatigue tests.

On the one hand, the hygrothermal effects change the properties of the adhesive joint. Most of the authors have been observed that the performance of the joint under fatigue decreases with the increase of the immersion time in water (Adams et al. 1984, Ferreira et al. 2002, Ferreira et al. 2007). The same tendency is observed in specimens exposed to hot/wet conditions similar to those which aircrafts experience during the service life (John and Buthus 1998, Chalambrides et al. 1998).

On the other hand, in the case of bonded joints for structural repairs, the influence of the pre-bond moisture in the pre-cured adherends must be taken into account. Few studies have been reported its effect on the mechanical properties, but there is not a clear

consensus on the results. From the revision of the state of the art it is observed that a small amount of pre-bond moisture (0.5% w/w) appears to have little effect on the strength of the repair, and large amounts up to 1.3% w/w causes a decrease in the tensile strength. However this is not a general tendency for all the adhesives.

In fact, the work presented in chapter 3 concludes that the pre-bond moisture decreases the performance of the joint. The presence of absorbed moisture in the adherend affects to the failure mode and thus to the value of the mode I fracture toughness (G_{IC}). In any case, these studies are carried out only under static testing and, as per the knowledge of the author; there is no study of the effect of pre-bond moisture under fatigue loading.

In this chapter, an experimental study of pre-bond moisture effects on co-bonded joints under fatigue loading is presented. The analysis is focused on the onset of propagation and the crack growth rate (da/dN) of DCB specimens. The tests have been run according to the methodology described in chapter 5. First, the details of the experimental testing campaign are described and then the results obtained are presented and discussed. In addition, the particularities of the onset and crack growth rate curves for this kind of specimens are analysed.

6.2 Experimental methodology

6.2.1 Materials and specimen preparation

The experimental study has been carried out with two different adhesive films, denoted by F1 and F2. The adhesives were epoxy films with an embedded carrier. The same specimens than in chapters 3 and 4 have been tested: adhesive co-bonded joints. The pre-cured and the co-bonded repair materials are $[0/90]_n$ plain weave carbon fabric epoxy pre-pregs. The pre-cured panel was cured in autoclave at 180ºC in a first cycle, and then the repair was cured together with the adhesive at 120ºC.

Before performing the second curing cycle, the CFRP substrates were immersed in distilled water at constant temperature of 70°C for 336±12 hours to promote moisture uptake. Then, the adherends were dried at 80°C for 1 hour and 24 hours after immersion, having moisture content in the adherend of 1.25% and 0.33% respectively. From the panels, specimens with a width of 25 mm and a length of 145 mm were cut,

with an initial pre-crack of 60 mm. The same non-destructive inspections than in chapters 3 and 4 were conducted for these specimens.

6.2.2 Testing

6.2.2.1 Quasi-static tests

Prior to fatigue testing, each specimen was tested individually under static loading. The reason to perform these tests was to provide values of G_{IC} in order to establish the energy release rate to be applied to the fatigue tests.

After pre-cracking the specimens, short propagation DCB tests were performed according to ISO 15024 standard with a MTS Insight testing machine and a 1 kN load cell. The tests were run at a crosshead rate of 5 mm/min in a laboratory controlled environment (23±2°C, 50±5% RH). They were stopped when the propagation reached 15 mm. In most of the specimens there was stick-slip, and the final crack length extended beyond this point.

The initial crack length was measured only at the beginning and at the end of the test with a microscope. The values of the force and the displacement were recorded continuously during the test. Only initiation values were taken into account, and among them the NL point was used. The data was analysed to determine the fracture toughness energy G_{IC} using the Corrected Beam Theory data reduction method. The results of the initiation values of G_{IC} according to the NL are listed in table 6.1. Only the average values for each batch are provided.

Batch	Substrate Condition	$[G_{IC}]_{av}$ (J/m^2)
T5DR	0% pre-bond moisture / Adhesive F1	644.34
T6DR	0% pre-bond moisture/Adhesive F2	682.04
T1DR	0.33% pre-bond moisture/Adhesive F1	713.71
T2DR	0.33% pre-bond moisture/Adhesive F2	677.75
T9DR	1.25% pre-bond moisture/Adhesive F1	364.25
T10DR	1.25% pre-bond moisture/Adhesive F2	432.82

Table 6.1 Initiation values of G_{IC} according to the NL point. Average values of each batch. Data reduction method: Corrected Beam Theory.

There is good reproducibility between the results of table 6.1 and those obtained in chapter 3, the only exceptions are specimens with adhesive F1 and with 0.33% and

1.25% pre-bond moisture. In the first case the value obtained is slightly above the values shown in figure 3.7, and in the latter case the values are slightly below. For the rest of the cases the values are inside the margins established by the standard deviation and in some cases they are almost coincident (e.g. F1 adhesive with 0% pre-bond moisture).

6.2.2.2 Compliance calibration tests

Instead of measuring the crack length during the fatigue test, it was estimated from compliance calibration tests. The calibrations were performed after the quasi-static tests and just before starting the fatigue testing campaign.

The compliance calibration tests were used to estimate the crack length and the level of energy release rate to be applied to each specimen when tested in fatigue.

The calibrations were performed according to the procedure described in section 5.2.3. Loading and unloading tests were performed at specimen crack lengths from a_p to $a_p - 10$, being a_p the final crack length after the quasi-static tests. In order to not cause propagation during the calibrations, the force applied was limited to the 90% of the force measured at the last propagation point of the quasi-static test. The following linear relationship between $C^{1/3}$ and a was considered:

$$\mathrm{C}^{1/3} = \mathrm{m} \cdot (\mathrm{a} + \Delta) \tag{6.1}$$

Where m and Δ are the adjustment parameters.

6. 2.2.3 Fatigue tests

The fatigue tests were performed after the short DCBs and the compliance calibrations. Six specimens were tested in a single station and mounted on each load cell as shown in figure 6.1. The cyclic fatigue tests were run in an MTS servo hydraulic machine. They were performed under displacement control at a frequency of 5 Hz, and at a load ratio R=0.1. Each specimen was tested at a different energy release rate percentage from 90% to 40%. To set the ERR, the initial crack length of the specimen was changed, the following equation was used:

$$a_0 = \left(\frac{3\delta_{max}^2}{2Bm^3 ERR[G_{IC}]_{av}}\right)^{1/4} - \Delta \tag{6.2}$$

Being B the specimen width, δ_{max} the maximum displacement applied during the fatigue test, $[G_{IC}]_{av}$ the average value of the mode I energy fracture toughness obtained from the quasi-static tests, and ERR the energy release rate percentage applied before the test by the user.

The run out was set to 2.5 million cycles in order to determine a threshold value. The maximum and minimum displacements applied during fatigue test were the same for all the specimens, 5 mm and 0.5 mm respectively. The load was measured individually at each specimen by means of 6 load cells of 1.25 kN that were attached to the 6 specimens. The fatigue tests were conducted in a laboratory controlled environment (23± 2°C, 50±5%RH). The load-displacement data of each specimen was acquired from each load cell with an external data acquisition system. This data was acquired together with the number of cycles.

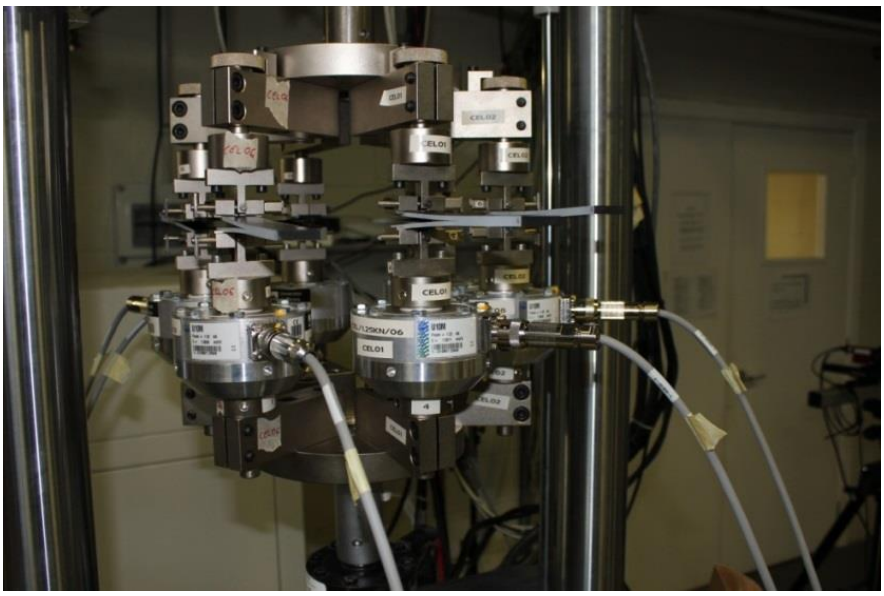

Figure 6.1 Multi-fatigue test device for testing 6 specimens at the same time

The methodology and the data reduction processes to obtain the onset and crack growth rate curves are detailed in chapter 5.

For the onset of propagation, three different criteria were taken into account: the 1%, 2% and 5% increase of the compliance with respect to the initial value. As the initial value, the compliance was measured and averaged in the first cycles of the test. The number of cycles at which the compliance increased a 1%, 2% and 5% was represented against the maximum value of the energy release rate measured from the test, G_{Imax}.

This latter value was calculated from the Corrected Beam Theory data reduction method:

$$G_{Imax} = \frac{3P_{max}\delta_{max}}{2B(a_0+\Delta)} \quad (6.3)$$

Being P_{max} and δ_{max} the maximum load and displacement applied during the first cycle respectively, B the specimen width, a_0 the initial crack length, and Δ the crack length correction parameter obtained from the compliance calibration tests.

Regarding to the crack growth rate curve, first a relationship between the crack length (a) against the number of cycles (N) was obtained. The crack length was estimated from the curve of the compliance versus the number of cycles and the compliance calibration tests. The continuous curve of $a(N)$ was differentiated with respect to the number of cycles (N) in order to obtain the crack growth rate (da/dN). The method to perform the derivative is based on grouping the data, and it is detailed in section 5.2.5.2.

Finally, the crack growth rate was represented against G_{Imax}. The maximum energy fracture toughness was calculated from equation (6.3), but taking P_{max} and δ_{max} as the maximum values of force and displacement of each cycle, respectively, and instead of the initial value (a_0), the crack length at each cycle (a) was used in the calculation.

6.3 Results and Discussion

The fatigue testing campaign involves the analysis of two adhesive joint configurations (with F1 and F2 adhesives) and three pre-bond moisture conditions in the adherends (0%, 0.33% and 1.25%). For each condition a batch of 6 specimens was tested. The six specimens of each batch were tested at different percentages of energy release rate, from 40% to 90%. The tests were performed in the multi-fatigue testing device. All the specimens tested and the test configurations are listed in table 6.2.

Adhesive	Batch	Adherent condition	%ERR	Specimen
F1	T5DR	0% pre-bond moisture	90%	T5DR03
			80%	T5DR05
			70%	T5DR07
			60%	T5DR02
			50%	T5DR04
			40%	T5DR06
	T1DR	0.33 % pre-bond moisture	90%	T1DR02
			80%	T1DR03
			70%	T1DR04
			60%	T1DR05
			50%	T1DR06
			40%	T1DR07
	T9DR	1.25 % pre-bond moisture	90%	T9DR02
			80%	T9DR03
			70%	T9DR04
			60%	T9DR05
			50%	T9DR06
			40%	T9DR07
F2	T6DR	0% pre-bond moisture	90%	T6DR03
			80%	T6DR05
			70%	T6DR07
			60%	T6DR02
			50%	T6DR04
			40%	T6DR06
	T2DR	0.33 % pre-bond moisture	90%	T2DR06
			80%	T2DR03
			70%	T2DR04
			60%	T2DR05
			50%	T2DR07
			40%	T2DR02
	T10DR	1.25 % pre-bond moisture	90%	T10DR02
			80%	T10DR03
			70%	T10DR04
			60%	T10DR05
			50%	T10DR06
			40%	T10DR07

Table 6.2 Specimen list and specimen configurations of the fatigue test campaign.

6.3.1 Analysis of the failure mode at the crack front

Before and after the fatigue tests, the zone near the crack tip was visually inspected in order to analyse the shape of the crack front. Different failure modes were observed for the joints with and without pre-bond moisture. But the same trend was observed in both adhesive films (F1 and F2). The failure mode was similar to that of quasi-static tests (see chapter 3).

The crack front of a specimen without pre-bond moisture is shown in figure 6.2a. The crack initiates at the interphase, however, additional cracks appear in the pre-cured adherend during the fatigue test. Multiple cracks are observed after the fatigue test. This failure mode is not observed in the specimens with pre-bond moisture content (1.25% and 0.33%) as shown in figure 6.2b, having a single crack front. The same failure mode occurs for the specimens with the other adhesive film F2.

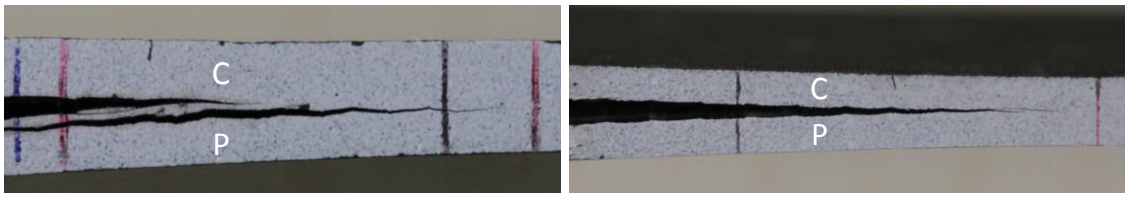

a) b)

Figure 6.2 Failure mode under fatigue loading of F1 bonded joints: a) without pre-bond moisture, specimen T6DR04; b) with 0.33% pre-bond moisture, specimen T1DR04. C means co-bonded and P pre-cured.

6.3.2 Onset of crack propagation

The standard ASTM D6115 recommends two criteria for the determination of the onset of propagation under fatigue loading, named as 1% and 5% increase of the compliance compared to the initial value measured at N=1 cycles. In this work, an intermediate increase has also been taken into account, a 2%. The onset lives of specimens tested at various percentages of energy release rate are summarized in tables 6.3 and 6.4.

Adherent condition	Specimen	Defined by the user		Measured from the test		$N^{1\%}$	$N^{2\%}$	$N^{5\%}$
		%ERR	G_{Imax} (J/m^2)	G_{Imax} (J/m^2)	%ERR			
0% pre-bond moisture	T5DR03	90%	579.91	553.71	86%	42	96	595
	T5DR05	80%	515.47	464.08	72%	88	266	2228
	T5DR07	70%	451.04	371.96	58%	221	954	3518
	T5DR02	60%	386.60	329.01	51%	1674	2697	12128
	T5DR04	50%	322.17	288.33	45%	8309	14504	35155
	T5DR06	40%	257.74	217.61	34%	> 2500000	> 2500000	> 2500000
0.33 % pre-bond moisture	T1DR02	90%	642.34	659.59	92%	14	31	67
	T1DR03	80%	570.97	561.02	79%	14	34	79
	T1DR04	70%	499.60	526.87	74%	31	134	256
	T1DR05	60%	428.23	498.47	70%	83	204	446
	T1DR06	50%	356.86	399.53	56%	73	294	1662
	T1DR07	40%	285.48	333.89	47%	204	857	3594
1.25 % pre-bond moisture	T9DR02	90%	327.83	320.03	88%	30	97	272
	T9DR03	80%	291.40	293.00	80%	93	257	627
	T9DR04	70%	254.98	271.64	75%	76	359	665
	T9DR05	60%	218.55	218.76	60%	210	467	936
	T9DR06	50%	182.13	183.86	50%	381	1596	12301
	T9DR07	40%	145.70	156.35	43%	1486	5575	22509

Table 6.3 Fatigue onset lives for the adhesive film (F1) composite bonded joints

Adherent condition	Specimen	Defined by the user		Measured from the test		$N^{1\%}$	$N^{2\%}$	$N^{5\%}$
		%ERR	G_{Imax} (J/m^2)	G_{Imax} (J/m^2)	%ERR			
0% pre-bond moisture	T6DR03	90%	613.83	521.77	77%	33	240	1270
	T6DR05	80%	545.63	480.96	71%	93	199	1457
	T6DR07	70%	477.43	407.49	60%	121	335	1852
	T6DR02	60%	409.22	286.48	42%	12963	97510	151084
	T6DR04	50%	341.02	281.58	41%	4129	12951	1259492
	T6DR06	40%	272.82	203.93	30%	> 2500000	> 2500000	> 2500000
0.33 % pre-bond moisture	T2DR06	90%	609.98	648.04	96%	30	97	272
	T2DR03	80%	542.20	553.80	82%	93	257	627
	T2DR04	70%	474.43	414.23	61%	76	359	665
	T2DR05	60%	406.65	416.95	62%	210	467	936
	T2DR07	50%	338.88	352.04	52%	381	1596	12301
	T2DR02	40%	271.10	261.90	39%	1486	5575	22509
1.25 % pre-bond moisture	T10DR02	90%	389.54	364.20	84%	92	250	600
	T10DR03	80%	346.26	350.64	81%	83	207	454
	T10DR04	70%	302.97	295.70	68%	249	594	1274
	T10DR05	60%	259.69	247.75	57%	456	903	2759
	T10DR06	50%	216.41	206.10	48%	2381	3701	10388
	T10DR07	40%	173.13	163.23	38%	16129	26721	46201

Table 6.4 Fatigue onset lives for the adhesive film (F2) composite bonded joints

As it was expected, the number of cycles to onset the crack propagation increases as G_{Imax} decreases. Lower values of G_{Imax} imply lower values of P_{max}, and thus, more cycles to start the crack propagation.

There are some differences between the values of G_Imax initially defined by the user and those measured from the test data. As previously stated, in chapter 5, these differences may be attributed to errors in the measurement of the crack front. However the analysis of these results requires further investigation.

From the values of the number of cycles it is observed that despite testing at percentages of ERR of 40%, there are not run out tests for the specimens with pre-bond moisture.

Only the dry specimens tested at this level of energy release rate need more than 2.5 million cycles to start to propagate. This is indicated as a $>2.5 \cdot 10^6$ in the tables. Besides, there are big differences in the number of cycles that each criterion (1%, 2% and 5%) defines as the onset of propagation. For the specimens with the lower values of energy release rate these differences are larger than one decade. In all the cases the 1% is the most conservative criterion and the 5% the less conservative one.

Despite being the less conservative, the author considers that the 5% increase of the compliance provides the most robust results for comparison purposes. This is mainly because it requires more cycles than the rest to reach the value of the compliance, thus having less scatter in the results and a better relationship between the number of cycles and G_{Imax}. On this basis, a comparison between the different levels of pre-bond moisture for the 2 adhesives, F1 and F2, is shown in figures 6.3 and 6.4; where the calculated value of G_{Imax} and the percentage of ERR have been plot against the number of cycles (N). In addition, and for each batch of specimens, a linear regression has been obtained in order to analyse the behaviour of each configuration. For the bonded joints with adhesive F2 and 0% pre-bond moisture there is not a linear tendency in the results. Therefore the linear regression is not included in the figures.

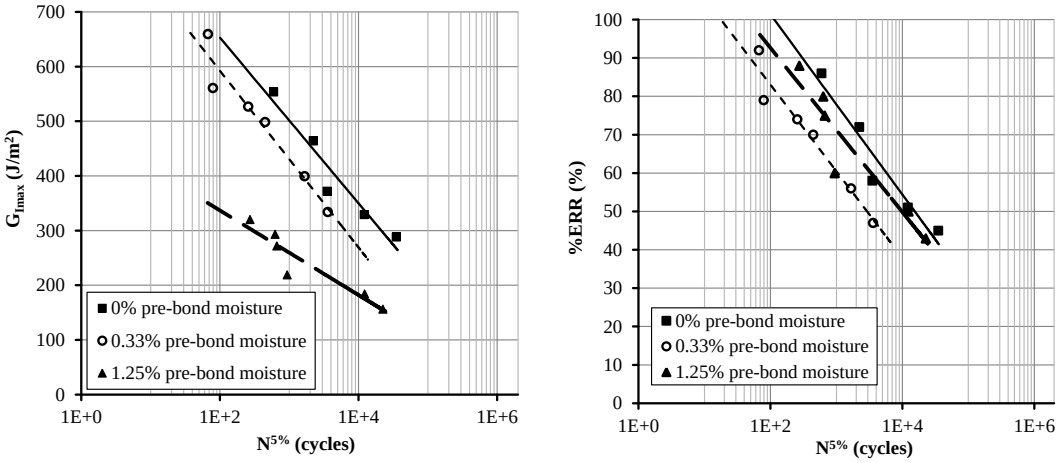

a) b)

Figure 6.3 Onset curves of the bonded joints with adhesive film F1 for different pre-bond moisture in the adherends: a) G_{Imax} calculated from the results of the test against the number of cycles; b) percentage of ERR calculated from the test results against the number of cycles.

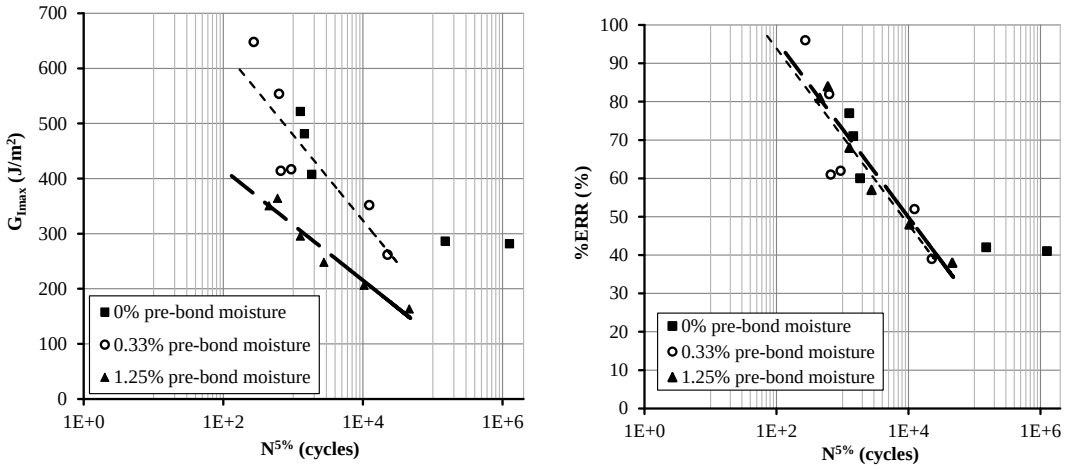

a) b)

Figure 6.4 Onset curves of the bonded joints with adhesive film F2 for different pre-bond moisture in the adherends: a) G_{Imax} calculated from the results of the test against the number of cycles; b) percentage of ERR calculated from the test results against the number of cycles.

It is observed, from the results of figures 6.3 and 6.4, that the crack initiation is delayed for the joints with a 0% pre-bond moisture content as compared to the joints with a 0.33% and 1.25%, i.e. more cycles are required to start the propagation. The delay in the crack initiation for the joints without pre-bond moisture is attributed to the multiple cracking, as seen in figure 6.2a. If comparing the results in terms of G_{Imax} it is observed that the presence of moisture causes more degradation to the adhesive joint. However, if they are compared in terms of the percentages of the energy release rate (%ERR) there are no appreciable differences between the configurations.

In the curves there is a lack of data of onset points at high cycles of fatigue. Thus, it is not clear that the behaviour exhibited in figures 6.3 and 6.4 can be extended to the whole curve. Repetitions of the same test at lower values percentages of energy release rate must be done in order to obtain a complete representation of the onset curves.

6.3.3 Analysis of the fatigue crack growth rate curves

The crack growth rate curves against G_{Imax} for the different levels of pre-bond moisture and the 2 adhesives (F1 and F2) are shown in figure 6.5. The results of the 6 specimens of the same batch tested at different levels of ERR are plot in a single graph.

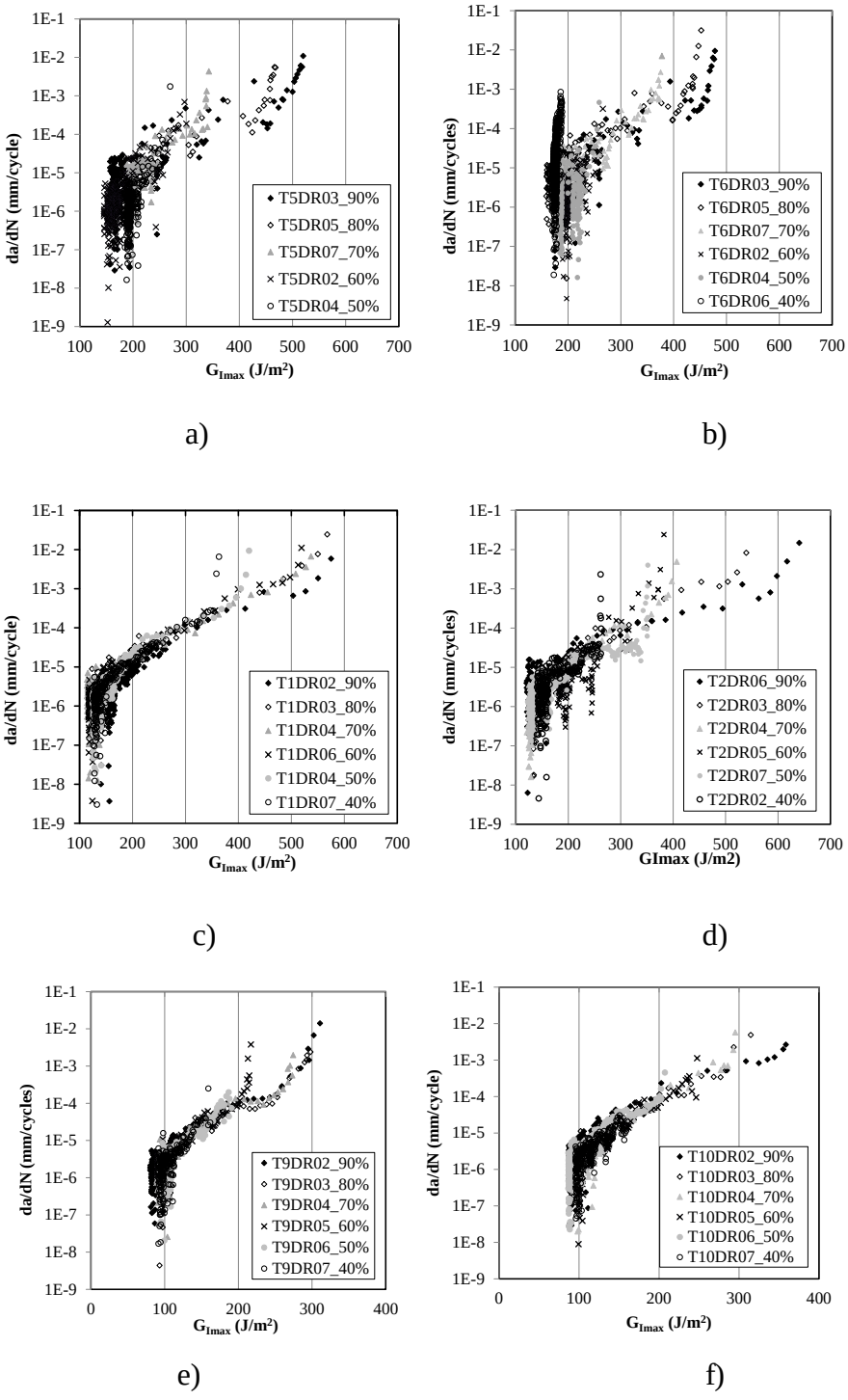

Figure 6.5 Fatigue crack growth rate curves of specimens tested at different energy release rate levels from 40% to 90%: a) F1 adhesive with 0% pre-bond moisture; b) F2 adhesive with 0% pre-bond moisture; c) F1 adhesive with 0.33% pre-bond moisture; d) F2 adhesive with 0.33% pre-bond moisture; e) F1 adhesive with 1.25% pre-bond moisture; f) F2 adhesive with 1.25% pre-bond moisture.

From the results it is observed that despite the percentage of energy release rate applied, all the curves of a batch represent the same crack growth rate behaviour. The specimens with the highest percentages reproduce almost the complete crack growth rate curve, whereas the specimens with the lowest ratios only reproduce a fragment. E.g. figure 6.6a shows the expected result for a batch of 3 specimens tested at a %ERR of 40%, 70% and 90%. For the percentage of 90% the whole crack growth rate curve is represented whereas for the 70% and 40% the curve starts in the linear region, at the level of G_{Imax} that coincides with the percentage of energy release rate applied, and only the last two regions (linear and crack growth arrest) are represented.

In all the cases the curves should follow the same trend. However, what is expected does not coincide with the experimental results that are obtained. E.g. figure 6.6b shows the results of 3 specimens tested at the percentages of energy release rate of 90%, 70% and 40%. The three curves exhibit a fast crack growth region at the initial part of the curve whilst they should start at the linear region. Apart from this, most of the curves of figure 6.5 present a wavy pattern in the linear crack growth rate region (region II of curve 5.1, defined by the Paris law relationship) instead of reproducing a straight line. All these deviations from the ideal curves are commented in the following subsections.

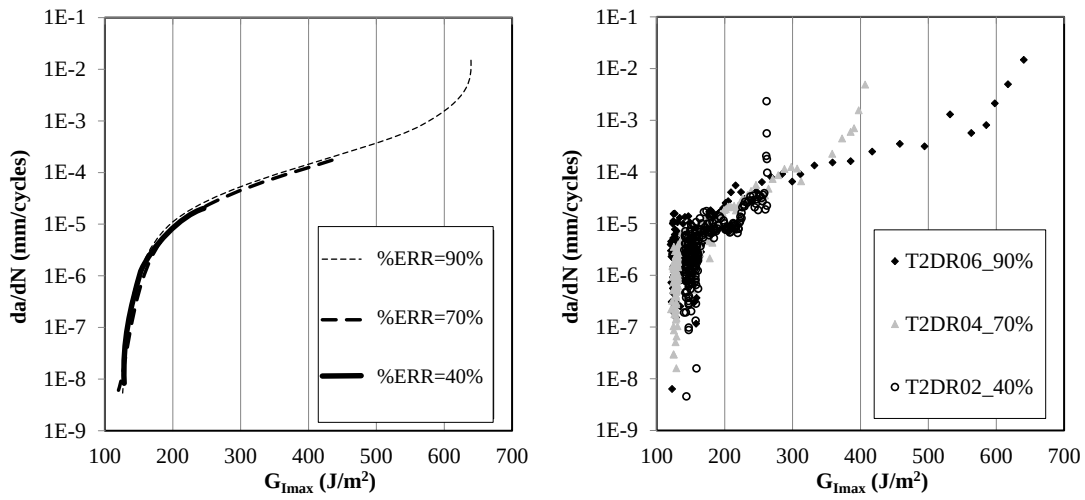

Figure 6.6 Crack growth rate curves: a) expected curve for a batch of 3 specimens tested at the %ERR from 40% to 90%; b) experimental results obtained from batch T2DR (F2 adhesive with 0.33% pre-bond moisture).

6.3.3.1 Analysis of region of fast crack growth (region III)

The fast crack propagation region occurs at the levels of the energy release rate close to the static mode I onset fracture toughness values (Sants et al. 2013). This region is characterized by a fast decrement of the crack growth ratio similar to the one in the quasi-static propagation tests

Only the specimens tested at the highest percentages of ERR should present this region. However from figure 6.5 and figure 6.6b it is observed that this trend also appears in the specimens tested at the lowest percentages. What would be expected in those specimens is that the curve started in the linear region but not having an initial decrement of da/dN. This behaviour may be caused by a change in the morphology of the crack front or it could be an internal problem caused by the test methodology or the equipment used.

In order to identify the source of the problem, a single specimen (specimen T1WL_09, adhesive F1, with 0.33% pre-bond moisture) was tested under the same conditions than those tested in the multi-fatigue device. The specimen was tested at a percentage of ERR of 90% and the test was stopped at a certain interval of cycles: $0.1 \cdot 10^6$, $0.5 \cdot 10^6$, $1 \cdot 10^6$ and $1.5 \cdot 10^6$ and $2 \cdot 10^6$ cycles. Then, the specimen was removed from the fixture, mounted and tested again until the next stop. The objective was to subdivide the test in several sub-tests performed at different initial crack lengths, and thus, at different percentages of the energy release rate.

The curve of the compliance against the number of cycles for this specimen is shown in figure 6.7. The curve is formed by several segments in between the test stops. Despite stopping the test and removing the specimen from the fixture, there is a continuity in the curve except for the stop at $1.5 \cdot 10^6$ cycles, where there is a small jump in the compliance.

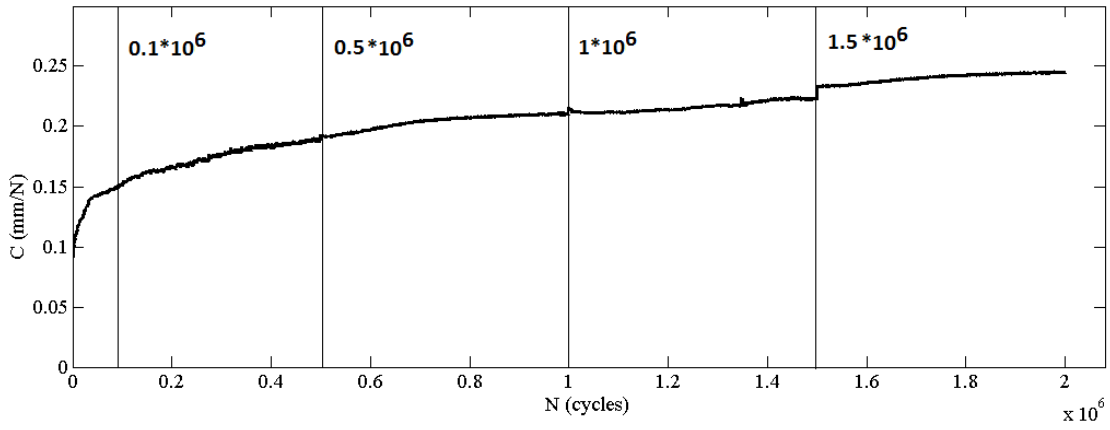

Figure 6.7 Curve of the compliance against the number of cycles for the specimen stopped at a certain interval of cycles, Specimen T1WL09. The vertical lines indicate the test stops.

For the same test, the crack growth rate curve was obtained, see figure 6.8. The same methodology described in chapter 5 was used to plot the curve.

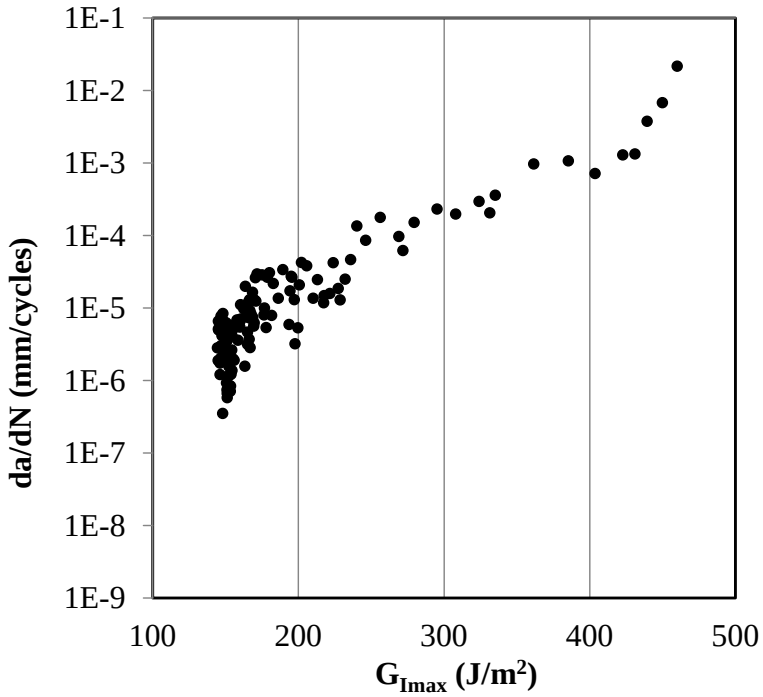

Figure 6.8 Crack growth rate curve of specimen T1WL09

For this specimen, the curve is continuous, and despite the stops there is only one fast crack growth region at the beginning of the test. There is continuity in the whole curve, even at the stop at $1.5 \cdot 10^6$ cycles.

Therefore, it can be concluded that the initial fast crack growth regions that appear in all of the curves should not be attributed to a problem in the methodology, but to a change of the morphology of the crack front when the material is subjected to cyclic loading.

6.3.3.2 Analysis of linear propagation region (region II)

After the fast crack growth the $da/dN(G_{Imax})$ curve is followed by a linear propagation region which is well described by the Paris law.

This region can be characterized by a straight line. However the curves represented in figures 6.5, 6.6 and 6.8 exhibit a wavy pattern. This behaviour is accentuated in bonded joint configurations with 0% pre-bond moisture.

In order to analyse this behaviour, the crack growth rate curves against G_{Imax} and the crack length for specimen T1DR02 have been plot in figure 6.9. This specimen contained 0.33% pre-bond moisture and it was tested at an energy release level of 90%. The author has chosen this specimen because only a single crack front was observed before and after the fatigue test.

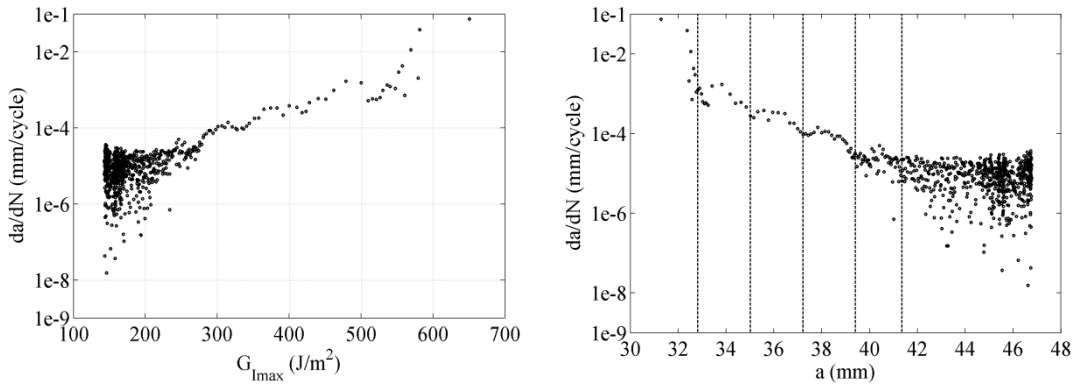

a) b)

Figure 6.9 Crack growth rate curve against G_{Imax} (a) and the crack length (b) of specimen T1DR02 (adhesive F1, 0.33% pre-bond moisture, specimen tested at %ERR = 90%). The vertical marks of figure b) indicate the zones of crack growth arrest.

Besides, a picture of the adhesive layer taken at the specimen side is plot in figure 6.10 for the same specimen.

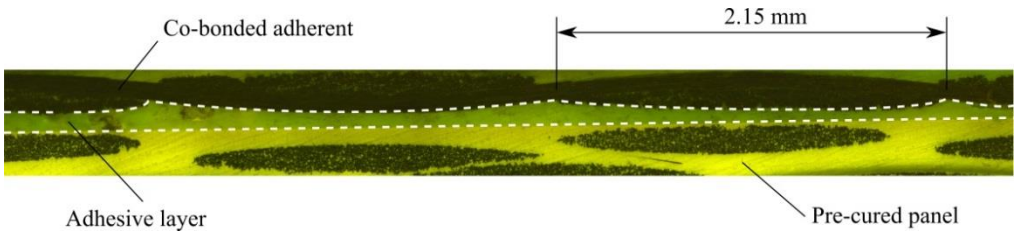

Figure 6.10 Image of the adhesive layer obtained at the specimen side with a stereomicroscope applying the fluorescence technique. The image is a mosaic composition of a series of concatenated pictures taken at the side.

From the plot of da/dN versus the crack length it is observed that the jump in the propagation occurs periodically at every 2.12 mm of crack propagation. On the other hand, it is observed in figure 6.10 that the adhesive thickness is not constant but varies following a wavy pattern. This wavy pattern is caused by the adherend fabric of the co-cured adherend. The distance at which the jumps shown in figure 6.9 occur coincides with the distance of the wavy pattern of figure 6.10. Therefore it can be concluded that the shape of the adhesive layer has an effect on the crack propagation during the fatigue tests.

This relationship is only valid for those specimens that have a single crack front, specimens with 0.33% and 1.25% pre-bond moisture content. For the specimens with 0% pre-bond moisture, the distance between the jumps and the wavy patterns is different, being longer than expected. A series of these measurements are listed in table 6.5.

Specimen	Parameter	1	2	3	4	5	6	7	$[\Delta_{arr}]_{av}$ (mm)
T5DR03	a_{arr} (mm)	39.78	42.48	45.31					
	Δ_{arr} (mm)	-	2.7	2.83					2.77
T6DR03	a_{arr} (mm)	39.03	41.82	44.62	47.38				
	Δ_{arr} (mm)	-	2.79	2.8	2.76				2.78
T1DR02	a_{arr} (mm)	32.82	35.02	37.22	39.41	41.35	43.45	45.56	
	Δ_{arr} (mm)	-	2.2	2.2	2.19	1.94	2.1	2.11	2.12
T2DR03	a_{arr} (mm)	32.82	35.02	37.55	39.89	42.03			
	Δ_{arr} (mm)	-	2.2	2.53	2.34	2.14			2.30

Table 6.5 Crack length of arrest fatigue propagation points (a_{arr}) of the wavy patter and increment between these arrest points (Δ_{arr}). For each specimen an average value of the increment has been obtained ($[\Delta_{arr}]_{av}$). Specimens T5DR03 and T6DR03 contain a 0% pre-bond moisture in the adherends. Specimens T1DR02 and T2DR03 contain a 0.33% pre-bond moisture.

For all the specimens, the distance between jumps remains the same during the whole fatigue test. For the specimens with 0.33% pre-bond moisture it is about 2 mm whereas for the dry specimens the distance increases up to 2.8 mm approximately. The author attributes this increment of the length between arrest points to the differences in the crack front. In specimens with 0% pre-bond moisture there are multiple crack fronts and the relationship between the jumps in the crack growth rate curve and the wavy pattern is not so direct.

What remains constant is the distance between jumps during the fatigue crack propagation. Therefore it can be concluded that whatever the failure mode at the crack tip, it remains constant during the test.

The study does not analyse if the arrest points correspond to the thick or thin regions of the adhesive layer, this requires further investigation.

6.3.3.3 Analysis of the arrest of propagation (region I)

The last part of the curve is the fatigue propagation arrest. In mode I fatigue tests controlled by displacement, there is an amount of crack propagation at which the crack stops even the number of cycles is increased. When this occurs, the crack growth rate decreases abruptly for a certain value of G_{Imax}. This value is defined as the threshold value (G_{th}). However, a consensus in the number of cycles at which a fatigue test should be stopped is still to be achieved (Argüelles et al. 2008, Argüelles et al. 2010, Kenane et al. 2011). What is commonly adopted, especially in propagation tests, is a crack growth rate limit. However there is a large disparity between the values proposed by the authors (Hojo 1987, Martin and Murri 1990, Stelzer et al. 2012, Stelzer et al.2013). In this work, the value of G_{Imax} measured after 2.5 million cycles has been taken as the threshold value. The results of the threshold values are listed in tables 6.6 and 6.7.

%ERR	Threshold values, G_{th} (J/m^2)		
	0% pre-bond moisture	**0.33 % pre-bond moisture**	**1.25% pre-bond moisture**
90%	162.2	139.1	80.6
80%	196.3	123.6	97.1
70%	195.8	114.3	94.4
60%	146.6	117.6	90.3
50%	175.2	125.6	97.0
40%	160.2	126.2	91.7
Av.	**172.7**	**124.4**	**91.9**
St. Dev.	**20.2**	**8.6**	**6.2**
C.V.	**11.7**	**6.9**	**6.7**

Table 6.6 Fatigue threshold values of adhesive film joints F1

%ERR	Threshold values, Gth (J/m^2)		
	0% pre-bond moisture	**0.33 % pre-bond moisture**	**1.25% pre-bond moisture**
90%	175.3	120.4	87.3
80%	165.2	131.1	87.6
70%	176.7	147.1	97.6
60%	186.1	125.9	99.5
50%	184.3	127.6	87.1
40%	151.2	137.6	95.6
Av.	**173.1**	**131.6**	**92.4**
St. Dev.	**13.1**	**9.5**	**5.7**
C.V.	**7.6**	**7.2**	**6.2**

Table 6.7 Fatigue threshold values of adhesive film joints F2.

There is a larger dispersion in the threshold values of specimens with 0% of pre-bond moisture. This scattering may be attributed to the failure mode at the crack tip. As it is shown in figure 6.2 the specimens with 0% pre-bond moisture have multiple crack fronts whereas specimens with 0.33% and 1.25% pre-bond moisture have a single crack tip. The images of the crack front of the batch with the largest scattering (T5DR) are compared to the crack front with the batch with the lowest (T10DR), see figure 6.11.

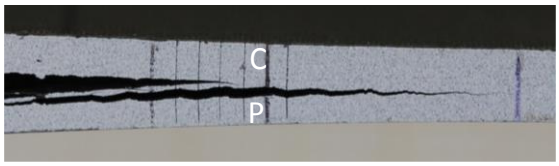

a) T5DR03 (%ERR = 90%)

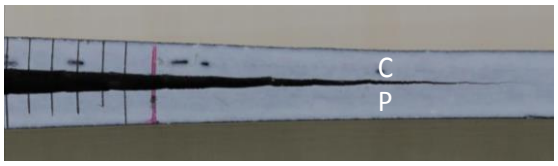

b) T10DR02 (%ERR = 90%)

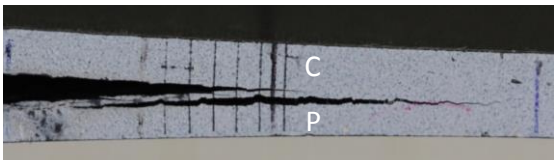

c) T5DR05 (%ERR = 80%)

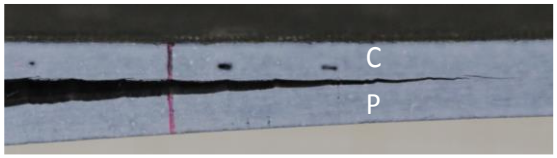

d) T10DR03 (%ERR = 80%)

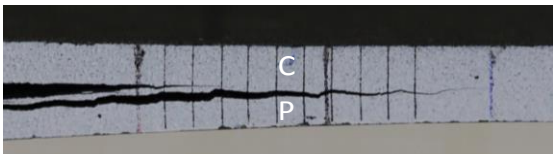

e) T5DR07 (%ERR = 70%)

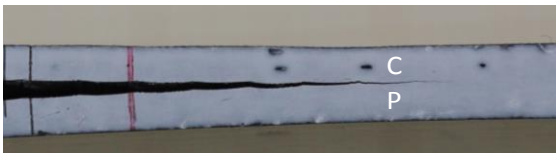

f) T10DR04 (%ERR = 70%)

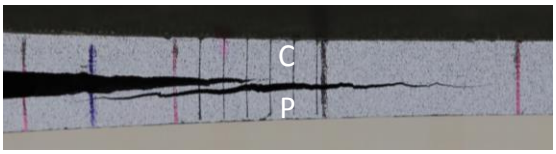

g) T5DR02 (%ERR = 60%)

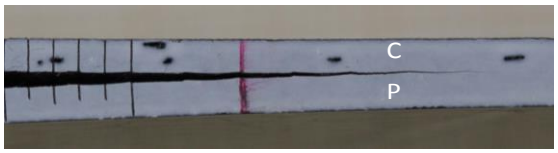

h) T10DR05 (%ERR = 60%)

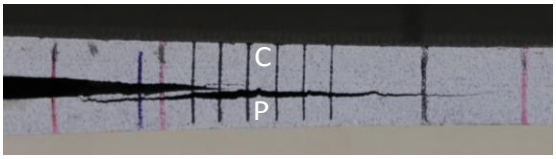

i) T5DR04 (%ERR = 50%)

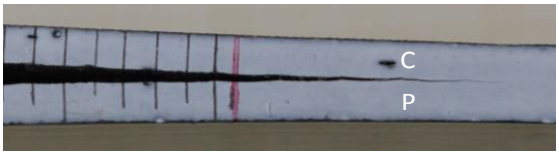

j) T10DR05 (%ERR = 50%)

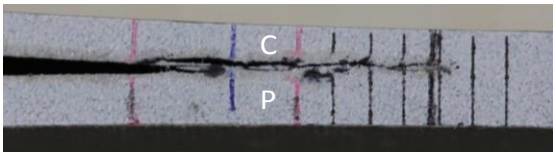

k) T5DR06 (%ERR = 40%)

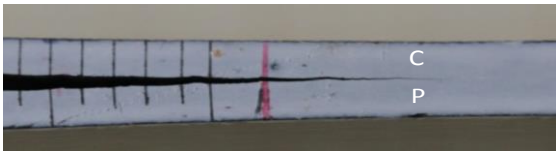

l) T10DR07 (%ERR = 40%)

Figure 6.11 Crack fronts after the fatigue test of specimens of batch T5DR (adhesive F1, 0% pre-bond moisture) and specimens of batch T10DR (adhesive F2, 1.25% pre-bond moisture). C is the co-cured adherend and P the pre-cured panel.

All the specimens of batch T5DR have multiple crack fronts causing a larger scattering in the results of the threshold value. On the contrary, one single crack tip is observed in specimens of batch T10DR.

6.3.4 Results of the fatigue crack growth rate curves

The pre-bond moisture effect on the fatigue crack propagation of the bonded joints has been analysed from the results of the crack growth rate curves. Two parameters have been measured: the slope of the linear propagation and the threshold values.

6.3.4.1 Slope of linear propagation curves

Despite having a wavy pattern in the linear region, as described in section 6.3.3.3, a linear regression of the linear part of the curve has been performed in order to obtain the slope of the curve (n) according to the Paris law.

Only one specimen per batch has been analysed, and the analysis has been conducted with those specimens with the highest percentages of applied energy release rate (%ERR=90%). Regions of fast crack growth and crack arrest have been deleted from the curve in order to perform the linear regression. Figure 6.12 shows how the linear region has been obtained for specimen T2DR06.

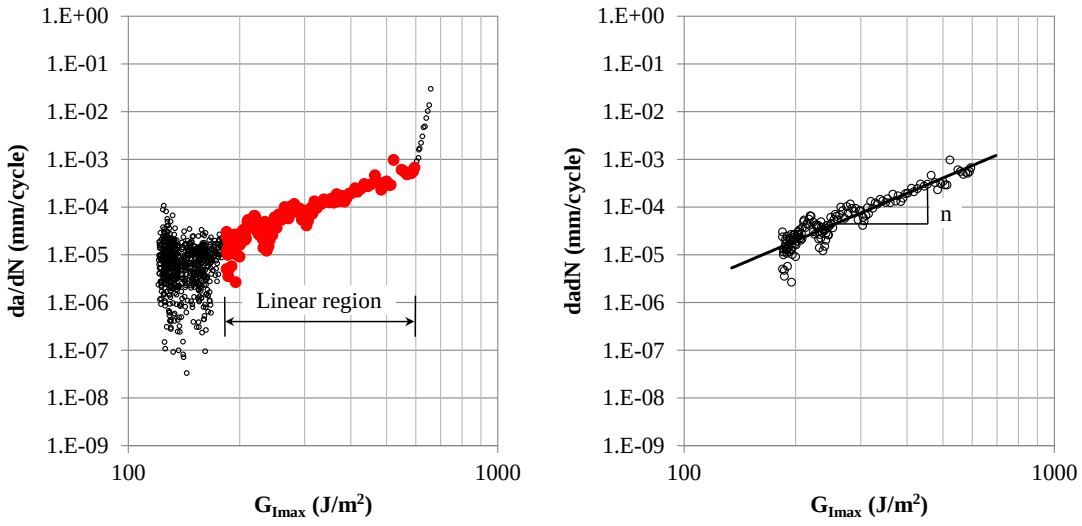

Figure 6.12 Zone at which the slope of the Paris law is obtained: a) linear region of the crack growth rate curve; b) determination of the slope of this linear region.

The results of this linear regressions and the slope for all the specimen configurations (two adhesives and 3 surface preparations) are shown in figure 6.13. The results have been divided for the two adhesives. The lines represent the curve fitting of the linear region of the crack growth rate curve.

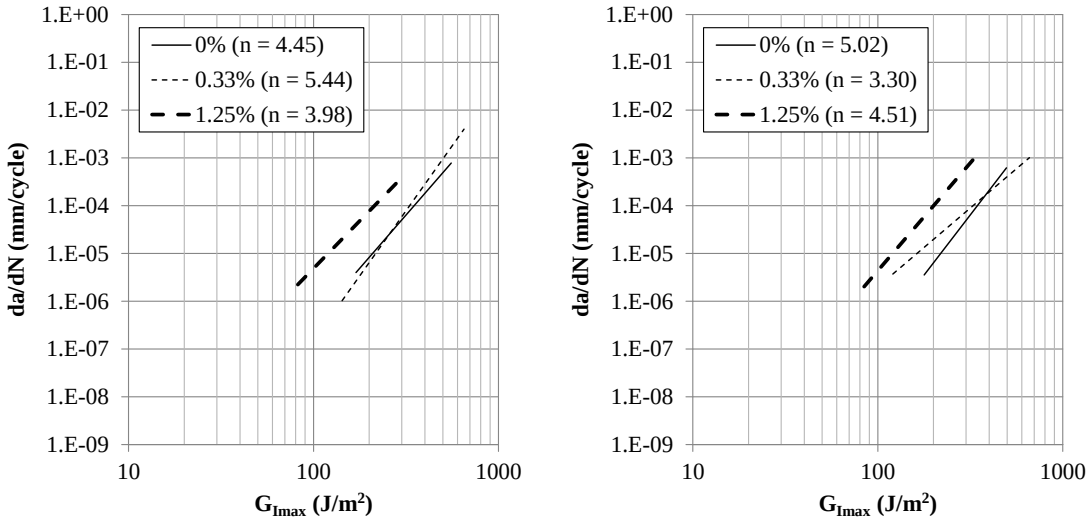

a) b)

Figure 6.13 Slopes of the linear region of the crack growth rate curves: a) bonded joints with F1 adhesive, b) bonded joints with F2 adhesive.

As expected from the results of the onset curves, the 1.25% pre-bond moisture specimens have the lowest values of G_{Imax} for the same crack growth rate. In relation to the slope of the linear region, there are not clear differences between the adhesive joint configurations. A trend for both adhesives is that 1.25% pre-bond moisture specimens have a lower gradient than the dry ones. The behaviour of 0.33% pre-bond moisture specimens is not so clear: for adhesive F1 the slope increases whereas for F2 adhesive it decreases.

6.3.4 Fatigue Threshold

The strain energy release rate corresponding to the threshold region has been calculated by using the Corrected Beam Theory data reduction method. The threshold values presented in this section are obtained from the crack growth rate curve. The values corresponding to the different preparation conditions are summarized in figure 6.14.

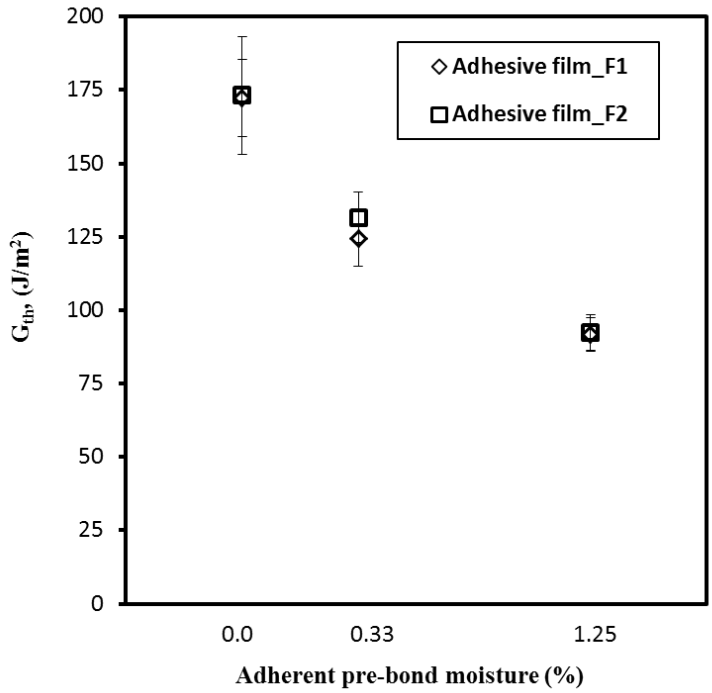

Figure 6.14 Effect of pre-bond moisture on fatigue threshold (G_{th}).

It is shown that the threshold values decrease with the increase in pre-bond moisture for both adhesive films. This reduction in the threshold value is noticed almost 40% and 70% for the joints with 0.33% and 1.25% pre-bond moisture respectively compared to the 0% pre-bond moisture content. For both adhesive film joints (F1 and F2) the reduction in threshold value is almost the same with the increase in pre-bond moisture. This indicates that the pre-bond moisture is an important factor for the decrease in threshold values.

6.4 Conclusions

The fatigue behaviour of adhesively bonded CFRP DCB joints has been analysed in specimens with different pre-bond moisture content. The results show that, a change in the pre-bond moisture significantly affects the fatigue behaviour of the examined bonded joints. The following conclusions have been obtained:

The specimens with 0% pre-bond moisture exhibited multiple cracks in the pre-cured adherend in addition to the insert plane, the same failure mode was observed in the static loading (see chapter 3). With increasing moisture, the failure mode turns into a single crack for both adhesive film joints.

Crack initiation is delayed for joints with 0% pre-bond moisture level with respect to the rest of the configurations. For the joints with pre-bond moisture, the degradation occurs with the joints that have the highest levels of moisture (1.25%), if the onset curve is represented in terms of G_{Imax}. However, if the curves are represented in terms of the percentage of the energy release rate, no differences are observed between the different configurations.

Regarding to the crack growth rate curves there are no significant variations in the slope of the linear region of the $da/dN(G_{Imax})$ curve for the different moisture configurations. On the contrary, these differences are clearly visible in the threshold values, in which the pre-bond moisture decreases the performance of the joint.

As a general conclusion, differences are observed for the levels of pre-bond moisture if the results are analysed in terms of the absolute values of G_{Imax}. The results are independent of the curve used: onset or crack growth rate. On the contrary, these differences are difficult to detect if the data is compared from incremental values, e.g. the slope of the onset curve or the crack growth rate curve.

Finally, the author wants to comment that there are differences in between the crack growth rate curves and the ideal ones represented in figure 5.1. These differences are attributed to the specimen configurations and the materials used.

Chapter 7

General Conclusions and Future Work

7.1 Conclusions

The main objective of the present work is to investigate the effect of the pre-bond moisture on the fracture toughness of adhesive bonded joints for composite structural repairs. The work is divided into two main tasks: the study of the effect of pre-bond moisture under static loading at room and at high temperatures and the fatigue behaviour of adhesive bonded joints under the influence of pre-bond moisture. Following, the main conclusions drawn from the present work are presented.

First, in chapter 2, an exhaustive revision of the state of the art about the environmental effects (moisture and temperature) on the mechanical performance of the bonded joints is presented. The revision shows that the humidity acquired by the substrate before the curing process directly affects the fracture properties of the joint. But there are very few studies of this kind, all of them with static tests, and the results do not provide a clear view on the pre-bond moisture effect on the values of the energy fracture toughness. In addition, and according to the best knowledge of the author, there is no study with specimens under fatigue loading.

In chapter 3, the effect of pre-bond moisture on fracture toughness under static loading at room temperature is presented. The work is performed with specimens simulating structural bonded repairs for real aircraft components. The results show a decrement in the fracture toughness with increasing pre-bond moisture level in the substrate from 0% to 1.25%. The fracture toughness of the two adhesive films used, F1 and F2, is found to be highly sensitive to the pre-bond moisture present in the pre-cured CFRP substrates before adhesive bonding.

Drying the substrate with pre-bond moisture from 1 hr to 24 hr causes an improvement in the fracture toughness of the joint. To that purpose, more exhaustive drying process might be necessary: while increasing significantly the drying time might not be practical and an increase of the drying temperature is still suitable. Fractographic inspections reveal an enhancement of the cohesive mode of failure with the decrease of the pre-bond moisture.

In fact, the failure mode changes dramatically with the pre-bond moisture, the joints with 0% pre-bond moisture exhibit multiple cracks in the pre-cured adherend in addition to the insert plane, this multiple failure is converted into a single crack growth and a wet-wet failure mode occurs when the moisture content in the substrates increases (0.33%, 1.25%). This wet-wet failure was more evident in the samples with high pre-bond moisture content (1.25%). Samples with lower pre-bond moisture (0.33%) exhibited a slight contribution of cohesive failure. The failure modes remain the same independently on the adhesive chosen, but the value of the mode I fracture toughness differs by 20-25%. Thus, special attention should be put in the selection of the adhesive material.

In chapter 4 the study continues with the same materials but with the tests performed at higher temperatures (80ºC and 120ºC) and the co-bonded specimens conditioned at 70ºC / 85% relative humidity.

0% pre-bond moisture conditioned joints showed also higher fracture toughness compared to the 1.25% and 0.33% pre-bond moisture joints at 80°C. Cohesive failure occurred in the specimens with 0% pre-bond moisture and this is a possible explanation for the increment in fracture toughness.

When comparing the two adhesive films tested in these conditions, F1 presents higher fracture toughness than adhesive F2 for all the pre-bond moisture conditions. This trend is opposite to that observed at room temperature. Adhesive F1, having lower values of G_{IC} at room temperature than F2, improves its toughness after being conditioned and tested at 80ºC, which seems to indicate that there is a higher plastic deformation in adhesive film F1.

At higher test temperatures, 120°C, and in specimens without pre-bond moisture, the co-bonded adherend appears to be the weakest part of the joint, suffering multiple cracks away from the bonded joint. In the presence of pre-bond moisture, the interface between the co-bonded adherend and the adhesive film weakened in the wet specimens tested at both 80ºC and 120ºC. The adhesive films remained bonded in all cases to the pre-cured adherend. This wet-wet failure had been also observed in the specimens with pre-bond moisture tested at room temperature.

These results indicate the need of a careful and detailed characterization of the bonded joints, paying attention not only to the fracture toughness values but also to the failure

mode. For the repair systems studied here, the presence of pre-bond moisture has a dramatic effect on the failure mode, moving it from the adherends themselves to the adhesive film or to the wet-wet interface, whichever the subsequent aging of the bonded joint and the test temperature.

Once the impact of the pre-bond moisture is eliminated by the proper drying process, careful choice of the adhesive and the repair pre-preg, and consideration of the operating conditions and in-service temperature should not be ignored. This is evidenced by the comparison of the different behaviour of the bonded joints with F1 and F2 at room temperature/as received versus 80ºC/wet and 120ºC/wet.

Chapters 5 and 6 are focused on the pre-bond moisture effects on specimens tested under fatigue conditions.

Chapter 5 proposes a multiple specimen testing device and the methodology for obtaining onset and crack growth rate curves of DCB specimens under fatigue loading. The device is successfully used to test batches of six specimens at the same time, it also allows to test at different energy release rates and load ratios. In addition, the methodology permits to monitor the compliance continuously during the tests and to obtain a continuous crack growth rate curves. The results of the onset and crack growth rate curves obtained from the multi-fatigue test device are comparable with to those obtained from the single specimen testing. The chapter demonstrates that the device and the methodology reduce the testing times of large fatigue campaigns, maintaining the level of precision of the tests.

In fact, the multi-fatigue testing device is used in chapter 6 for the analysis of pre-bond moisture effects in specimens submitted to fatigue loading. The results show that the pre-bond moisture in the substrate has a significant effect on the fatigue behaviour of the examined adhesively-bonded joints. The degradation of the bonded joint increases when there is moisture in the substrate (0.33% and 1.25%) in comparison to joints without pre-bond moisture.

In relation to the onset curves, crack initiation delays for the joints with 0% pre-bond moisture level as compared to those with 0.33% and 1.25% pre-bond moisture, this tendency occurs for both adhesive films (F1 and F2), but for F2 adhesive film joints it is delayed the double as compared to F1 joints. Therefore, proper selection of the adhesive material is important in order to increase the fatigue life of the repairs.

Pre-bond moisture has a considerable effect on the fatigue threshold behaviour of the crack growth rate curves. The fatigue threshold energy decreases with the increasing pre-bond moisture level in the adherend for both film joints. Failure modes drastically change from multiple crack growth to the single crack with increasing pre-bond moisture from 0% to 0.33% and 1.25%. Same failure modes were also observed in the static loading condition. Onset and crack growth rate curves are sensible to pre-bond moisture effects if the results are analysed in terms of the absolute values of the energy fracture toughness. On the contrary the pre-bond moisture effect is difficult to detect if the data is compared from incremental values, e.g. the slopes of the onset curve or the crack growth rate curve.

7.2 Future work

The most promising future work that come out from this thesis is detailed below.

From the results of chapter 3 it is observed that extending the drying time improves the fracture toughness of the joint but the mechanical properties are not fully recovered. Therefore, there is need to extend the drying time or drying temperature in order to have significant increment of G_{IC}.

Bonded joints in the absence of pre-bond moisture present, for the materials considered in this work, several failure modes as a function of the test temperature. The pre-cured adherend is found to be the weakest part of the bond at room temperature, the co-bonded adherend is found to be the weakest at 120ºC, while only at 80ºC, the adhesive films fail with cohesive failure. The introduction of pre-bond moisture in the system leads to a unique failure mode, in the interface between the co-bonded adherend and the adhesive films. The determination of the pre-bond moisture value that triggers this change for different repair systems would permit the optimization of the drying conditions.

Both the adhesive films showed different fracture toughness values despite being under the same pre-bond moisture conditions. Therefore special care must be taken into account when selecting the adhesive for the bonded joint. In order to establish general guidelines for the selection of the adhesives, an extension of this study involving different adherend-adhesive combination could be performed in order to better

understand the effects of adhesive or the adherend in the final properties of the bonded joint. In this study the content of pre-bond moisture also should be taken into account.

In the analysis conducted in chapters 3 and 4 the pre-bond moisture effect has been taken into account only in the pre-cured substrate. However in real repair processes is difficult to avoid the upraising moisture of the fresh repair materials. The fresh repair materials (adhesive films and repair prepregs) absorb moisture while they are out of the fridge and being handled in the repair shops. The contribution of this moisture to the degradation of the bond line has to be also quantified and studied in combination with the pre-bond moisture in the substrate, in order to set proper work time limits.

Chapter 5 and chapter 6 are focused on the study of the pre-bond moisture effect in specimens under fatigue loading conditions. For this purpose a multi-fatigue device capable to test 6 specimens was developed. The device allows testing at multiple percentages of the energy release rate and at multiple levels of load. In this work the specimens have been tested at various levels of ERR but all have been tested at the same load level (R = 0.1). The study could be continued by testing more specimens at different load ratios and simultaneously at different levels of ERR. Like in the static tests, this testing campaign could be extended to different temperatures and to different combinations of adhesive-adherend. The multi-fatigue testing device was designed to be included in a climatic chamber.

In any case, in relation to the fatigue tests that have been presented in this work, more results are needed for the actual configurations to complete the onset curves.

Bibliography

Bibliography

Abdelaziz. A. Taib., Rachid. Boukhili., Said. Achious., Sebastien. Gordon., Hychem. Boukehili., "Bonded joints with composite adherends. Part I. Effect of specimen configuration, adhesive thickness, spew fillet and adherent stiffness on fracture", International Journal of Adhesion and Adhesives, 2006, vol-26, pp: 226-236.

Abdel-Wahab. M. M., Ashcroft. I. A., Crocombe. A. D., Smith. P. A., "Finite element prediction of fatigue crack propagation lifetime in composite bonded joints", Composite Part A- Applied science, 2004, vol-35(2), pp: 213-22.

Adams. R. D., Wake. W. C., "Structural adhesive joints in engineering", 1984, vol-15, (Elsevier, New York).

AITM1-0053., "Carbon Fibre Reinforced Plastics. Determination of mode I fracture toughness energy of bonded Joints", Airbus Test Method, 2013.

Akay. M., kong. S., Stanley. A., "Influence of moisture on the thermal and mechanical properties of autoclaved and oven cured Kevlar-49/epoxy laminates", Composite Science and Technology, 1997, vol-57, pp: 565-571.

Ameli. A., Papini. M., Spelt. J. K., "Hygrothermal degradation of two rubber-toughened epoxy adhesives: Application of open face fracture tests", International Journal of adhesion and adhesive, 2011, vol-31, pp: 9-19.

Arguelles. A., Vina. J., Canteli. A. F., Castrillo. M. A., Bonhomme. J., "Interlaminar crack initiation and growth rate in a carbon-fiber epoxy composite under mode-I fatigue loading", Composite Science and Technology, 2008, vol-68, pp: 2325-2331.

Argüelles. A., Viña. J., Canteli. A., Bonhomme. J., "Influence of Resin type on the Delamination Behaviour of Carbon Fiber Reinforced Composites Under Mode-II Loading", International Journal of Damage Mechanics, 2011, vol-20, pp: 963-978.

Armstrong. K. B., Cole. W., Bevan. W. G., "Care and repair of advanced composites", London: SAE International; 2005.

Armstrong. K., "Effects of absorbed water in CFRP composites on adhesive bonding", International journal of Adhesion and Adhesive, 1996, vol-16, pp: 21-28.

Ashcroft. I. A., Hughes. D. J., Shaw. S. J., "Adhesive bonding of fibre reinforced polymer composite materials", Assembly Automation, 2000, vol-20, pp: 150–161.

Ashcroft. I. A., Hughes. D. J., Shaw. S. J., "Mode I fracture of epoxy bonded composite joints: 1 Quasi –static loading", International Journal of Adhesion and Adhesives, 2001, vol-21, pp: 87-99.

Ashcroft. I. A., Hughes. D. J., Shaw. S. J., Wahab. M. A., Crocombe. A., "Effect of temperature on the quasi-static strength and fatigue resistance of bonded composite double lap joints", Journal of Adhesion, 2001, vol-75, pp: 61–88.

Ashcroft. I. A., Shaw. S. J., "Mode I fracture of epoxy bonded composite joints 2. Fatigue loading," International Journal of Adhesion and Adhesives, 2002, vol-22, pp: 151–167.

Asp. L., "The effect of moisture and temperature on the interlaminar delamination toughness of carbon/epoxy composites", Composite Science and Technology, 1998, vol-58, pp: 967-977.

ASTM D5229/D5229M, "Standard test method for Moisture Absorption Properties and Equilibrium Conditioning of Polymer Matrix Composite Materials", 2004.

ASTM D5528-01, "Standard Test Method for Mode I Interlaminar Fracture Toughness of Unidirectional Fiber-Reinforced Polymer Matrix Composites", American Society for Testing and Materials (ASTM), V. 15.03, Philadelphia (USA), 2007.

ASTM D6115-97, "Standard Test Method for Mode I Fatigue Delamination Growth Onset of Unidirectional Fiber-Reinforced Polymer Matrix Composites", American Society for Testing and Materials (ASTM), vol-15.03, Philadelphia (USA), 2004.

ASTM E647-13a, "Standard test method for Measurement of Fatigue Crack Growth Rates", American Society for Testing and Materials (ASTM), V.03.10, Philadelphia (USA), 2013.

Azari. S., M. Papini., Spelt. J. K., "Effect of adhesive thickness on fatigue and fracture of toughened epoxy joints- Part I: Experiments", 2011, vol-78, pp: 153-162.

Baldan. A., "Adhesively bonded joints and repairs in metallic alloys, polymer and composite materials: adhesives, adhesion theories and surface pretreatment", Journal of materials science, 2004, vol-39, pp: 1-49.

Banea. M. D., Silva. L. F. M., "Adhesively bonded joints in composite materials: an overview", Journal of Material design and applications, 2008, vol-223, pp: 1-18.

Banea. M. D., Silva. L. F. M., Campilho. R. D. S. G., "Mode I fracture toughness of adhesively bonded joints as a function of temperature: Experimental and numerical study" Journal of adhesion and adhesives, 2011, vol-31, pp: 273-279.

Benard. Q., Fois. M., Grisel., "Influence of fiber reinforcement and peel ply surface treatment towards adhesion of composite surfaces", International Journal of Adhesion and Adhesives, 2005, vol-25, pp: 404-409.

Benoit. Landry., Gabriel. LaPalnet., Luc. R. Le. Blanc., "Environment effects on mode II fatigue delamination growth in an aerospace grade carbon /epoxy composite", Composite part A, 2012, vol-43, pp: 475-485.

Blackman. B. R. K., Johnson. B., Kinloch. A., Teo. W., "The effect of pre-bond moisture on the fracture behaviour of adhesively bonded composite joints", Journal of Adhesion, 2008, vol- 84, pp: 256-276.

Blackman. B. R. K., Kinloch. A. J., "Fracture tests for structural adhesive joints, Fracture mechanics testing methods for polymers, adhesives and composites", Elsevier Science, 2001.

Blackman. B. R. K., Kinloch. A. J., Paraschi. M., Teo. W., "Measuring the mode I adhesive fracture energy, G_{IC}, of structural adhesive joints: the results of an international round-robin", International Journal of Adhesion and Adhesive, vol-23, 2003, pp: 293-305.

Bowditch. M. R., "The durability of adhesive joints in the presence of water", International Journal of Adhesion and Adhesive, 1996, vol-16, pp: 73-79.

Brunner. A. J., Murphy. N., Pinter. G., "Development of a standardized procedure for the characterization of interlaminar delamination propagation in advanced composites under fatigue mode I loading conditions", Engineering Fracture Mechanics, 2009, vol-76, pp: 2678-2689.

Brunner. A. J., Stelzer. S., Pinter. G., Terrasi. G. P., "Mode II fatigue delamination resistance of advanced fiber-reinforced polymer-matrix laminates: towards the development of a standardized test procedure", International Journal of Fatigue, 2013, vol-50, pp: 57-62.

BS 7991, "Determination of the mode I adhesive fracture energy, G_{IC}, of structural adhesives using the double cantilever beam (DCB) and tapered double cantilever beam (TDCB) specimens", 2001.

Budhe. S., Rodriguez-Bellido. A., Renart. J., Mayugo. J. A., Costa. J., "Influence of pre-bond moisture in the adherent on the fracture toughness of bonded joints for composite repairs", International journal of adhesion and adhesive, 2014, vol-49, pp: 80-89.

Caminero. M. A., Pavlopoulou. S., Lopez-Pedrosa. M., Nicolaisson. B. G., Pinna. C., Soutis. C., "Analysis of adhesively bonded repairs in composites: Damage detection and prognosis", Composite Structure, 2013, vol-95, pp: 500-517.

Chapman. T. J., Smiley. A. J., Pipes. R. B., "Rate and temperature effect of mode II interlaminar fracture toughness in composite materials- Deformation and fracture of

laminated composites", In: proceedings of the 6th international conference on Composite materials (ICCM-6), 1987, pp: 3295-3304.

Charalambides. M. N., Hardouin. R., Kinloch. A. J., Matthews. F. L., "Adhesively-bonded repairs to fibre-composite materials I. Experimental", Composites Part Applied Science and Manufacturing, 1998, vol-29(11), pp: 1371–1381.

Chen. Chang- Rong., Yiu-Wing. Mai., "Comparison of cohesive zone model and linear elastic fracture mechanics for a mode I crack near a compliant/stiff interface", Engineering Fracture Mechanics, 2010, vol-77, pp: 3408-3417.

Cheng. P., Gong. X. J., Hearn. D., Aivazzadeh. S., "Tensile behavior of patch-repaired CFRP laminates", Composite Structure, 2011, vol-93, pp: 582-589.

Choi. H. S., Ahn. K. J., Nam. J. d., Chun. H. J., "Hygroscopic aspects of epoxy/carbon fiber composite laminated in aircraft environments", Composites Part A-Applied science and manufacturing, 2001, vol-32, pp: 707-720.

Comyn. J., Mascia. L., Xiao. G., Parker. B. M., "Corona discharge treatment of polyetheretherketone (PEEK) for adhesive bonding", International Journal of Adhesion and Adhesives, 1996, vol-16(4), pp: 301–304.

Coronado. P., Arguelles. A., Vina. J., Mollon. V., Vina. I., "Influence of temperature on a carbon-fiber epoxy composite subjected to static and fatigue loading under mode-I delamination", Journal of solids and structures, 2012, vol-49, pp: 2934-2940.

Cowley. K. D., Beaumont. P. W. R., "The interlaminar and intralaminar fracture toughness of carbon-fiber polymer composites: the effect of temperature", Composite Science and Technology, 1997, vol-57, pp: 1433-44.

Crichtlow. G. W., Cottam. C. A., Brewis. D. M., Emmony. D. C., "Thermal studies into the effectiveness of CO2-Laser treatment of metals for adhesive bonding", International Journal of Adhesion and Adhesives, 1997, vol-17(2), pp: 143–50.

Critkovich. M. K., O'Brien. T. K., Minguet. P. J., "Fatigue debonding characterization in composite skin/stringer configurations", Composites Material: Fatigue and Fracture, vol-1330 (seventh volume), 1998, pp: 97-121.

Datla. N. V., Ulicny. J., Carlson. B., Papini. M., Spelt. J. K., "Mixed-mode fatigue behaviour of degraded toughened epoxy adhesive joints", International Journal of Adhesion and Adhesives, 2011, vol-31, pp: 88-96.

Davidson. B. D., Kumar. M., Soffa. M. A., "Influence of mode ration and hygrothermal condition on the delamination toughness of a thermoplastic particulate interlayered

carbon/epoxy composite", Composite. Part A: Applied Science Manufacturing, 2009, vol-40, pp: 67-79.

Davis. P., Charentenary. F. X., "Effect of temperature to on the interlaminar fracture of tough composites. Deformation and fracture of laminated composites". In: proceedings of the 6th international conference on Composite materials (ICCM-6), 1987, pp: 3284-3294.

Degrieck. J., W. Van. Paepegaon., "Fatigue damage modelling of fiber reinforced composite materials: Review", Applied Mechanical Research, 2001, vol-54, pp: 279-300.

Edward. M. Petrie., "Handbook of adhesives and sealant", McGraw Hill Professional, second edition, 2007.

Fereira. J. M., J. T. B. Pires., Costa. J. D., Errajhi. O. A., Richardson. M., "Fatigue damage and environment interaction of polyester aluminized glass fiber composites", Composite Structure, 2007, vol-78, pp: 397-401.

Fereira. J. M., Reis. P. N., Costa. J. D. M., Richardson. M. O.W., "Fatigue behavior of composite adhesive lap joints, Composite Science and Technology, 2002, vol-62, pp: 1373-1379.

Found. M. S., Friend. M. J., "Evaluation of CFRP panels with scarf repair patches", Composites structures, 1995, vol-32, pp: 115-122.

Gao. L. L., L. Wang., Gao. H., Chen. G., Chen. X., "Fatigue life evaluation of anisotropic conductive adhesive film joints under mechanical and hygrothermal loads," Microelectronics Reliability, 2011, vol-51, pp: 1393–1397.

Gao. S., Kim. J., "Cooling rate influences in carbon fibre/PEEK Composites. Part II: interlaminar fracture toughness", Composite. Part A: Applied Science Manufacturing, 2001, vol-32, pp: 763-774.

Garg. A., Ishai. O., "Hygrothermal influence on delamination behaviour of graphite/epoxy Laminates", Journal of Engineering fracture mechanics, 1985, vol-22, pp: 413-427.

Gefu. Ji., Zhenyu. Ouyang., Guoqiang. Li., Samuel. Ibekwe., Su-Seng. Pang., "Effects of adhesive thickness on global and local Mode-I interfacial fracture of bonded joints" International journal of Solids and structures, 2010, vol-47, pp: 2445-2458.

Hadavinia. A. D., Kinloch. A. J., Little. M. S. G., Taylor. A. C., "The prediction of crack growth in bonded joints under cyclic-fatigue loading I Experimental studies", International journal of Adhesion and Adhesive, 2003, vol-23(6), pp: 449-461.

Harris. A. F., Beevers. A., "The effect of grit-blasting on surface properties for adhesion", International Journal of Adhesion and Adhesives, 1999, vol-19(16), pp: 445-452.

Hashemi. S., Kinloch. A. J., Williams. J. G., "The effect of geometry, rate and temperature on Mode-I, Mode-II and Mixed Mode.I/IIinterlaminar fracture of carbon-fiber/poly(ether-ether ketone) composites", Journal of Composite Materials, 1990, vol-24, pp: 918-939.

Heung. Soap. Choi., Yong. Hoon. Jang., "Bondline Strength evaluation of co-cure/procured honeycomb sandwich structures under aircraft hygro and repair environments", Composites part A, 2010, vol-41, pp: 1138-1147.

Hojo. M., Matsuda. S., Tanaka. M., Ochiai. S., Murakami. A., "Mode I delamination fatigue properties of interlayed – toughened CF/epoxy laminates", Composites Science and Technology, 2006, vol-66 (5), pp: 665-675.

Hojo. M., Ochiai. S., Gustafson. C. G., Tanaka. K., "Effect of matrix resin on delamination fatigue-crack growth in CFRP laminates", Engineering Fracture Mechanics, 1994, vol-49(1), pp: 35-47.

Hu. F. Z., Soutis. C., "Strength prediction of patch-repaired CFRP laminates loaded in Compression". Composite Science and Technology, 2000, vol-60, pp: 1103–1114.

Hutapea. P., Yuan. F. G., "The effect of thermal ageing on the Mode-I interlaminar fracture behavior of a high-temperature IM7/LaRC-RP46 composite" Journal of Composites Science and Technology, 1999, vol-59, pp: 1271-1286.

ISO 15024: 2001, Fibre-reinforced plastic composites - Determination of mode I interlaminar fracture toughness, GIC, for unidirectional reinforced materials. International Organization for Standardization (ISO), Geneva, Switzerland, 2001.

ISO 25217: 2009, Adhesives - Determination of the mode 1 adhesive fracture energy of structural adhesive joints using double cantilever beam and tapered double cantilever beam specimens. International Organization for Standardization (ISO), Geneva, Switzerland, 2009.

Jen. Y. M., "Fatigue life evaluation of adhesively bonded scarf joints," International journal of Fatigue, 2012, vol-36, pp: 30-39.

Johnson. J. A., Provan. J. W., Krygier. J. J., Chan. K. H., Miller. J., "Fatigue of acrylic bone cement-effect of frequency and environments", Journal Biomedical Material Research, 1989, vol-23, pp: 819-831.

Johnson. W. S., Butkus. L. M., "Considering environmental conditions in the design of bonded structures: a fracture mechanics approach," Fatigue & Fracture of Engineering Materials & Structures, 1998, vol. 21, pp: 65-478.

Jordi. Renart., "Desarrollo de un Nuevo ensayo experimental para la evalucion de la calidad de uniones adhesive entre componentes estructurales de composite", Doctoral thesis, 2010.

Kanerva. M., Saarela. O., "The peel ply surface treatment for adhesive bonding of composites: A review", International Journal of Adhesion and Adhesives, 2013, vol-43, pp: 60-69.

Kawashaki. L. F., A. J. Kinloch., D. R. Moore., J. G. Williams., "The influence of bond line thickness and peel arm thickness on adhesive fracture toughness of rubber toughened epoxy-aluminium alloy laminates", International journal of Adhesion and Adhesives, 2008, vol-28, pp: 199-210.

Kenane. M., Azari. Z., Benmedakhene. S., Benzeggagh. M. L., "Experimental development of fatigue delamination threshold criterion", Composites Part B: Engineering, 2011, vol-42, pp: 367-375.

Kevin. C. D., Beaumont. P. W. R., "The interlaminar and intralaminar fracture toughness of carbon-fibre/polymer composites: the effect of temperature" Journal of composite science and technology, 1997, vol-57, pp: 1433-1444.

Khalili. S. M. R., Shokuhfar. A., Hoseini. S. D., Bidkhori. M., Khalili. S., Mittal. R. K., "Experimental study of the influence of adhesive reinforcement in lap joints for composite structures subjected to mechanical loads," International Journal of Adhesion and Adhesives, 2008, vol-28, pp: 436-444.

Kim. J. K., Lee. D. G., "Characteristics of plasma surface treated composite adhesive joints at high environmental temperature", Composite structure, 2002, vol-57(1-4), pp: 37-46.

Kim. K. Y., Ye. L., "Interlaminar fracture toughness of CF/PEI composites at elevated temperatures: roles of matrix toughness and fiber/matrix adhesion" Journal of composites part A, 2004, vol-35, pp: 477-487.

Kinard. J., Colton. J., "Material system for rapid manufacture of composite structure" polymer Composites, 2009, vol-21, pp: 918-930.

Kinloch. A. J., "Durability of structural adhesives, 1983, Applied Science Publishers, London.

Knight. G. A., Hou. T. H., Belcher. M. A., Palmieri. F. L., Wohl. C. J., Connell. J. W., "Hygrothermal aging of composite single lap shear specimens comprised of AF-555M

adhesive and T800H/3900-2 adherennds", International Journal of Adhesion and Adhesives, 2012, vol-39, pp: 2-7.

Koh. S. K., Cho. J. S., Yom. S. S., Beah. Y. W., "Hydrophilic surface formation on polymers and its applications", Current applied physics, 2001, vol-1(2–3), pp: 133–138.

Kohan. M. I., Nylon Plastics Handbook (Hanser-Gardner Publications, Cincinnati, OH) 1995.

Kohli. D. K., "Improved 121°C curing epoxy film adhesive for composite bonding and repair applications: FM300-2 adhesive system" International Journal of Adhesion and Adhesives, 1999, vol-19, pp: 231-242.

Krause. W., Mathis. R. S., "Fatigue properties of acrylic bone cement: review of the literature", Journal of Biomedical Materials Research, 1988, vol-22, pp: 37-53.

Kwang-Soo. Kim., Jae-Seok. Yoo., Yeong-Moo. Yi., Chun-Gon. Kim., "Failure mode and strength of unidirectional composite single lap bonded joints different bonding methods", Composite structures, 2006, vol-72, pp: 477-485.

Lang. R. W., Manson. J. A., "Crack tip heating in short fiber-fiber composites under fatigue loading conditions", Journal Material Science, 1987, vol-22, pp: 3576-3580.

Mall. S., Ramamurthy. G., "Effect of bond thickness on fracture and fatigue strength of adhesively bonded composite joints" International journal of Adhesion and Adhesive, 1989, vol-9, pp: 33-37.

Markatos. D. N., Tserpes. K. I., Rau. E., Markus. S., Ehrhart. B., Pantelakis. S., "The effects of manufacturing-induced and in-service related bonding quality reduction on the mode-I fracture toughness of composite bonded joints for aeronautical use", Journal of Composites: Part B, 2013, vol-45, pp: 556-564.

Martin. R. H., Murri. G. B., "Characterization of Mode I and Mode II Delamination Growth and Thresholds in AS4/PEEK Composites. Composite Materials: Testing and Design (Ninth Volume)", ASTM STP 1059, S.P. Garbo, Ed., American Society for Testing and Materials, Philadelphia, 1990, pp: 251-260.

Matthews. F. L., Tester. T. T., "The influence of stacking sequence on the strength of bonded CFRP single lap joints", International Journal of Adhesion and Adhesives, 1985, vol-5, pp: 13-18.

Melcher. R. J., Johnson. W. S., "Mode I fracture toughness of an adhesively bonded composite-composite joint in a cryogenic environment", Composite Science of Technology, 2007, vol-70, pp: 501-506.

Military Handbook, (2002), "Composite Material Handbook, Volume 1, Chapter 7 Structural Element Characterization", U. S. Department of Defence, 2002.

Mosaki. Hojo., Keisuke. Tanaka., Claes-Goran. Gustafson., Ryuichi. Hayashi., "Fracture mechanics for delamination fatigue crack propagation of CFRP in air and in water", Engineering materials, 1989, vol-37, pp: 149-160.

Mostovoy. S., Crosley. P. B., Ripling. E, J., "Use of crack-line-loaded specimens for measuring plane strain fracture toughness", Journal of Material, 1967, vol-2, pp: 661-681.

Moura. M. F. S. F. de., Campilho. R. D. S. G., Goncalves. J. P. M., "Crack equivalent concept applied to the fracture characterization of bonded joints under pure mode I loading", Composite Science of Technology, 2008, vol-68, pp: 2224-2230.

Myhre. S., Labor. J., Aker. S., "Moisture problem in advanced composite structural repair", Composites, 1982, vol-10, pp: 289-297.

Ogasawara. Toshio., Shifumi. Aizawa., Takeshi. Ogawa., Takashi. Ishikawa., "Sensitive strain monitoring of SiC fiber/Eepoxy composite using electrical resistance changes" Composites science and technology, 2007, vol-67, pp: 955-962.

Olsson. R., "A simplified improved beam analysis of the DCB specimens", Computer Science Technology, 1992, vol-43, pp: 329-338.

Ouezdou. Ben., Chudnovsky. A., "Stress and energy analysis of toughness measurement for adhesive bonds", Engineering Fracture Mechanics, 1988, vol-29, pp: 253-261.

Parker. B. M., "Effect of extended exposure to hot-humid conditions and subsequent drying on adhesive bonded CFRP-CFRP joints", composites, 1983, vol-14, pp: 226-232.

Parker. B. M., "The effect of composite pre-bond moisture on adhesive-bonded CFRP-CFRP joints", Composites, 1983, vol-14, pp: 226-232.

Parker. B., "Some effects of moisture on adhesive bonded CFRP-CFRP joints", Composites", 1986, vol-6, pp: 123-139.

Parker. B., "The strength of bonded carbon fibre composite joints exposed to high humidity", International Journal of Adhesion and Adhesives, 1990, vol-10, pp: 187-191.

Penado. F. E., "A closed form solution for the energy release rate of the double cantilever beam specimen with an adhesive layer", Journal of composite Material, 1933, vol-27, pp: 383-407.

Renart. J., Blanco. N., Pajares. E., Costa. J., Lazcano. S., Santacruz. G., "Side Clamped Beam (SCB) hinge system for delamination in beam-type composite specimens",

Composites Science and Technology, 2011, vol-71, pp: 1023-1029.

Renart. J., Vicens. P., Budhe. S., Costa. J., Mayugo. J. A, "Compliance real time monitoring in delamination fatigue tests". To be submitted to International Journal of Fatigue. 2014.

Ripling. E. J., Mostovoy. S., Patrick. R. L., "Measuring fracture toughness of adhesive joints", Mater. Res. Stands, 1964, vol-4, pp: 129-134.

Roberts. T. M., Talebzadeh. M., "Acoustic emission monitoring of fatigue crack propagation", Journal of Constructional Steel Research, 2003, vol-59, pp: 695–712.

Robson. J., Matthews. F., Kinloch. A., "The bonded repair of fibre composites: effect of composite moisture content", Composite Science and Technology, 1994, vol-52, pp: 235-246.

Rodrigo. A., Silva-Muñoz. Roberto., Lopez-Anido. A., "Structural health monitoring of marine composite structural joints using fiber Bragg grating sensors", Composite structures, 2009, vol-89, pp: 224-243.

Roizard. X., Wery. M., Kirmann. J., "Effects of alkaline etching on the surface roughness of a fibre-reinforced epoxy composite", Composite Structure, 2002, vol-56(3), pp: 223–228.

Russell. A. J., Street, K. N., "Moisture and temperature effects on the mixed-mode delamination fracture of unidirectional graphite/epoxy. Delamination and Debonding of materials", ASTM STP 876, ed. W.S: Johnson. American Society for Testing and Materials, Philadelphia, PA 1985, pp: 349-370.

Sage. G., Tiu., "The effect of glue line voids and inclusions on the fatigue strength of bonded joints in composites", Composites, 1982, vol-13, pp: 228-232.

Sans. D., Renart. J., Costa. J., Gascons. N., Mayugo. J. A., "Assessment of the influence of the crack monitoring method in interlaminar fatigue tests using fiber Bragg grating sensors", Composites Science and Technology, 2013, vol-84, pp: 44-50.

Sans. D., S. Stutz., Renart. J., Mayugo. J. A., Botsis. J., "Crack tip identification with long FBG sensors in mixed-mode delamination", Composite structures, 2012, vol-94, pp: 2879-2887.

Sarfaraz. R., Vassilopoulos. A. P., Keller. T., "Experimental investigation of the fatigue behaviour of adhesively-bonded pultruded GFRP joints under different load ratios", International Journal of fatigue, 2011, vol-33, pp: 1451-1460.

Sela. N., O. Ishai., L. Banks-sills., "The effect of adhesive thickness on interlaminar fracture toughness of interleaved CFRP specimens" Journal of composites", 1989, vol-20, pp: 257-264.

Selzer. R., Fredrich. K., "Influence of water up take on interlaminar fracture properties of carbon-reinforced polymer composites", Journal of Material Science, 1995, vol-30, pp: 334-338.

Selzer. R., Fredrich. K., "Mechanical properties and failure behaviour of carbon fibre-reinforced polymer composites under the influence of moisture", Composites. Part A: Applied science of manufacturing, 1997, vol-28A, pp: 595-604.

Shanahan. M. E. R., Bourge-Monnier. C., "Effects of plasma treatment on the adhesion of an epoxy composite", International Journal of Adhesion and Adhesives, 1996, vol-16(2), pp: 129-35.

Shaw. Y., K. Liao., "Environmental fatigue of unidirectional fiber reinforced hybrid composite", Composites Part B, 2001, vol-32, pp: 353-363.

Song. Min-Gyu., Jin-Hwe. Kweon., Jin-Ho. Choi., Jai-Hyun. Byun., Min-Hwan. Song., Sang-joon. Shin., Tae-Joo. Lee., "Effects of manufacturing methods on the shear strength of composite single–lap bonded joints", Composite structures, 2010, vol-92, pp: 2194-2202.

Soutic. C., Hu. F. Z., "Design and performance of bonded patch repairs of composite structures" In proceedings of the Institution of Mechanical Engineers", Part G. Journal of Aerospace Engineering, 1997, vol-211(4), pp: 263-271.

Soutis. C., Duan. D. M., Goutas. P., "Compressive behavior of scarf-patch-repaired composite laminates loaded in compression", International journal of Adhesion and Adhesive, 2000, vol-38(4), pp: 737-740.

Stelzer. S., Brunner. A. J., Argüelles. A., Murphy. N., Cano. G. M., Pinter. G., "Mode I delamination fatigue crack growth in unidirectional fiber reinforced composites: Results from ESIS TC4 round-robins", Engineering Fracture Mechanics, 2014, vol-116, pp: 92-107.

Stelzer. S., Brunner. A. J., Argüelles. A., Murphy. N., Pinter. G., "Mode I delamination fatigue crack growth in unidirectional fiber reinforced composites: development of a standardized test procedure", Composites Science and Technology, 2012, vol-72(10), pp: 1102-1107.

Stephan. Marzi., Andres. Biel., Ulf. Stigh., "On experimental methods to investigate the effect of layer thickness on the fracture behavior of adhesively bonded joints", International Journal of Adhesion and Adhesives, 2011, vol-31, pp: 840-850.

Thunga. M., Lio. W. Y., Akinc. M., Kessler. M. R., "Adhesive repair of bismaleimide/carbon fiber composites with bisphenol E cyanate ester" Journal of composite and science technology, 2011, vol-71, pp: 239-245.

Turon. A., Costa. J., Camanho. P. P., Davila. C. G., "Simulation of delamination under high-cycle fatigue", Composites Part A–Applied Science Manufacturing, 2007, vol-38 (11), pp: 2270-82.

Vanlanduit. Steve., Joris. Vanherzeele., Roberto. Longo., Patric. Guillaume., "A digital image correlation method for fatigue test experiment", Optics and laser engineering, 2009, vol-47, pp: 371-378.

Vinciquerra. A. J., Barry. D. Davidson., "Effect of crack length measurement technique and data reduction procedures on the perceived toughness from four-point bend end-notched flexure tests", Journal of reinforced plastics and composites, July 2004, vol-23, pp: 1051-1062.

Vodicka. R., "Accelerated environmental testing of composite materials", Report DSTO-TR-0657, 1997.

Wang. C. H., Gunnion. A. J., "Optimum shapes of scarf repair Composites", PartA: Applied Science and Manufacturing, 2009, vol-40(9), pp: 1407–1418.

Wang. J., Zhou. Z., Vodicka. R., Chiu. W. K., "Selection of aptch and adhesive materials for helicopter battle damage repair applications", Composite structures, 2009, vol-91, pp: 278-285.

Whittingham. A., Baker. A., Harman. A., Bitton. D., "Micrographic studies on adhesively bonded scarf repairs to thick composite aircraft structure", Composite Part A Applied science and manufacturing, 2009, vol-40(9), pp: 1419-1432.

Wood. K., "In-situ composite repair builds on basics High Performance" Composites, 2008.

Wright. W. W., "The effect of diffusion of water into epoxy resins and their carbon-fibre reinforced composites", Composites, 1981, vol-81, pp: 201-205.

Zhang. Ye., Anastasios. P. Vassilopoulos., Thomas. Keller., "Environmental effects on fatigue behavior of adhesively-bonded pultruded structural joints", Journal of Composite Science and Technology, 2009, vol-69, pp: 1022-1028.